Dynamic wind turbine and farm models for power system studies

Authors Sanna Uski-Joutsenvuo & Bettina Lemström

Confidentiality Public

Report's title

Dynamic wind turbine and farm models for power system studies

Customer, contact person, address	Order reference
ABB Oyj, Fingrid Oyj, Kraftnät Åland AB, Nordisk Energiforskning, Ålands Vindenergiandelslag, Ålands Vindkraft AB	NEF Project No. 63-02
Project name	Project number/Short name
Tuulivoimamallit sähköverkkotarkasteluissa	TUUMA
Author(s)	Pages
Sanna Uski-Joutsenvuo & Bettina Lemström	9
Keywords	Report identification code
wind turbine, wind farm, model, modeling, dynamic	VTT-R-00531-07

Summary

This report discusses the dynamic wind turbine and farm models for power system studies. It focuses on the modeling issues concerning the turbine/farm interaction with the power system, i.e. what phenomena of a turbine/farm need to be modeled and in what degree of accuracy e.g. in case of studying grid contingencies.

Fixed speed wind turbines are covered most thoroughly. Fixed speed wind turbine theory, building turbine and farm models, as well as performing simulations and evaluations on different modeling accuracy and parameter sensitivity analysis were carried out, and finally model validation against measurement data was conducted. The fixed speed wind turbine being the simplest wind turbine type, experience and knowledge gained from them can be, and was used as the base for studying the other turbine types.

Two doubly-fed induction generator wind turbine models that were available, were tested, but not found suitable. Problems were encountered even before entering the validation procedure against measurement data. In addition to testing the models, variable speed wind turbines models, especially DFIGs, were analyzed based on literature, measurements and other available information e.g. from manufacturers.

Conclusion of the work is that the fixed speed wind turbine models are rather good, and validated today. There are lot of variable speed turbine models built, but rarely validated, nor they are publicly available. Also getting sufficient information for modeling on specific turbines is difficult and turbine control schemes are complex. There is still work to be done.

Confidentiality	Public

Espoo 12.10.2007

Signatures

Bettina Lemström	Esa Peltola	Kari Larjava
Project leader	Team leader	Technology Director

VTT's contact address

VTT Technical Research Centre of Finland, P.O.Box 1000, FI-02044 VTT, Finland

Distribution (customer and VTT)

ABB Oyj, Fingrid Oyj, Kraftnät Åland AB, Nordisk Energiforskning, Ålands Vindenergiandelslag, Ålands Vindkraft AB.

Preface

This report is the final report of national *TUUMA*-project which is a part of the Nordic co-operation *Nordic Grid* directed by Sweden (Chalmers), and with Norway (SINTEF), Denmark (Risø) and Finland (VTT). The aim of the *TUUMA*-project was to investigate and study wind turbine modeling. One of the topics was to find out what kind of wind turbine models there are available and ensure and evaluate their validity. To fill in the lacking of models, models were also to be created within the project. One of the aims was also to maintain and broaden the know-how in the field of wind turbine dynamic modeling for power systems in Finland.

The domestic steering group was formed by industrial financiers' representatives Jouko Niiranen (ABB), who also attended the Nordic meetings, Matti Lahtinen (Fingrid), Sven-Anders Eriksson (Kraftnät Åland), and Henrik Lindqvist (Ålands Vindenergiandelslag). Financing was also received from Ålands Vindkraft AB.

This report contains some parts, e.g. ch 3.1, in which several persons at VTT have contributed through other projects as well in some extent. Juha Kiviluoma has implemented the PSCAD/EMTDC-Simulink dynamic data exchange during simulation, and Simo Rissanen (formely with VTT) the data exchange between ADAMS and Simulink as well as he has taken care of ADAMS simulation part of joined PSCAD-ADAMS simulations. The wind turbine model in ADAMS has been produced and improved under previous projects by several people.

The papers written and co-written within this project are mainly delivered to the project partners in NEF-project report and all the papers are available to them on confidential project CD. Due to publication rights, papers are not included in this report.

Espoo 12.10.2007

Sanna Uski-Joutsenvuo and Bettina Lemström

ELECTRICAL FILES ON CONFIDENTIAL CD:

- Matlab m-code for calculating active and reactive power by positive sequence fundamental frequency current and voltage phasors from instantaneous three phase voltage and current data series “laske_fundUI.m”
- PSCAD/EMTDC component library “FSWT_Comps.psl” containing
  - fixed speed wind turbine aerodynamic -component ”Fixed Speed Wind Turbine”
  - rotational sampling-wind speed model ”Wind field to equivalent wind speed”
- PSCD/EMTDC-models:
  - 600/120 kW fixed speed wind turbine model as page module ”Bonus600_120kW_pagemodule.psc”
  - measurement voltage data input model as page module “Vinput_pagemodule.psc”
  - soft-starter model as page module ”SoftStarter_pagemodule.psc”
  - 600/120 kW fixed speed wind turbine model with soft-starter and voltage source grid equivalent ”2gen_fixed_spd_with softstarter.psc”
  - Hagesholm 2 MW fixed speed wind turbine model (benchmark case) with wind turbine aerodynamic component ”Hagesholm_Singlecage_WT.psc”
  - Alsvik 180 kW fixed speed wind turbine model ”Alsvik.psc”
- Collected wind turbine Cp-data “tuulivoimaloiden_Cp-käyriä.xls”
- Olos disturbance data ” Olos disturbance update1.zip”
- Conference/workshop papers (co-)written – PUBLIC
  - Nordic Wind Power Conference ’04 paper ”adjoint simulation.pdf”
  - Fifth International Workshop on Large-Scale Integration of Wind Power and Transmission Networks for Offshore Wind Farms ’05 paper ”Dynamic_fault_simulation_of_wind_turbines_using_commercial.pdf”
  - Boreas VII ’05 paper ” Boreas VII Rissanen, Uski_Final.pdf”
  - European Wind Energy Conference ’06 paper ”EWEC_Measurements_Uski.pdf”
  - Nordic Wind Power Conference ’06 paper ”Perdana&Uski_NWPC06.pdf”
  - The report “TUUMA-project report.pdf”

1 Wind turbine modeling

In this project PSCAD/EMTDC was the simulation tool, and the modeling purpose was wind turbine and farm dynamic models for power system studies. Therefore, in the following the wind turbines are mainly discussed and analyzed regarding the issues related to the time scale of couple of seconds, and especially behavior during and after grid faults. The observation angle of view to the models and simulation is principally from the power systems viewpoint. Wind turbine and farm models for PSCAD/EMTDC were studied, analyzed and simulated in the project and are described in this report.

1.1 Modeling issues – significance of model components and parameters in different time-scales

The wind conditions control the output power of wind turbines. Wind conditions change e.g. by season, or by the time of the day, as well as by hours due to moving weather fronts, and stochastically in short term time in terms of gusts and slight changes in wind direction.

In terms of considering wind power as part of the electricity system, the wind turbine or farm can be seen as a production unit as any other in long-term studies, but with more unpredictability and variability (time-scale from hours to years). The focus is almost totally on the windyness and wind conditions. Of the power system transmission issues, the transmission capacity may need to be considered.

When it comes to shorter observation periods, as minutes to an hour time-scale, some more aspects about wind turbines and farms need to be considered in modeling. E.g. the influence of wind power variations on the rest of the system, as well as the response of wind power to changes in system – in general the interaction of wind power with the system – becomes important. This means the consideration of the difference between wind power and conventional power production units, and their different control strategies.

On about a second to few minutes time-scale, the changing wind conditions start to become less significant and significance of the electrical issues gain more importance. Studying a wind turbine or farm on this time-scale, there are several issues to be considered, such as that the wind may change due to gusts etc, and therefore the aerodynamics and turbine construction may be of significance on this time-scale. Also the electrical issues of the wind turbine and farm, as well as the grid, are of significance. Observation of electrical units may still be kept on power-level. Due to post-fault oscillations, the correct modeling of wind turbine inertias may be important.

On less than a second time-scale, the modeling of wind turbine may usually be narrowed down majorily to electrical issues, as the wind conditions or the rotating turbine causes hardly any changes on turbine torque during observation period. The changes in generator speed, caused by a fault in the grid, have hardly any affect on turbine aerodynamics and the torque through the turbine speed when during-fault phenomena are studied. Therefore the assumption of constant torque may be used. The turbine inertias still need to be modeled.

1.2 Wind turbine types

There are three major types of wind turbines in use today. The so-called Danish concept, i.e. fixed speed wind turbine, is the oldest and most simple wind turbine type of the three major types. This turbine type has been dominant in the past, and therefore there are quite a number of turbines of this type still in operation. However, the turbines are usually low-rated, and distributed production units. There are some exceptions also, e.g. the Nysted wind farm, one of the world's largest ones, consists of 72 units of 2.3 MW fixed speed wind turbines.

The major variable turbine types today are double fed induction generator or called also as doubly fed induction generator (DFIG) equipped wind turbine, and the (direct driven) synchronous generator equipped wind turbine with full converter. The variable speed wind turbines have thriven due to their better controllability compared to the fixed speed turbines', which are losing their popularity.

The DFIG concept is nowadays the most used concept in new wind turbines and farms. Its converter is smaller than the converter needed for the same size full converter equipped wind turbine, and the price due to converter costs has been its advantage over the full converter concept. The converter costs are coming down and thus the full converter concept may gain more market penetration in the future.

1.2.1 Fixed speed wind turbine type

Fixed speed wind turbines operate at fixed speed. They are equipped with induction generator (usually squirrel cage induction generator) and a capacitor bank to compensate the reactive power needed by the induction machine. The fixed speed wind turbines are also equipped with a gearbox to couple the turbine and the generator. Often the turbine generator is a two-speed generator, thus allowing the turbine to operate on two speed-modes, i.e. at two different fixed speeds. One of the modes is for small wind speeds and small power, and the other for higher wind speeds and larger power. The change from one mode to another is done in halt when the wind conditions change suitably.

Fixed speed wind turbine power to the grid is not controlled during operation. The generator and other electrical parts are dynamically uncontrollable. The only control of the turbine during operation is stall control. It means that at high enough wind speeds, i.e. when nominal power is reached, the turbine blades stall and thus provide power control for the turbine. The stall control can be either passive, when the control occurs by itself at wind speeds high enough, or active, when the blades are twisted mechanically meaning that the blades' angle of attack are controlled in order to make the blades stall.

Passive stall control is such that after the nominal power is reached as the wind speed increases, at first the turbine power exceeds slightly the nominal power, and then at higher wind speeds the power sways around nominal speed, and might go under (or above) nominal power again. In active stall control the blades are turned to the opposite direction than in blade pitching, which causes the blade to stall. By this exceeding the nominal power is avoided and the power is able to be kept in nominal value. Pitch and stall of the blades and other fundamental wind turbine operation basics are explained e.g. in [1].

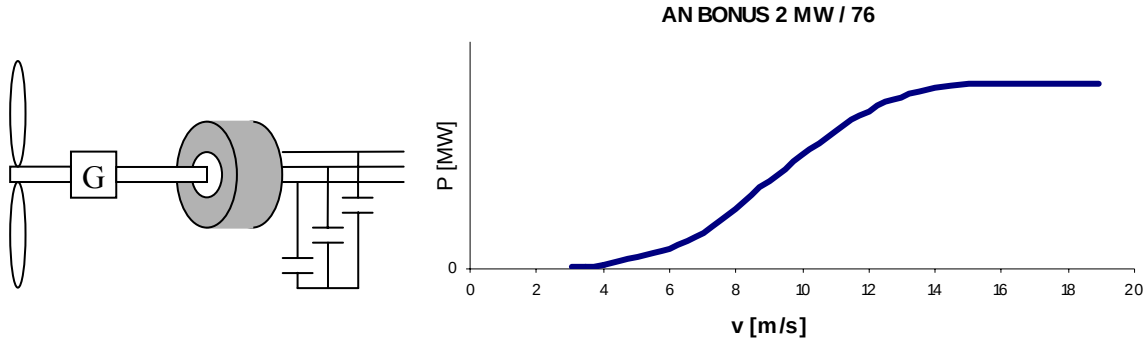

Figure 1. Fixed speed wind turbine schematic diagram and power curve of an active stall controlled turbine.

1.2.2 DFIG equipped variable speed wind turbine type

The doubly fed induction generator, i.e. DFIG concept, which is used in some variable speed wind turbines, is a wound rotor induction generator. The rotor circuit is connected to the grid via a converter bridge, and the stator circuit is directly connected to the grid. In Figure 2 is shown an elementary diagram of the turbine type and a power curve from one turbine.

The power transmitted via the rotor circuit is dependent on the machine slip. About up to one third of the generator power, power can be fed via the rotor/converter circuit. The machine can operate in sub- or super-synchronous speed when feeding power to the grid and the converter can control the output active and reactive power. Fixed speed wind turbines are equipped with capacitor banks to compensate the reactive power used by induction machine, but DFIG equipped wind turbines do not need to have capacitors, as the reactive power can be controlled. The power electronic converter bridge provides also a smoothing effect of power fed to the grid due to wind speed variations, as well as e.g. transients due to grid faults, as the speed of the generator is allowed to vary and thus absorb or free energy within operating speed limits. The variable speed wind turbines are equipped with blade pitch control.

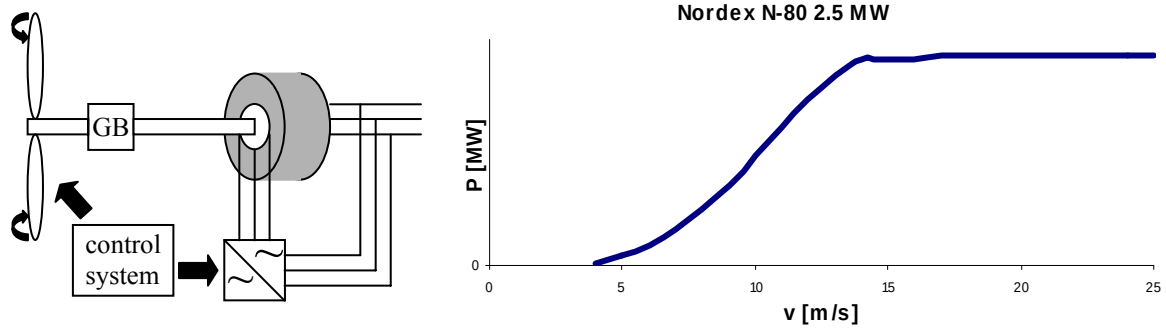

Figure 2. Variable speed wind turbine equipped with DFIG, schematic diagram and power curve of a turbine. The turbine may or may not have a gearbox. Curve from a turbine with pitch control.

In variable speed wind turbines the turbine rotor speed as well as the generator rotor speed are variable. In DFIG equipped wind turbine there is a gearbox coupling the turbine and the generator rotor as in fixed speed wind turbines. The speed of the turbine is controlled in two ways. At lower wind speeds, the generator speed is smaller, and at slightly higher wind speeds

the generator speed is controlled to be higher. The generator speed is controlled in this manner by the power electronics up to speed just about the nominal speed of the turbine. The speed range – and the maximum speed – of the turbine is a bit larger, though. The nominal speed is reached somewhere below the turbine nominal power.

Theoretically, as the nominal speed is reached, speed control is not done anymore in the manner explained earlier for lower wind speeds, but the control is now on blade pitch control. In practice it is not necessarily a specific point at which the speed control is abandoned and pitch control is taken in use (see Figure 3, which applies to both variable speed wind turbine types). Anyway, at higher wind speeds the generator speed is kept just about constant, and the turbine power is kept constant by blade pitching. If blade pitching would not be used, the turbine would behave like a fixed speed wind turbine in this operation area, but pitch control keeps the power well in nominal value.

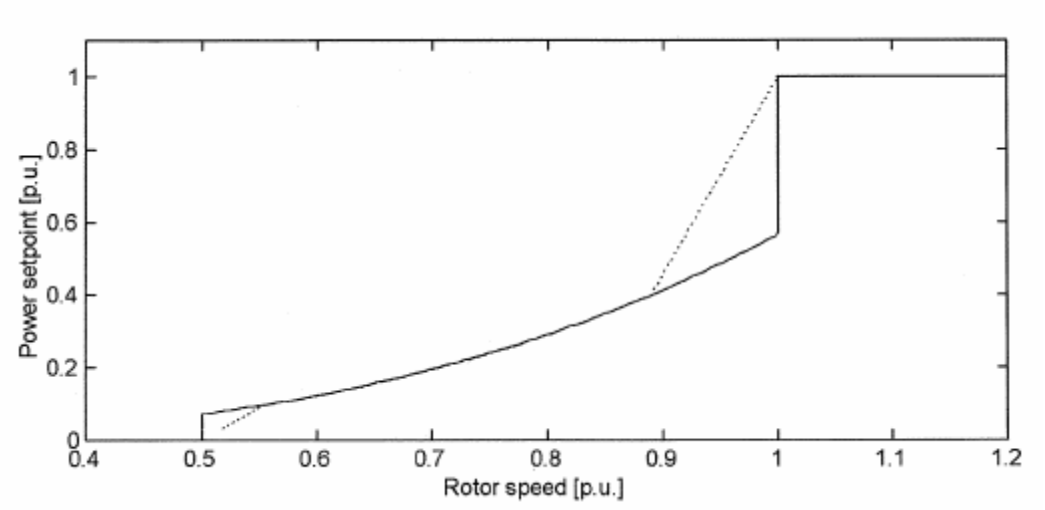

Figure 3. Optimal (solid curve) and practical (dotted curve) rotor speed-power characteristic of a typical variable speed wind turbine. [2]

The power electronic devices are vulnerable to grid faults, i.e. low voltages causing large currents, which could brake the equipment in DFIGs. The DFIG machines may therefore be equipped with crowbar protection, which short circuits the rotor circuit and thus bypasses the converters. When crowbar has operated and the rotor circuit is shorted, the machine functions like the squirrel cage induction machine in a fixed speed wind turbine.

Based on the old practice, the wind turbine is disconnected from the grid due to a grid fault, but nowadays and even more in the future, the wind turbines must fulfill new requirements and remain connected during a fault. This is called fault ride through, or low voltage ride though and requires e.g. DFIG machine crowbar the capability of being switched off and returning to converter operation while the wind turbine is connected to the grid. Crowbar which has no ability to be deactivated during operation when turbine is connected to the grid, is of passive type, and the crowbar capable of being used in low voltage ride though is active crowbar.

1.2.3 Full converter concept

Another variable speed wind turbine type in addition to DFIG equipped turbines, and the third major turbine type, is the wind turbine with full converter. This wind turbine type generator, usually synchronous generator, is connected to the grid via a converter, whereas the DFIG stator circuit is connected directly to the grid and the rotor circuit only via a converter, thus allowing the DFIG converter to be about a third of the converter size in the same size wind turbine equipped with full converter.

Full converter concept wind turbines my or may not be equipped with a gearbox. The term "direct driven" in context of this third major turbine type refers to the direct coupling between the turbine and the generator, whereas in the fixed speed type turbines and DFIG equipped turbines there are used gearboxes to couple the turbine and the generator. Some full converter equipped wind turbines do have a gearbox, but often it is considered as one additional failure component, and thus not used.

Another difference to previously described two other major types is also that in full converter equipped wind turbine the generator is a synchronous generator, whereas in the other two types it is asynchronous induction machine. In the direct driven wind turbine the generator rotor rotates at the same speed with the turbine rotor. This requires the number of generator pole pairs to be very large, although the electrical frequency does not need to be the same as grid frequency because of the decoupling converter.

Although the generator frequency is decoupled from grid frequency by the converter, the generator rotor and also the turbine rotor speed is limited by blade tip speed. Thus the maximum rotor speed on wind turbines of different rated power is different. The bigger rated the wind turbine is, the smaller is the maximum rotor speed. E.g. rotor speed maximum for Enercon 1 MW wind turbine is 24 rpm, and 22 rpm for 1.5 MW wind turbine. The same speed control and blade pitch control principles apply to this wind turbine type as for DFIG equipped wind turbine described in previous section 1.2.2.

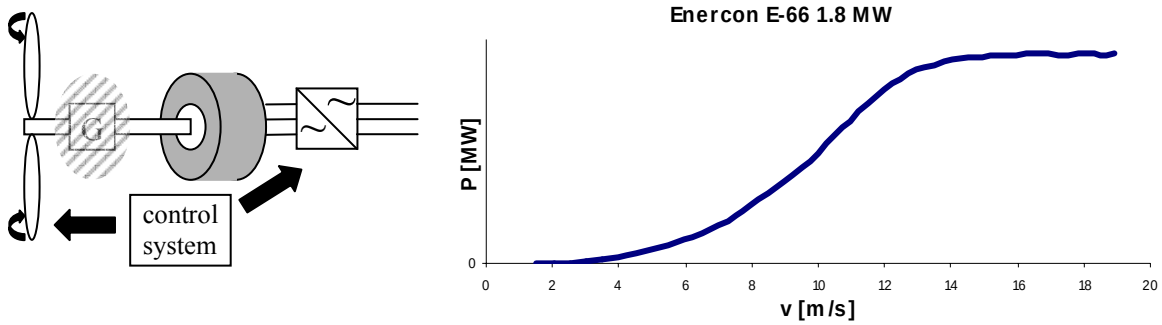

Figure 4. Variable speed wind turbine equipped with synchronous generator, schematic diagram and power curve of a turbine. Curve from a direct drive turbine with pitch control.

1.3 Wind turbine models – modeling purposes

There are several purposes which wind turbine and farm simulation models are needed for. First of all, the model needed must be suitable for the purpose of the study. The modeling tool should also be selected suitably being capable of representing the model in the degree of

detail wanted and required, at the same time enabling sufficiently simplified modeling and providing a reasonable simulation time.

Involving electrical modeling of the wind turbine, different needs for models are e.g. wind turbine mechanics and aerodynamic studies, generator or generator & power electronic devices-setup studies, power quality studies, grid connection studies, power system load flow studies, power system dynamics studies, etc.

In studies where the wind turbine itself is being studied, the mechanical and aerodynamical modeling of the wind turbine is of great importance. On the other hand, in power system studies mechanical and aerodynamical parts can be modeled very simplified, the main focus being on the electrical modeling of the wind turbine. A number of wind turbines may be even simplified as one or some aggregate models also in terms of their electrical quantities.

The generator and other electrical components (e.g. power electronics) can be the scope of the study, where the generator itself may be modeled in such detail that focus is on the transient events, and the mechanical parts can be omitted, e.g. [3], [4].

If studying the turbine mechanics, e.g. stresses the turbine is exposed to, the electrical parts of the wind turbine can be included in the model in order to be able to study stresses caused by the electrical faults in the grid. This topic is discussed a little bit further in section 3.1.

In power quality studies e.g. the flicker is an important issue. The aerodynamics of the turbine need to be modeled at least in some extent in power quality studies. In [5] two modeling approaches were used, a more advanced and a simplified one for aerodynamic conversion system. The conclusion was to recommend not to use the simplified aerodynamic modeling approach for short time flicker severity index impact prediction. The flicker appears due to power variation caused by rotating turbine which extracts different amount of power from the wind depending on position of the blades, and varying wind speed and wind field. Power quality of wind turbines is modeled and studied e.g. in [6] and [5]. Modeling the wind and turbine aerodynamics in a simple way is discussed in sections 3.2.4 and 4.5.

In this report the main focus is on the dynamic wind turbine models for (power system) dynamic studies, which represent the behavior of the turbine in case of disturbances in the grid and can be used e.g. in grid studies involving wind turbine low voltage ride through capability. Concerning these models the simulation/study periods are usually short enough that wind speed variations are not significant, so wind and the aerodynamics of the turbine are not needed to be modeled. This is investigated and shown in section 3.2.4.2. The mechanics of the turbine are usually sufficiently modeled when using a two mass model of the wind turbine.

Power system studies usually involve the whole power system or a portion of it. Being of rather small capacity size compared to the system under study, single wind turbines are not of significance. However, as wind turbines are forming larger wind farms in the system, the number of single units makes them significant as a whole. It is not reasonable, nor compulsory, to represent each wind turbine individually, but instead one or a few aggregate models to represent the wind farm can be used. Aggregate wind farm models are discussed in sections 3.4, 3.5, 3.6, 4.9, and 3.7.

1.4 Dynamic models for PSCAD/EMTDC

PSCAD/EMTDC is one of the foremost commercial electromagnetic transient simulation tools. It has been developed by Manitoba Hydro and later Manitoba HVDC Research Center since the 1970's.

During the last few years, there has been lot of discussion about dynamic models for wind turbines and farms, and model development, which can been seen as numerous presentations given in conferences and workshops, as well as in terms of e.g. an International Energy Agency (IEA) Wind Energy R&D Annex XXI [7] working on around the task [8]. Despite of the popularity of the subject and numerous models developed by number of different instances, there are very few publicly available models around, and even fewer such for PSCAD/EMTDC. Validated models are even more rare, and many of the models of different instances that are not even public, are not validated either, e.g. [8].

Commonly found in publications, a good, sufficient and adequate wind turbine model for power system studies consists of the generator, 2-mass model system representing the wind turbine system inertias, capacitor bank for fixed speed wind turbine and converter control (P and Q) and blade pitch control for variable speed wind turbines. E.g. [9].

Concerning the wind turbine models for dynamic studies (of transient voltage stability), modeling the aerodynamics of the wind turbine provides a coupling between the turbine speed deviation/pitch angle and the mechanical power produced by the turbine at constant wind speed. Thus also the blade angle control system of pitch or active-stall system is needed, and the turbine shaft system modeling represents the interaction between the mechanical and electrical parameters. On the other hand, what usually are not needed, are the wind speed fluctuations – long-term or turbulent – or mechanical oscillations in the blades or the tower influence. [9]

The dynamic models two of the three major types of wind turbines are discussed in chapters 3, fixed speed wind turbines, and 4, DFIG equipped wind turbines. Full converter equipped wind turbine models are not focused in this report due to the lacking of available models for testing, as well as the fact that even available DFIG models were not found valid yet. Therefore full converter equipped wind turbine model was not even attempted to be built in the project.

2 Model validation

Model validation is most reliable when comparing simulation results against actual measurements of the real system. The model needs to be able to show the response of the actual system, for example to a fault.

Usually the fault characteristics, such as location or fault impedance, in real systems are not exactly known. Measurements of current and voltage can be done, however, of actual fault incidents. Measurements are discussed in section 2.1.1 and measurement data handling in section 2.1.2. Usually real-life faults are not ideal, i.e. they do not have known, or even constant, fault impedance. In many cases the fault impedance and even the fault type is changing throughout the fault period.

In validation procedure described in this report, the measured phase voltages during, before, and after the fault are inputted as the phase voltages to the model in corresponding location, as discussed in section 2.2. Then the simulated phase currents are compared to the measured currents. If the model is good, the simulated phase currents should correspond fairly well to the measured phase currents, as well as the calculated active and reactive power of measurements and simulation.

Single operating point validation may not be enough to prove the validity of the model extensively over the whole operating scale of the turbine. These issues are discussed in section 2.3.

2.1 Validation data

2.1.1 Measurement data

Validity of the measurement data is important in model validation. Usually the data is taken of all three phases, and it is essential to know which phase voltages are pairs with which currents, as well as that the measured quantities are in synchronism. Usually there are three possibilities which give reasonable values for both, active and reactive power and based on which the "correct" solution/pairs are chosen.

The data may be unsynchronized due to e.g. mistakes done in the measuring set up synchronization, or data recording set up. Also, one should be careful in case the phases are not named correctly, in terms of the voltage and the current pairs, or the phase sequence (a,b,c), which makes significance when calculating the fundamental positive and negative sequence vector components for active and reactive power calculation discussed in the following section 2.1.2.

However, in case the voltage and current data are not in synchronism, there are even more possibilities of interpreting the data wrong. There may easily be "suitable" short time shift in the current data relative to the voltage data. In case there is a time shift, the data may seem fine, but when calculating active and reactive power, they may not be as expected.

The best way to check the synchronism of the data is to compare the singular points (e.g. due to faults), which can be timed to be taking place simultaneously in both, voltage and current data. Also, the model to be validated may give hints of problems with the measurement data if the simulated currents do not match reasonably to the measured ones when using the measured voltage as input to the simulation.

In addition, if the data still seems fine, a larger number of measurements sets may reveal the problem. E.g. the plot of the pre-fault P(Q)-data operating point curve of the wind turbine of number of measurement cases, should resemble the turbine characteristic P(Q)-curve in case there are many enough measurement cases throughout the wind turbine operating area.

The sign of instantaneous current depends on in which direction the current was measured, and it is not of significance when the data is in synchronism. In case the current is measured in "wrong" direction its sign can be simply changed.

Problems with the data used for validation in this project, were encountered. Data interpretation problem was discovered with help of P(Q)-curve, as well as data synchronism

problem was discovered by model (to be validated) simulation and singular point comparison [10].

2.1.2 Data handling

Usually the measurements and simulations have been compared to each other by the active and reactive power, and this is also recommended by the IEA Annex XXI.

Active power is that part of the electrical power that can be transformed to mechanical power or vice versa. By definition as described in [11], active power is defined as average over one period, apparent power is the product of rms current and voltage, and reactive power is the non-active power what is left of apparent power

$$Q = \sqrt{S^2 - P^2} \,.$$

One of the easiest and quite widely used ways of calculating the active and reactive power of measured instantaneous phase voltages and currents is using equations

$$P = u_1 i_1 + u_2 i_2 + u_3 i_3 \tag{2.1}$$

$$Q = -\frac{(u_2 - u_3) i_1 + (u_3 - u_1) i_2 + (u_1 - u_2) i_3}{\sqrt{3}}, \tag{2.2}$$

which, however, apply only to (at all times) balanced three-phase system. Especially equation (2.2) relies greatly on symmetry of voltages.

The equations (2.1) and (2.2) were used e.g. in [12] for comparative purposes of measurement and simulation in case of an unbalanced fault, as both, the measured and simulated active and reactive power were calculated in the same manner. It was, however, stated that the shown reactive power during unbalanced operation should not be considered for any other purpose but comparison of the measurement and simulation results. In [11] it was shown that in case of an unbalanced fault the different methods of active and reactive power calculation give differing values, especially for reactive power.

Especially in unbalanced situations, but preferably in all cases, instead of equations (2.1) and (2.2) active and reactive power should be calculated using the fundamental positive sequence voltage and current phasors. This is also recommended in [13] and rationalized in [11], where equations are also given. The Fourier coefficients for phase-a are

$$u_{a1,\cos} = \frac{2}{T} \int_{t-T}^{t} u_a \cos \omega_1 t \mathrm{d}t \tag{2.3}$$

$$u_{a1,\sin} = \frac{2}{T} \int_{t-T}^{t} u_a \sin \omega_1 t \mathrm{d}t \tag{2.4}$$

and phase-a rms voltage is

$$U_{a1} = \sqrt{\frac{u_{a1,\cos}^2 + u_{a1,\sin}^2}{2}} \,. \tag{2.5}$$

After solving Fourier coefficients for each phase with above equations, the fundamental positive sequence vector components for voltage and current are calculated by

$$u_{1+,\cos} = \frac{1}{6}\left[2u_{a1,\cos} - u_{b1,\cos} + u_{c1,\cos} - \sqrt{3}\left(u_{c1,\sin} - u_{b1,\sin}\right)\right] \tag{2.6}$$

$$u_{1+,\sin} = \frac{1}{6}\left[2u_{a1,\sin} - u_{b1,\sin} + u_{c1,\sin} - \sqrt{3}\left(u_{b1,\cos} - u_{c1,\cos}\right)\right] \quad (2.7)$$

$$i_{1+,\cos} = \frac{1}{6}\left[2i_{a1,\cos} - i_{b1,\cos} + i_{c1,\cos} - \sqrt{3}\left(i_{c1,\sin} - i_{b1,\sin}\right)\right] \quad (2.8)$$

$$i_{1+,\sin} = \frac{1}{6}\left[2i_{a1,\sin} - i_{b1,\sin} + i_{c1,\sin} - \sqrt{3}\left(i_{b1,\cos} - i_{c1,\cos}\right)\right]. \quad (2.9)$$

With voltage and current vector components can be calculated

$$P_{1+} = \frac{3}{2}\left(u_{1+,\cos}i_{1+,\cos} + u_{1+,\sin}i_{1+,\sin}\right) \quad (2.10)$$

$$Q_{1+} = \frac{3}{2}\left(u_{1+,\cos}i_{1+,\sin} - u_{1+,\sin}i_{1+,\sin}\right). \quad (2.11)$$

As dealing with sequence systems, it should be remembered to take care of the order of phases when naming the phases. In the positive sequence system phases b and c lag phase a by 120 and 240 degrees respectively – according to which the instantaneous phase quantities should be named – and in the negative sequence system phases b and c lead phase a.

A Matlab code calculating the active and reactive power based on fundamental positive sequence voltage and current phasors is available in appendix file on the CD.

2.2 Using measured voltage as input in model validation

2.2.1 Backgroung

Usually the measurements taken are of real life faults instead of being results of artificial fault tests performed on the field. Thus, the fault impedance is not usually known, and it often can be of varying magnitude throughout the fault as well. In addition, the most common “natural” faults are of unbalanced type, and the fault type can be changing, e.g. a single phase fault may evolve to a two phase to ground fault. [14]

In order to be able to compare simulation result to the measurements, similar fault and conditions to the measured system should be created in the model. However, it is not easy to create the similar fault conditions for simulation model due to the fact that the fault impedance is not known, nor it can be calculated accurately as the fault location or other information of the system may not be known.

The measurements are taken from one particular point. Usually when wind turbine model validation data is in question, the measurement point is at the wind turbine terminals or near to it. By using the measured phase voltage time series as the voltage conditions in the model at corresponding location to the measuring point, simulations can be performed. In addition, using this method the connection grid does not need to be modeled.

When inputting the measured voltage to the model emulating the actual system in question, the response of the model is expected to correspond to the measurements. Thus the simulated currents and active and reactive power are compared to the measurements. If the correspondence between the simulation and measurement is good, the model is good, and in case there are differences between the simulation and measurement, there are some things in the model that are not being modeled correctly, or features are even missing.

The power output of the generator and slip of induction generator are related strongly, and thus the rotor slip oscillation will cause power oscillation. As the torsional shaft mode is the natural frequency of power oscillations, the oscillations at this frequency will be seen on voltage fluctuation. This means that voltage fluctuations and slower recovery of voltage after a grid fault are results of the transient mechanical behavior of the twisted shaft [9]. This means that the voltage seen at the wind turbine terminals is (partly) caused by the mechanics of the wind turbine system.

Thus, it may seem like if inputting the measured voltage to the system, the influence of the wind turbine is experienced twice, first in the input voltage, and then as the response of the model. However, as the inputted voltage is set, and the uncontrolled model response can not change it, the model response must be seen somewhere else, and that is in current. As the voltage is "fixed" and the model can not change it, the current must change accordingly.

In following section 2.2.2 is shown that using measured voltage as input in fixed speed wind turbine model simulation is justified and in case the model is accurate, the simulation results should correspond to the measured ones. Implementation of measured voltage input to simulation in PSCAD/EMTDC is discussed in section 2.2.4.

2.2.2 Justification

A test for validity of using measured voltage as input voltage in model validation procedure (in PSCAD/EMTDC), was arranged as follows. The absolute model parameters are not, however, of interest in this context, i.e. if or if not the model used represents any particular wind turbine.

The model parameters used here, were parameters for Bonus 600 kW turbine. 600 kW generator mode of the generator and turbine were used in the model with generator parameters:

Rs = 0.006548 pu
Xs = 0.089442 pu
Rr = 0.009334 pu
Xr = 0.111314 pu
Xm = 3.886948 pu

The wind turbine model has capacitor banks connected of reactive power supply at nominal voltage 50+50+62.5 kVAr. The turbine is modeled as a two mass model with turbine and other components on the low speed side as one mass, and the generator and high speed side components as the other mass.

Two sets of the wind turbine model to be validated were set up. One setup was with ordinary voltage source emulating the connection grid, and the other with component capable to model the measured voltage (exactly) as the voltage at the point. This was implemented basically by inputting time series of measured voltage data as the voltage at input point, to the simulation.

Later in section 2.2.4 real measurement data is used as input. In the model with ordinary voltage source component, there were also added components that create a varying fault, starting at 2.5 s after the initialization of the simulation. The fault starts as a two-phase short circuit, then after 83 ms transforms to a two-phase-to-ground fault of duration of 38 ms, and changing finally to a three-phase short circuit, which lasts for 158 ms. The fault is cleared by

itself at 2.779 s, and is to take place at the voltage source terminals. Varying and unbalanced fault type was selected in order to the test being as diversified as possible.

A simulation on the model with ordinary voltage source and a fault taking place at the source terminals was performed. The simulation phase voltages and currents were stored between the fault point and the wind turbine. In Figure 5 and Figure 6 are presented the phase voltages and phase currents of the simulation with ordinary voltage source in case of a fault. Simulation time step used is 50 µs, and sampling time step of saving data is 100 µs.

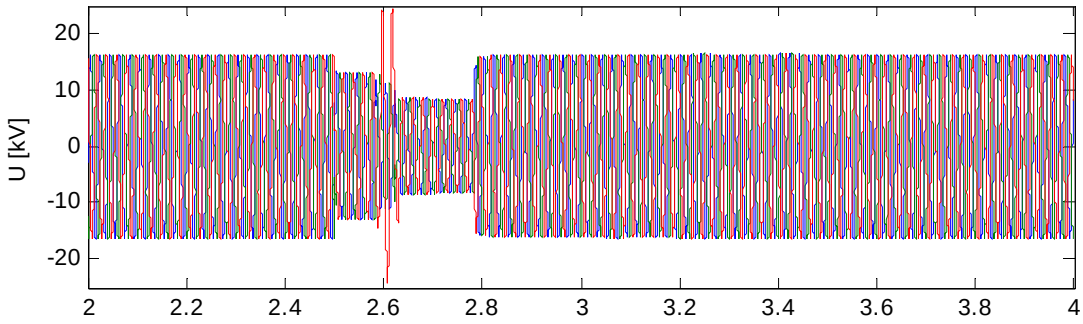

Figure 5. Phase voltages in case of a varying fault occurring at 2.5 s. The fault starts as a two-phase short circuit (83 ms of duration), changes to a two-phase-to-ground fault (38 ms of duration) and finally to a three-phase short circuit (158 ms of duration), and the fault is cleared by itself at 2.779 s after simulation initialization.

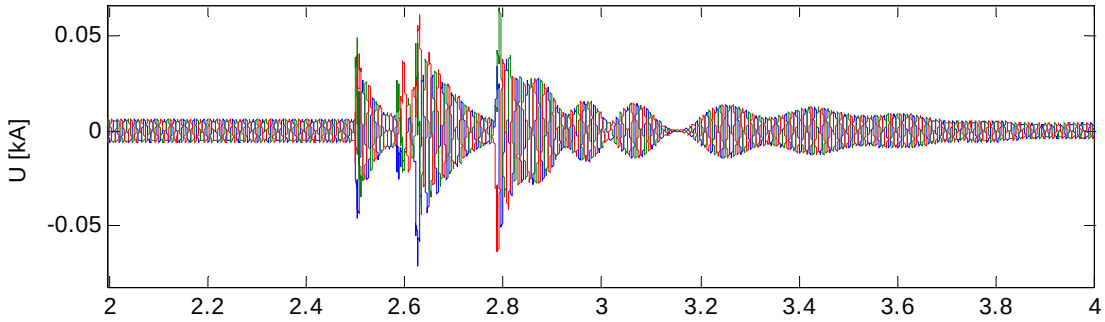

Figure 6. Phase currents corresponding to voltages and the fault described in Figure 5.

The phase voltages stored of the simulation are then used as input to the second model simulation as the voltages at corresponding point of the system where they were measured in the first simulation. The simulation time step is the same as in the first simulation, 50 µs, and data sampling time step 100 µs. The voltage data is inputted at frequency of 10 kHz, which corresponds to the sampling frequency of data saving in the simulations.

Now only one phase is compared and shown for clarity. The phase voltage stored in the first simulation and the phase voltage measured at the voltage input component terminals (voltages at the same point in the system) are shown in Figure 7. In Figure 8 the corresponding phase currents are shown. The match is fairly perfect in both figures. The largest mismatch in the particular phase shown here, is 1.5 A, and the largest mismatch in any phase is 3 A. The largest mismatch takes place in instant when the change rate of the current is very large, and therefore these mismatches are not really shown.

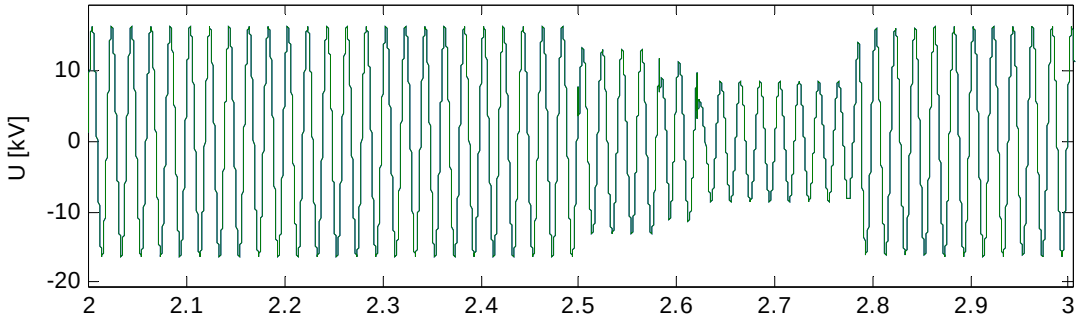

Figure 7. Phase voltages of one phase in voltage source simulation (blue line), and voltage input simulation (green line) with sampling frequency of 10 kHz. The voltage input voltage corresponds perfectly to the voltage in voltage source simulation (overlaps the blue line).

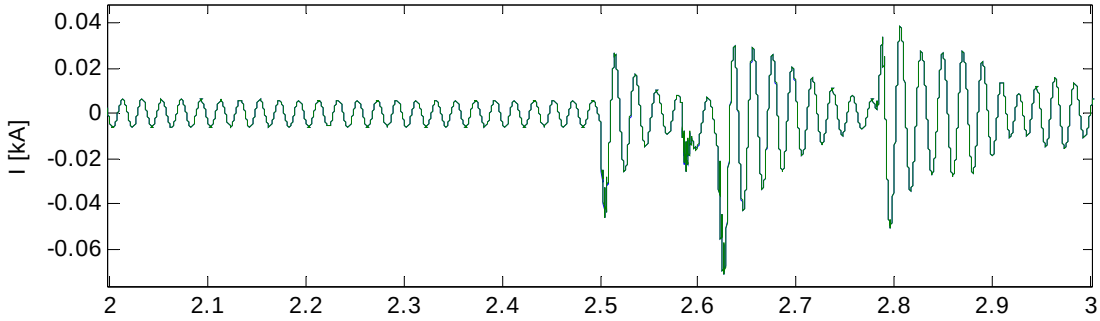

Figure 8. Phase currents of the same phase of which voltages are shown in Figure 7. Voltage source simulation (blue line), and voltage input simulation (green line). The voltage input current corresponds perfectly to the current in voltage source simulation (overlaps the blue line).

When using sampling frequency of data corresponding to the simulation time step in both simulations (50 µs simulation time step, 50 µs saving data sampling time step), the input sampling frequency of voltage data in voltage input simulation corresponds to the time step size. In this case the largest difference in currents becomes less than 70 µs. Real-life data measurements are usually carried out at smaller sampling frequencies.

The larger the input data sampling frequency, the better correspondence there is seen in the results. Reduction of the sampling frequency to 5 kHz, the largest mismatches seen in phase currents are 1.5, 2.8 and 1.3 A. With sampling frequency of 1 kHz, the mismatches are getting visible in figures (Figure 9) and are at maximum in phases 11, 22.5 and 11.8 A. Sampling frequency of voltage source simulation data is also 1 kHz.

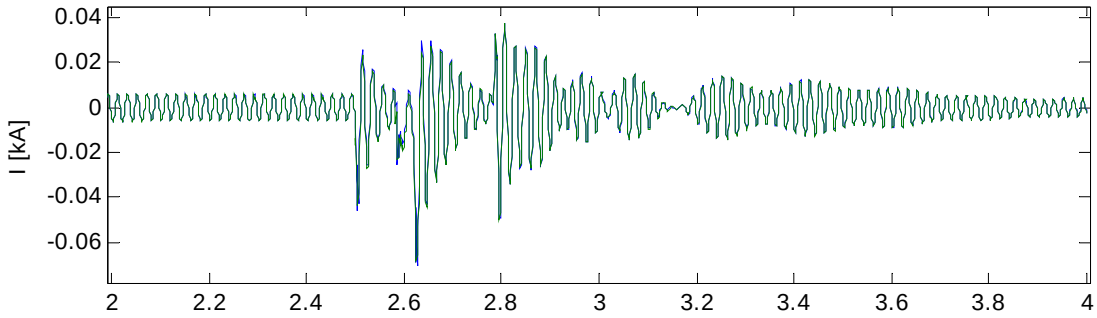

Figure 9. Phase currents of a phase with voltage input sampling frequency of 1 kHz to the simulation. Voltage source simulation (blue line), and voltage input simulation (green line).

Most, and the largest mismatches, in currents occur in data period when there are large changes in current. The steady state stage currents correspond better to each other. There are larger differences in currents in post-fault stage as well. The mismatch in post-fault stage is larger than in pre-fault steady state, but somewhat smaller than mismatch in during-fault stage.

When using voltage data input sampling frequency of 500 Hz, there become large inconsistencies in steady state data as well. The currents of the two simulations are shown in Figure 10.

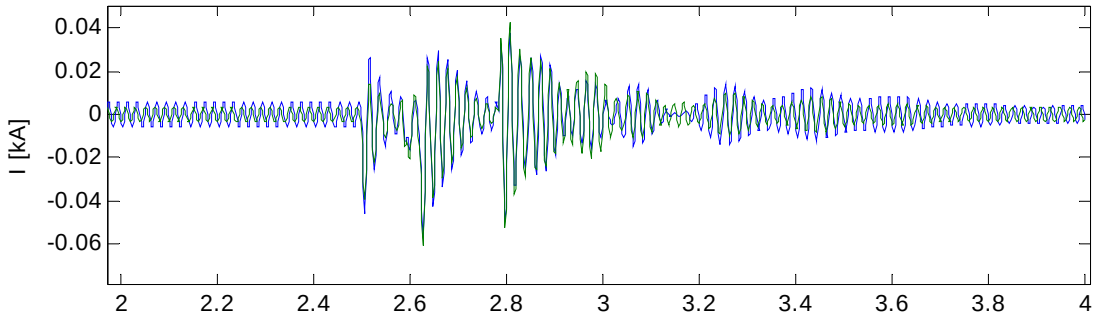

Figure 10. Phase currents of a phase with voltage input sampling frequency of 500 Hz to the simulation. Voltage source simulation (blue line), and voltage input simulation (green line).

The simulations in PSCAD/EMTDC are always started from flat, or from a snapshot stored of a previous simulation. Using a flat start simulation, the system needs a while to reach the steady state. In the simulations shown in this context, the simulations are flat started simulations.

In voltage input simulation with 500 Hz sampling frequency, the phase currents are at the beginning of the simulation in phase with the currents simulated with voltage source component. At the beginning of the simulation, there is a phase shift between the currents (leading) and voltages. However, starting right at the beginning of simulation, the phase shift in the input voltage simulation starts to decrease, and after a short while after the beginning of the simulation, the voltages and currents are in phase. There occurs also a decrease in currents in magnitude. These things can be seen also when comparing the currents of input voltage simulation, to currents of voltage source simulation in Figure 11. As the fault begins, the current phase shift seems to change closer to what it should be, but after the fault again starts

to drift from what it should be. Due to the changed current (in phase shift angle in respect to voltage and the magnitude) it is not possible to determine the active and reactive power of the simulation results.

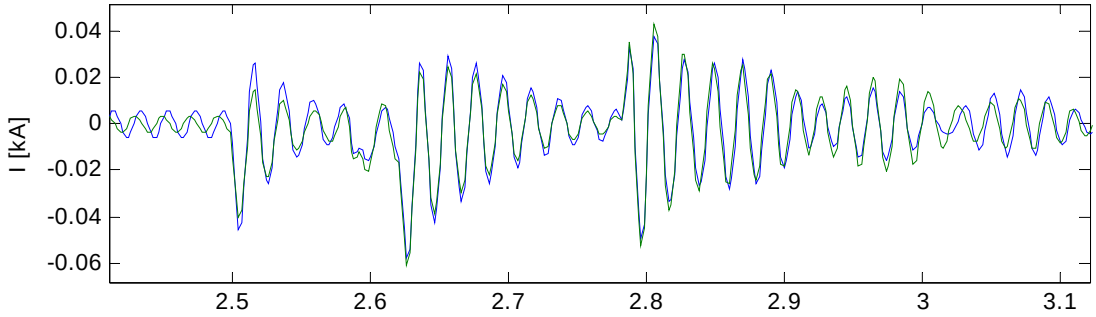

Figure 11. Phase currents of a phase with voltage input sampling frequency of 500 Hz to the simulation. Voltage source simulation (blue line), and voltage input simulation (green line).

The problem regarding too low a voltage input sampling is not due to too large steps of the step-wise voltage resulting of low sampling frequency. Expanding the voltage input data to be inputted as 1.5 kHz data (as genuine 1 kHz sampling frequency data gave fairly good results) by interpolating two additional data-point values to the data set between each measured value, does not give any better solution, but instead identical to the simulation with genuine 500 Hz data input (in Figure 11). Therefore, measurement data of too low a sampling frequency can not be used directly as voltage input to simulation.

Using spline-interpolation is useful and helps to expand the measurement data of too low sampling frequency to the sampling frequency suitable for inputting the measured voltage data in simulation. In Figure 10 phase current of simulation with 500 Hz sampling frequency measured voltage used as input to simulation was compared to the measurement of current (of the voltage source simulation). The results were not good. This 500 Hz voltage measurement data is expanded to 5 kHz data by spline-interpolation, and the expanded data is used as input voltage to the simulation. The correspondence of a phase current in simulation and the measured current of the voltage source simulation creating the measured values, is shown in Figure 12. The correspondence seems to be rather good, the largest mismatches of phases are 20.1, 20.1 and 23.2 A. Voltage measurement data of sampling frequencies 333 Hz, 250 Hz and 200 Hz give also good correspondence when data is used as input voltage to simulation after spline-interpolation to 5 kHz data. The active power of these simulations is shown in Figure 13.

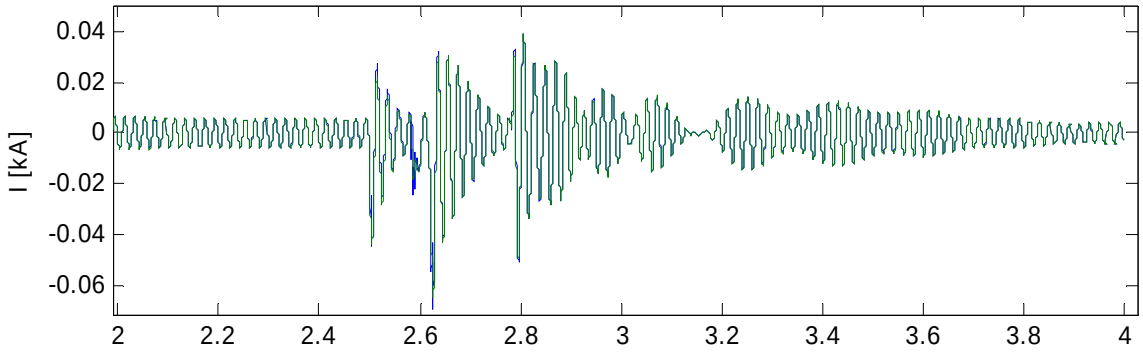

Figure 12. Phase currents of a phase with voltage input sampling frequency of 5 kHz of spline-interpolated measurement data of 500 Hz to the simulation. Voltage source simulation (blue line), and voltage input simulation (green line).

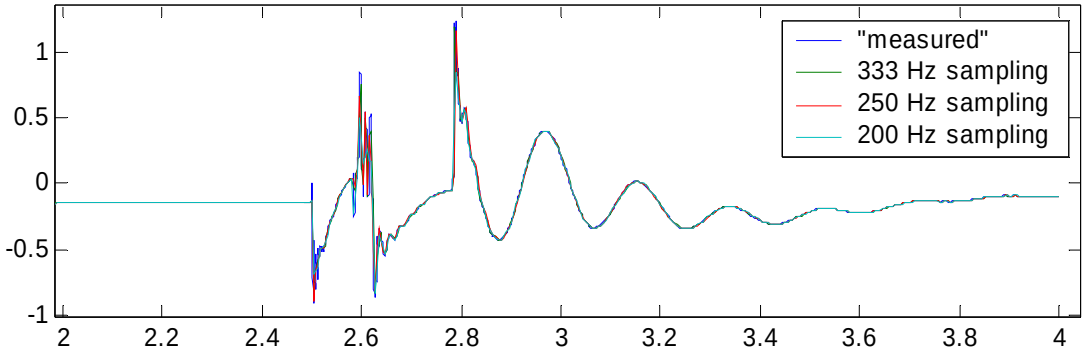

Figure 13. Small measurement sampling frequency voltage data used as input voltage data after spline-interpolation to 5 kHz data. Comparison of active power of simulations to the "measured" power.

It can be concluded that using spline-inperpolated measured phase voltages as input to simulation, rather small sampling frequency measurement data can be used. It should be remembered, though, that in this experiment where simulated values were taken as "measurement", and then used as input to another simulation with exact same model of wind turbine, the "measurement" data was accurate. I.e. there were no errors in the measurement accuracy, scaling, nor timing. And further more, the fault simulated was rather unrealistic with constant fault impedance in each fault type period, thus producing rather ideal-like voltage waveforms, which are easier to interpolate closer to actual value.

2.2.3 Influence of model parameter accuracy

The basic idea is, if the model is correct, that the simulated current should correspond to the measured currents. Now it is investigated how errors in model parameters affect the simulation results. Later in section 3.2.3 Figure 25 - Figure 29 is seen that the mechanical parameter values influence the model performance only in post fault state, and not in during fault period.

In Figure 14 - Figure 18 is shown how inaccuracy of electrical parameter values of the model generator influence the output current of simulation. In each case one parameter is varied at the time to both directions from its actual value. The parameter value variations are not very large, but are significant in the order of magnitude of each parameter when the parameters are estimated to the correct order of magnitude.

When inspecting the significance of parameter accuracy in the figures below, it should be remembered that the sensitivity study done here is done for one generator type with certain parameter values.

From Figure 14 it can be concluded that moderate error in stator resistance parameter value has almost no influence on the output of the model. Equal error in pu done in stator and rotor reactance, produce almost perfectly identical difference in output phase current (Figure 15 and Figure 18). Errors done in magnetizing reactance parameter value also have rather slight influence on the output current. Contrary to the stator resistance which makes almost no significance, the error in rotor resistance parameter value has more influence on output current. The smaller the resistance, the looser the system seems to be, when comparing the influence of parameter values to the post fault oscillation.

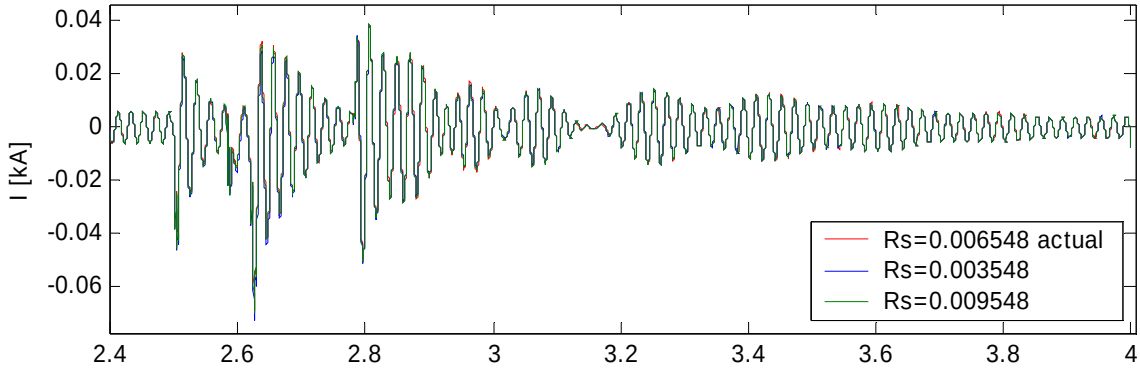

Figure 14. Influence of inaccurate parameter value of stator resistance in the model to output current.

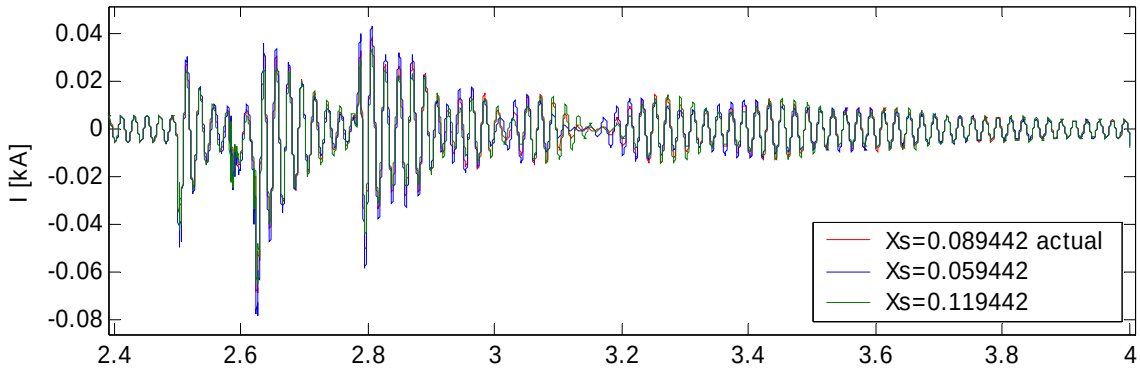

Figure 15. Influence of inaccurate parameter value of stator reactance in the model to output current.

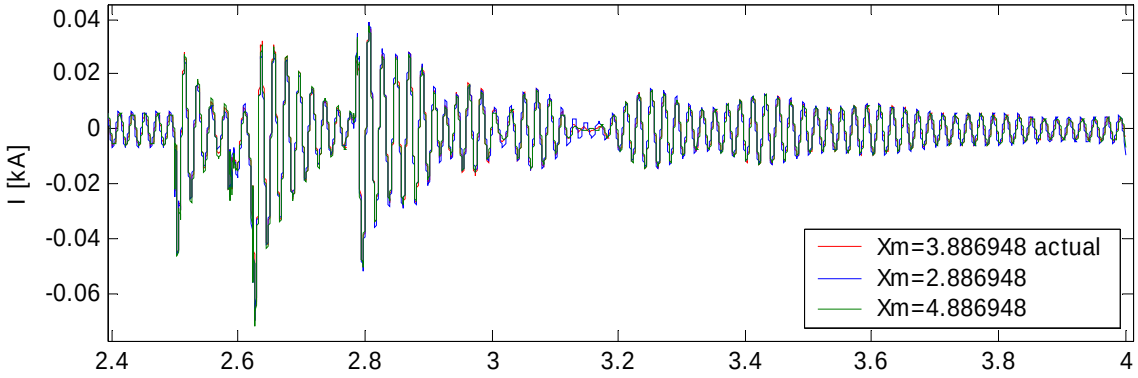

Figure 16. Influence of inaccurate parameter value of magnetizing reactance in the model to output current.

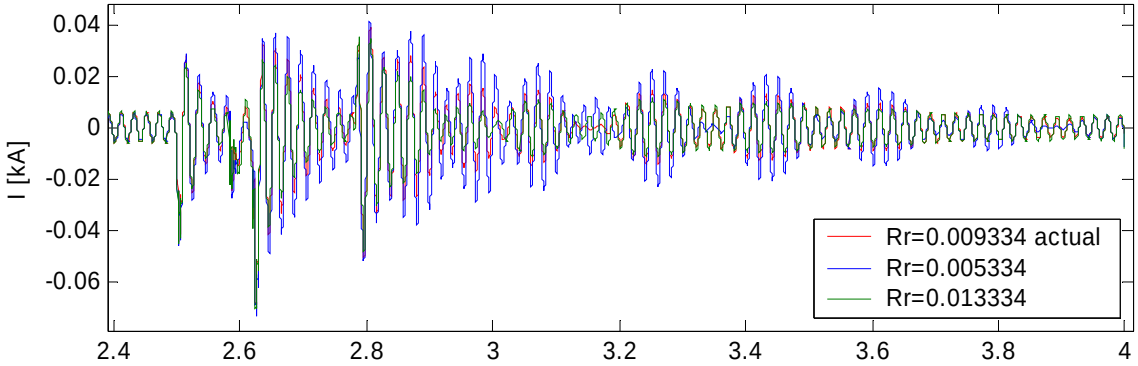

Figure 17. Influence of inaccurate parameter value of rotor resistance in the model to output current.

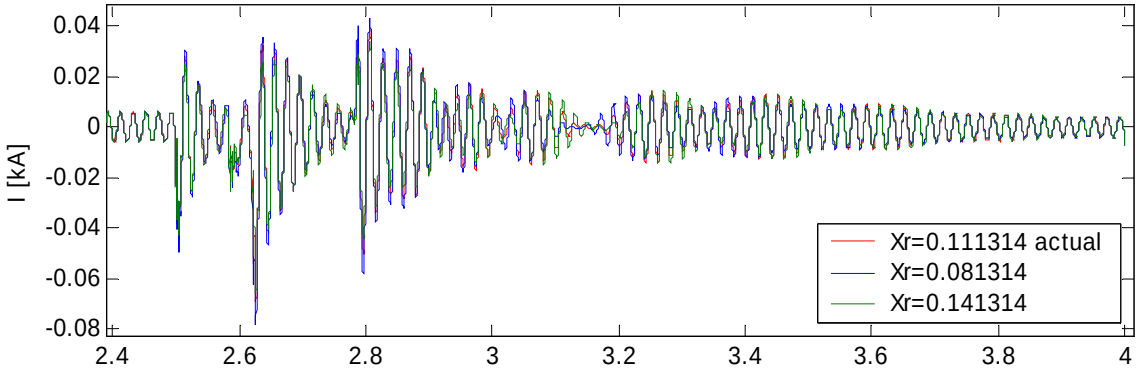

Figure 18. Influence of inaccurate parameter value of rotor reactance in the model to output current.

2.2.4 Implementation

The measured voltage input to simulation in PSCAD/EMTDC is not as simple as it might be for example in Matlab, where is dealt only with equations. In PSCAD/EMTDC, the "electricity is flowing" so to speak. The voltages are generated by voltage source components, and such a component is needed in every PSCAD/EMTDC model consisting of electrical components in order to get the system energized. In addition the PSCAD/EMTDC model is

such that the voltages and currents entering and leaving the components (e.g. voltage source, generator) are electrical quantities, and no data values can be added to these electrical quantities, nor they (e.g. voltage) can be a series of data.

There are some 3-phase voltage sources in PSCAD/EMTDC standard library in which an external voltage source control is possible. This control value, however, is a single value indicating the three-phase voltage magnitude, and thus voltages of the three individual phases are not possible to be inputted accurately through these voltage sources.

There is a component *Single-Phase Voltage Source Model 2* in which also the control voltage input is available, and in addition the voltage source can be used as an AC and DC source. This voltage source can be used in inputting measured voltages in simulation when setting the "Source Impedance" to ideal, selecting the DC "Source Type" and "External" "Input Method". This way the user can use the instantaneous voltage data series of AC as DC voltage, and is able to input exactly the measured voltage waveforms at each phase. The voltage data is imported from a text-file via *File Read* component. The sampling frequency of the data in the user specified data file can be chosen in *File Read* component.

There might not be enough data (several seconds) measured before the fault so the PSCAD/EMTDC simulation system would have time to reach stable operation condition before the fault injection, as the simulation system starts from zero. On the other hand, there is no point measuring several seconds of stable operation, nor usually there is not too long a period of pre-fault data in the dataset.

The simulation system may be started with a separate dataset of ideal and symmetric sinusoidal data to be inputted before the measured dataset. This sinusoidal, ideal data may be just one period long, and the data may be rewound and replayed a suitable number of times in order to get the system in steady operating state. After this, the measured voltage data with fault may be inputted. The two datasets need to be synchronized at the moment of transition from one dataset to another.

2.3 Validation cases

The International Energy Agency (IEA) Wind R&D working group, Annex XXI, has been a recently operating forum under task "Dynamic models of wind farms for power system studies". The Annex XXI, consisting of number of experts in the field of wind power modeling from several countries, has given out recommendations on wind turbine/farm model validation. In [8] the Annex XXI suggested the first set of recommendations, where there is stated that a voltage time series should be used as input, and time series plot of active power, reactive power and voltage at wind turbine terminals ought to be the observed outputs.

The measurement data available for wind turbine model validation is not very much or extensively available. The data is usually owned by different institutions or companies, and it is not distributed freely. The measurement data is also from certain wind turbines or farms of certain turbine types and sizes. There is no extensive database where one could get measurement data for model validation purposes of all the turbine types of different sizes and different operating points. The IEA Annex XXI has managed to achieve a very good base of such a database, although in small-scale, for Annex participant use. Usually the measurement data is of random operating stage as the measurement system has recorded the voltage dip and the turbine response due to the fault taking place coincidentally.

If possible, model validation should be done, not only against a single measurement data case, but against measurement cases of different types, i.e. using voltage dip measurements of different duration, and wide range of dip depths. Wind turbine models should be tested for different operating points (production levels) as well. Variable speed wind turbines should be tested for cases when power electronic converters are in operation at all times, i.e. in case of faults causing small voltage dips, or full converter equipped wind turbines for their possible fault ride through capability and DFIGs for crowbar operation, both for passive and especially active crowbar operation if the model should be used for active crowbar operation simulations.

After validating the model against measurements of different voltage dip depths and different turbine/farm operating points, the model operation in different grid environments should be tested. In [15] is suggested to use a universal simple power system model for this purpose.

Wind turbine/farm interaction with grid may vary in different grids. It is equally important to know the model performance in different grid conditions as showing how the model works in the validation grid or proving that the model is good under the conditions in validation case. And besides, as mentioned earlier, there is not always many validation case data available to use, and then this suggested universal grid model tests should be performed.

When using a universal simplified grid model, it is easy to test the model in different grids, as well as different model performances can be easily compared to each other. However, the models should be put in order of superiority only when simulation results are compared against measurements. In [15] is suggested to test the models on the universal test grid against four characteristics;

i) strong grid/weak grid
ii) full wind turbine power/ low wind turbine power
iii) full grid load/low grid load
iv) high X/R ratio/low X/R ratio.

When testing for all combinations of the four categories, there will be as many as 16 cases.

In addition, typical simulation studies listed in [15] were

a) remote fault
b) close fault to connection point of the wind energy unit
c) line or other plant tripping
d) voltage disturbance and oscillation
e) frequency disturbance (islanding)
f) system power oscillation.

Using these different study cases with earlier listed operating characteristics, makes a very large number of possible combinations of simulation cases. Not all the cases need necessarily be tested, but maybe some carefully selected ones. The cases can be chosen e.g. by experience of which cases would be the most important, and the set of cased gives a good selection of simulations in different operating conditions and interaction between the wind turbine/farm and the grid.

3 Fixed speed wind turbine models

3.1 Joint PSCAD/EMTDC and ADAMS model of fixed speed induction generator wind turbine

VTT has a detailed mechanical aerodynamical model of Bonus 600 kW fixed speed wind turbine in ADAMS program. It was therefore not a very extensive effort to conduct an electrical study of fixed speed wind turbine with detailed mechanical aerodynamical model. The purpose was to study how much the detailed model adds value to power system study simulations instead of using a simplified model.

Three commercial programs, ADAMS, PSCAD/EMTDC and Simulink were first linked together to be used for continuous and simultaneous simulation of a wind turbine in a power system [16]. A multi-body dynamics code ADAMS is used for modeling the turbine dynamics, whereas the electrical components of the turbine as well as the grid are modeled in PSCAD/EMTDC. Matlab/Simulink is used to combine the simulations of the two programs.

The dynamic model of the wind turbine is created using a graphical modeling program ADAMS from MSC Software Corporation. ADAMS is a commercial general-purpose multi-body dynamics code. Wind turbine design is assisted with a special NREL produced package ADAMS/WT [17]. ADAMS/WT has been replaced nowadays by FAST, which is a medium-complexity code for aero-elastic analysis of wind turbines developed by NREL. ADAMS is not available for purchase any more.

ADAMS models are usually constructed of flexible main components such as blades, tower and drive train. Typically a model consists of a few hundred degrees of freedom. The modeled wind turbine is a Bonus 600 kW Mark IV with arctic equipment (e.g. blade heating). It is a stall regulated two-speed wind turbine, but only the higher rotation speed has been used in simulations. The model consists of three flexible blades, low speed shaft, gearbox, high-speed shaft, generator, flexible tower and nacelle. The blades are divided into ten parts and tower into nine parts. The parts are connected to each other with flexible connections. Because every part has three translational and three rotational degrees of freedom the whole model has about 250 degrees of freedom. Every blade part has two aerodynamic points where the aerodynamical forces are calculated. The drive train model consists of a flexible main shaft, high speed shaft and gearbox. In this turbine model the gearbox contains a planetary stage and two helical stages.

The effect of the wind on the blades is added into ADAMS simulation with Aerodyn from NREL [18]. Aerodyn runs as a separate program, which takes blade angles as input from ADAMS and sends calculated output forces back. Aerodyn uses a three-dimensional wind field to calculate the forces created by the wind and the blade profile. The Aerodyn code has been modified by VTT and a new code can use different lift and drag coefficient tables for every blade and the tables can be changed during simulation. The code can now be used to simulate aerodynamical imbalance of an iced rotor, and incidents like ice accretion during wind turbine operation can be studied. There are also improvements for tower shadow model. The original Aerodyn v12.57 code does not calculate the wind speed deficit caused by the tower for upwind turbines.

The described turbine model is a two-speed, passive stall wind turbine with squirrel cage induction generator. The control system is not modeled for this turbine. In this joint modeling environment it is most convenient to model control systems for blade pitching, yawing, vibration control, generator control and other systems to the dynamic wind turbine model etc. in Matlab/Simulink. Simulink works also as the platform for connecting the electromagnetic simulation (PSCAD) to the mechanical simulation (ADAMS).

The electrical parts of the wind turbine, i.e. generator, capacitor banks and transformer, and the electrical network, as well as network faults and system disturbances are modeled in PSCAD/EMTDC. The PSCAD/EMTDC model consists of a standard induction generator model with parameters set to respond the high speed mode of the generator used in the Bonus 600 wind turbine. The capacitor banks and the wind turbine transformer are modeled with standard components with their corresponding parameter values as well.

The two simulation tools, ADAMS and PSCAD/EMTDC, are communicating during the simulation via Matlab/Simulink. Both ADAMS and PSCAD have their own Simulink interface. ADAMS uses an additional product called ADAMS/Controls from MSC Software. PSCAD/EMTDC standard interface to Simulink does not enable continuous and simultaneous simulation with ADAMS. Therefore new interface modules were developed at VTT for the communication [19]. The principle of ADAMS-PSCAD simulation is quite simple. Rotor rotation speed information of the generator is transferred from ADAMS to PSCAD. PSCAD calculates electrical counter torque and returns the value to ADAMS. The programs exchange information with a time step of 5 ms. ADAMS runs with variable time step, but it is always smaller than or equal to the data exchange time step. PSCAD/EMTDC uses a smaller time step of 50 μs. Data exchange between the simulation programs can be seen in Figure 19. Joint simulation with ADAMS, PSCAD/EMTDC and Matlab/Simulink has successfully been conducted by VTT [16], [20].

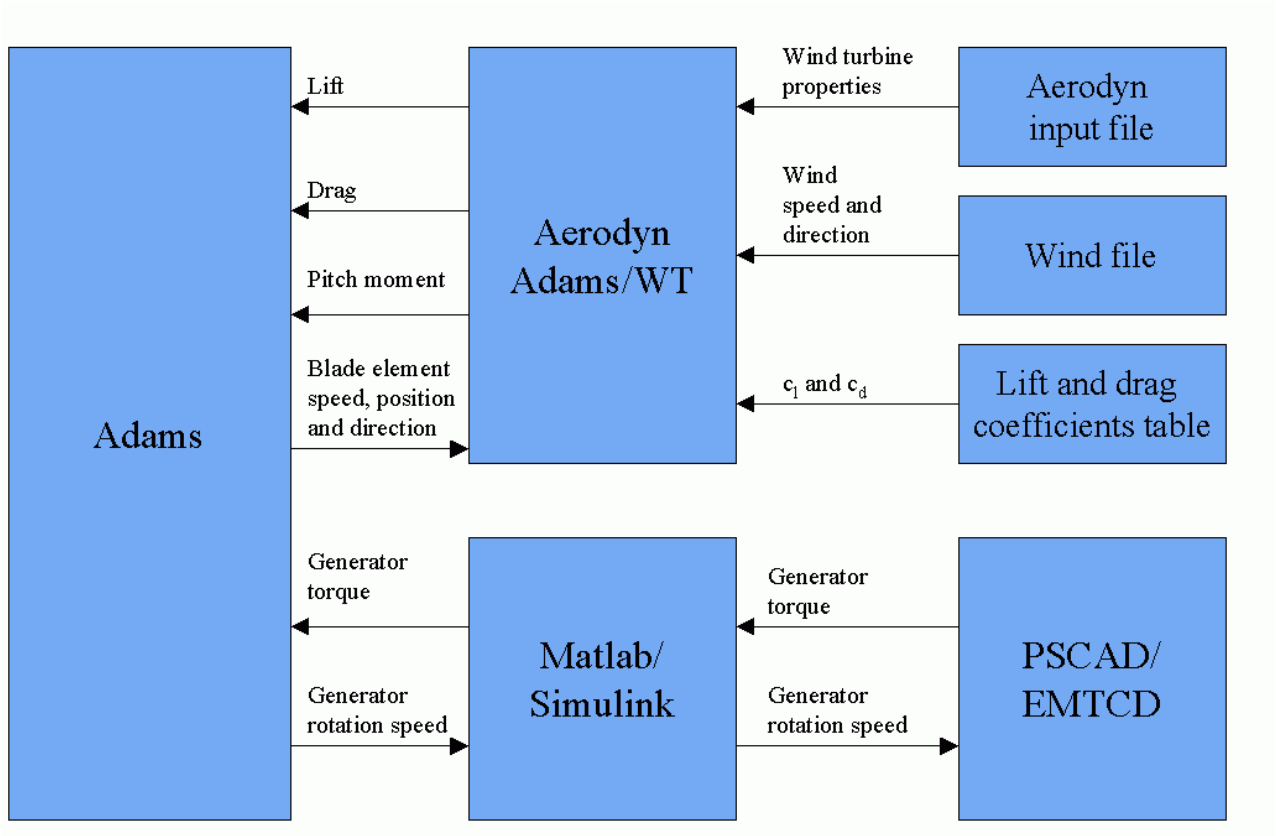

Figure 19. Data exchange between simulation programs.

In Figure 20 and Figure 21 are shown active and reactive power simulation results of PSCAD-ADAMS-simulation, and the corresponding simulation with only simple 2-mass model of the turbine in PSCAD. The fault simulated in both cases was identical (three phase short-circuit with constant fault resistance) as well as the electrical components in PSCAD-models. There is also plotted measured active and reactive power in the figures for comparison. The initial operating point of the turbine in case of the measurement is different than in the simulations ($P \approx 50$ kW vs. $P \approx 150$ kW), as well as is the reactive power consumption of the turbine ($Q \approx 60$ kVAr vs. $Q \approx 20$ kVAr). In the simulations the full compensation of reactive power is in use, but in case of the measurement, one of the steps in three-step capacitor bank was out of operation. The capacitors are disconnected during the fault in the measurement, whereas they were kept connected in the simulations. Also the fault in the measurement is different from the one in the simulations. The actual faults are rarely of constant fault resistance, and it is not unusual that they vary in type as well. In the case of the fault in the measurement, the fault was a three-stage fault consisting of a two-phase short-circuit, a two-phase-to-ground fault and a three-phase short-circuit. The fault duration in the simulations and of the measured case is slightly different as well.

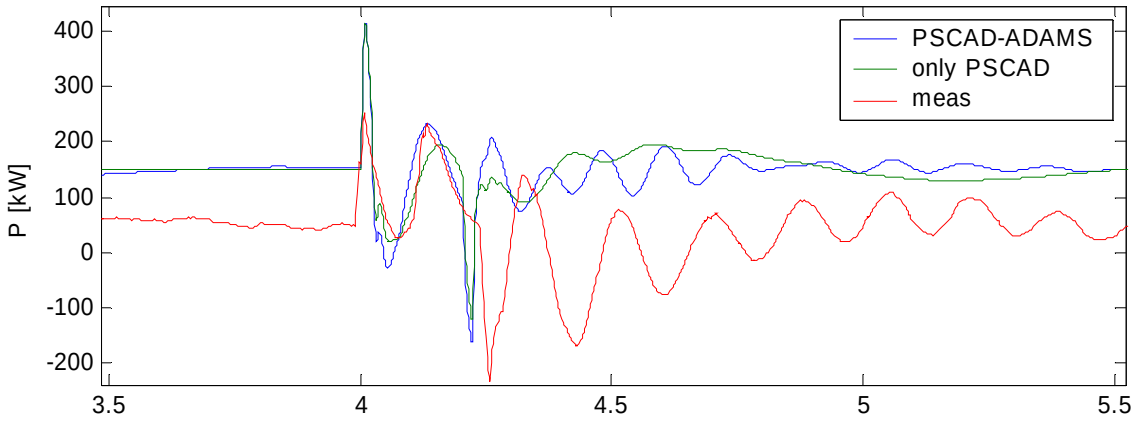

Figure 20. Active power response to voltage dip. Simulation results of PSCAD-ADAMS simulation and PSCAD simulation with simplified turbine model, as well as measurement taken from the turbine being modeled.

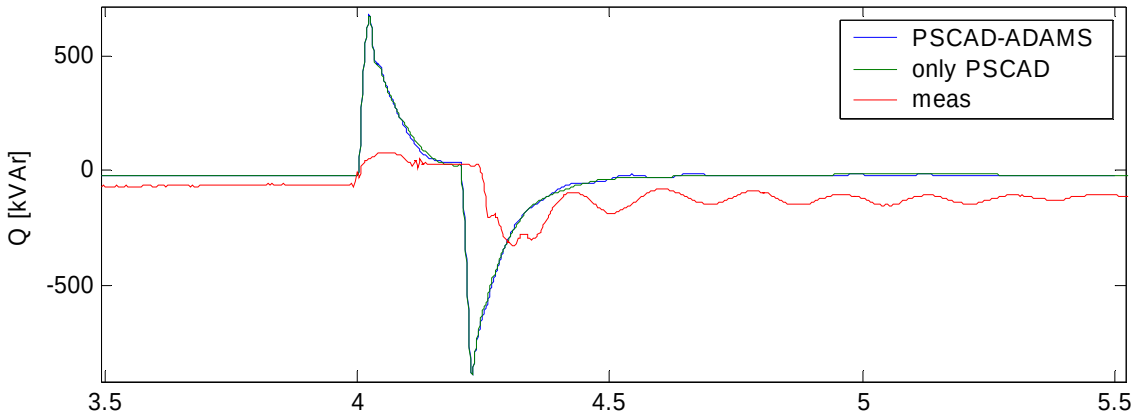

Figure 21. Reactive power response to voltage dip. Simulation results of PSCAD-ADAMS simulation and PSCAD simulation with simplified turbine model, as well as measurement taken from the turbine being modeled.

The most post-fault oscillations are seen in the measurement, and some oscillations in the PSCAD-ADAMS-model simulation. In reactive power, almost no difference is seen between the simulations with detailed model in ADAMS and simple 2-mass model in PSCAD. The PSCAD-ADAMS model does not really seem to reveal very significant issues in active power response either, except some oscillations, compared to the very much simplified model with turbine modeled as a 2-mass model in only PSCAD. One of the reasons why the oscillations in active power are smaller in amplitude in the simulations, is that the back-ground grid in the simulations was too strong (Z_k about 10 times too large), which has influence on the oscillations as is shown in chapter 3.2.1.

It ought to be remembered that the ADAMS-turbine model is very much heavier to run in power system simulations than the turbine 2-mass model in PSCAD. It also takes rather much time, effort and information gathering of the turbine to be modeled in detail in ADAMS in case a new model should be needed. It should be kept in mind that the more components and parameters the model includes, the more there are possible error sources as well. This is further discussed in section 3.2.3.

The greatest use of joint simulation seems to be when one wants to analyze the impact of grid disturbances and faults on the wind turbine and its components. Joint simulation is also useful for developing control and control strategies for wind turbines in case of grid disturbances and for example for fault-ride-through capability. A third practical use is for development of simplified mechanical and aerodynamic models of wind turbine models for power system studies. A verified joint model can be used for comparison when only little measured data is available. In order to model the mechanical part of a wind turbine in ADAMS a large amount of data describing individual components of the turbine is needed. Model setup in ADAMS is time consuming and not usually worth to do only for power system studies.

Simulations and comparisons by VTT verify that power system studies can be accurate enough when conducted solely with PSCAD/EMTDC. User defined models (or even standard models) of wind turbine mechanics and aerodynamics are then used instead of the detailed ADAMS wind turbine model. Joint simulation is, however, beneficial when modeling the impact of complex mechanical events on the power system; for example how a mechanical failure or ice accretion on the blades affects the power quality.

Simulink has a power system blockset named SimPowerSystems that can be purchased separately and probably be used instead of PSCAD/EMTDC together with ADAMS. This has, however, not been tested.

3.2 Fixed speed wind turbine PSCAD/EMTDC-model

The fixed speed wind turbine model for PSCAD/EMTDC described here is built within this project. The model consists of the squirrel cage induction machine, multi-mass to represent the inertias and flexibility of the masses, the wind turbine transformer, and the capacitor bank of the wind turbine. In the model shown in Figure 22 both speed modes of two-speed machine are modeled as separate generators and multi-masses. Also aerodynamics can be modeled with user-built component or in turbine start-up simulations user-built soft-starter model can be used.

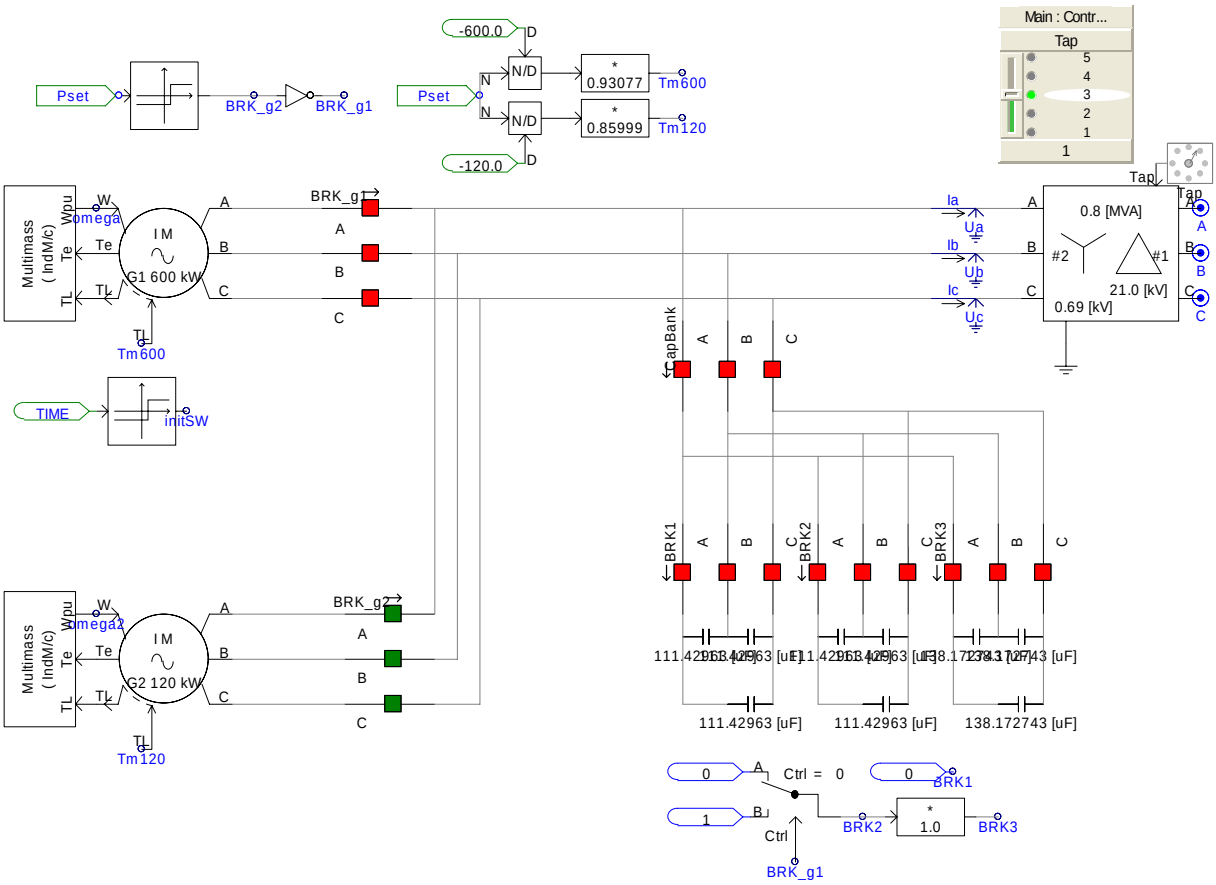

Figure 22. Bonus 600/120kW fixed speed wind turbine model for PSCAD/EMTDC.

3.2.1 Grid

The fixed speed wind turbine setup shown in Figure 22 is of general type. The model can be used as a page module in a grid model in PSCAD/EMTDC. Essential in modeling a certain size of a wind turbine or even a specific wind turbine, parameter selection is of significance.

The grid to which the wind turbine is connected, has influence on the wind turbine behavior. It is important to distinguish between the phenomena of the wind turbine (and the model of one) and the connection grid.

In Figure 23 is shown the influence of the stiffness of the grid to the wind turbine model response to a fault. In the simulations of Figure 23 a three phase fault is applied at the wind turbine terminals at high voltage level side of the wind turbine step-up transformer. In the figure is seen that the post-fault oscillation frequency and amplitude may vary slightly due to the magnitude of the short circuit impedance at the wind turbine connection point, but the influence is rather small.

A change in impedance angle makes no significance. Thus, the approximate magnitude of short circuit impedance at the connection point should be known, accuracy of which can be assessed based on Figure 23. When the impedance is in the correct order of magnitude, model validation simulations should not be very much disturbed (in case using a voltage source instead of measured voltage as input voltage) by the connection grid modeling.

Also in defining the mechanical parameters of the wind turbine based on measurements taken of a turbine, possible tuning of the model can be done safely as far as the approximate magnitude of short circuit impedance at the connection point is known with sufficient accuracy.

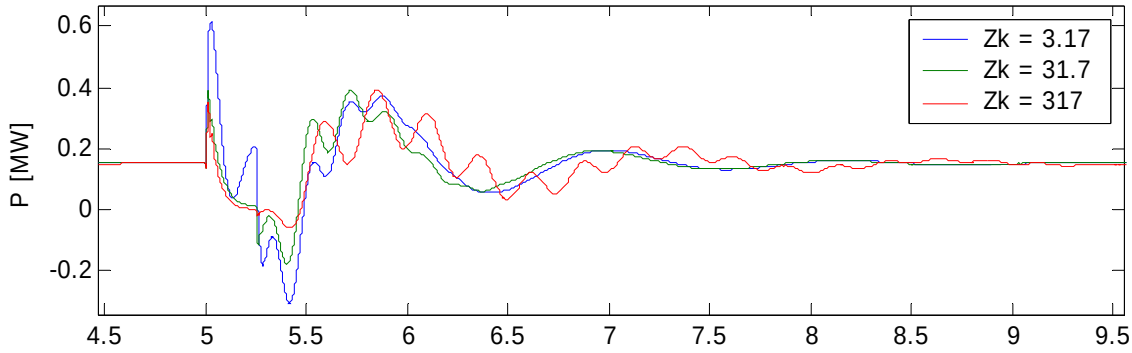

Figure 23. Comparison of the influence of the connection grid stiffness, i.e. the short circuit impedance at the wind turbine (model) grid connection point. The actual (known/approximated) impedance value is compared to tenfold and one tenth of the actual value in case of a severe fault.

The smaller the short circuit impedance is, the larger the short circuit power at the point, and thus the stronger the grid is. A stronger grid produces more stiff voltage, and in case of a fault at connection point, the stronger the grid is seen at this point, the less the fault affects the voltage. Therefore the current of the wind turbine or farm also is less affected than in case the connection grid was weaker.

Magnitude of fault resistance (in test simulations at wind turbine terminals on high voltage side of the step up transformer) has no influence on the frequency components of a two mass system.

3.2.2 Generator

The induction generator detailed model typically represents the dynamics of the machine stator and the rotor, as well as the deep-bar and saturation effects [12]. The PSCAD/EMTDC rotating machine models are modeled in state variable form using generalized machine theory [21]. The PSCAD/EMTDC *Squirrel Cage Induction Machine*-component is a fifth order model. The squirrel cage induction machine standard library component is modeled as a two cage machine to account for the deep bar effect of the rotor cage. The *Squirrel Cage Induction Machine*-component two cage parameter inputs can be used for inputting the parameters as of single cage machine by setting *Second Cage Resistance* and *Second Cage Unsaturated Reactance* very large values (e.g. 100 pu). Parameter *Rotor Unsaturated Mutual Reactance* is then used for inputting the single cage rotor reactance value. In usual fifth-order model used also in fixed speed wind turbine induction machine modeling omits for example the skin effect [22]. Skin effect is not even significant but maybe on large slip operating conditions. Thus, the single cage machine parameters may well be used in the generator component.

The fifth-order model stator and rotor equations are described in vector notation as

$$\underline{u}_s = \underline{i}_s R_s + j\omega_s \underline{\psi}_s + \frac{d\underline{\psi}_s}{dt}, \qquad (3.1)$$

$$0 = \underline{i}_r R_r + j(\omega_s - \omega_r)\underline{\psi}_r + \frac{d\underline{\psi}_r}{dt}, \tag{3.2}$$

where $\underline{\psi}$, $\underline{i}$ and $\underline{u}$ are the vectors of flux, current and voltage, R resistance and ω rotation speed [12]. Subscript s refers to the stator and r to the rotor. The model is reduced to third order model by removing the stator flux transients, and the model is capable of being used for symmetrical condition simulations of fundamental frequency [12].

3.2.3 Multi-mass

In [9] it is stated that a two-mass representation of a wind turbine is sufficient, and requisite. Especially in case of a fixed speed wind turbines, which are equipped with gearboxes thus causing very different rotating speed of turbine and generator, there is so-called soft shaft between the low and high speed inertias. The gearbox is widely used as the interface of the two masses in two-mass models, [9], [23] etc. The two-mass system is defined by equations [9]

$$\begin{cases} 2H_T \dfrac{d\omega_T}{dt} = T_T - K_S\theta_S - D_T\omega_T \\ 2H_G \dfrac{d\omega_G}{dt} = K_S\theta_S - T_E - D_G\omega_G, \\ \dfrac{d\theta_S}{dt} = \omega_0(\omega_T - \omega_G) \end{cases} \tag{3.3}$$

where ω_0 is the fundamental electric system angular speed, H is inertia, T torque, K spring constant (stiffness), D damping coefficient, θ torsional twist of the shaft, ω the rotation speed, and subscripts T refers to turbine (i.e. low speed parts of the turbine and shaft system), G generator (i.e. the high speed parts of the generator and shaft system), and S to the shaft.

The needed parameters, high speed lumped mass inertia, low speed lumped inertia and the spring constant are not given wind turbine parameters in turbine brochures and by the manufacturers.

In PSCAD/EMTDC the two mass representation in implemented by using the *Multi-Mass*-component (named *Torsional Shaft Model*), where the parameters are given as transformed to the high speed side. If the moments of inertia J of the components are known, the inertia for the lumped masses can be calculated as

$$H_G = \frac{\frac{1}{2}J\left(\frac{\omega_0}{p}\right)^2}{S_n}, \tag{3.4}$$

$$H_T = \frac{\frac{1}{2}J\left(\frac{\omega_0}{p \cdot GR}\right)^2}{S_n}, \tag{3.5}$$

where p is the number of pole pairs in the generator, GR the gear ratio and S_n the nominal power of the generator.

When the oscillating frequency of a turbine is known (from measurements), the spring constant (shaft stiffness) can be calculated with equation [9]

$$K_S = \frac{8\pi^2 f_T^2}{\omega_0} \cdot \frac{H_T H_G}{H_T + H_G}, \quad (3.6)$$

where f_T is the shaft torsional mode, i.e. the natural frequency of electrical oscillations e.g. after a grid component tripping experiment.

Example case here is the Olos wind turbine, where from measurements have been taken. The 2-mass representation inertias of the wind turbine were defined to be Hg = 0.5768 s and Ht = 3.91 s. Of the measured phase voltages and currents in case of a disturbance in the grid, active power was calculated applying the positive sequence method described in 2.1.2. In active power calculated of 500 Hz measurement data of 2.5 second period, two major oscillating frequencies were found; 5.65 Hz and 0.8 Hz. Also some 9.8 Hz oscillation seems to be involved. The frequency f_T in question in (3.6) in this case is 5.65 Hz oscillation frequency. Equation (3.6) gives K = 4.032 pu/el.rad, which equals to 443.6pu/mech.rad (in which units the spring constant is given in the PSCAD/EMTDC model), as the number of pole pairs in the generator is 2 and gear ratio of the gear-box is 55.

In another study [24] the natural oscillating frequency for this Bonus 600 kW wind turbine type (not for those particular ones at Olos the measurements taken are from) was defined to be 0.98 Hz for the 600 kW mode.

Calculating the spring constant with equation

$$K = \omega^2 J_t = 2\omega^2 H_t$$

gives 197.58 pu/mech.rad for 0.8 Hz and 296.50 pu/mech.rad for 0.98 Hz. It is not totally clear on which frequency the spring constant should be really calculated at. Calculating the spring constant at frequencies 0.8 and 0.98 Hz on (3.6) does not give any reasonable value (8.89 and 13.3 pu/mech.rad respectively). In order the simulations to produce reasonable results, spring constant should be of magnitude of about 300…400 pu/mech.rad.

There are different approaches and equations with which spring constant value is determined, and it has been somewhat confusing which would be the correct method to use, and to what some of the given equations are based on, or if they are even used correctly (e.g. maybe a single mass equation is used for 2-mass system?). [9][8]. With equation

$$K = \frac{2(2\pi f_0)^2 H_t}{2\pi f_n} \quad (3.7)$$

given in [8], K = 2,496pu/el.rad = 274,56pu/mech.rad.

Akhmatov states in [9] that in case the shaft system is sufficiently stiff, ideally $K \rightarrow \infty$, the lumped single mass model can be used. Further more he suggests that experience based value of K = 3.0 pu/el.rad could be used as the boundary value for single lumped mass representation instead of two-mass representation of a wind turbine model. In the Olos wind turbine example case a value greater than the above mentioned 3.0 pu/el.rad was calculated.

In Figure 24 is shown the simulation power outputs of the two-mass model (with K = 443 pu/mech.rad) and single-mass model with lumped inertia of Olos wind turbine. It can be clearly seen that the single mass model gives much worse response than the two-mass model of this particular case.

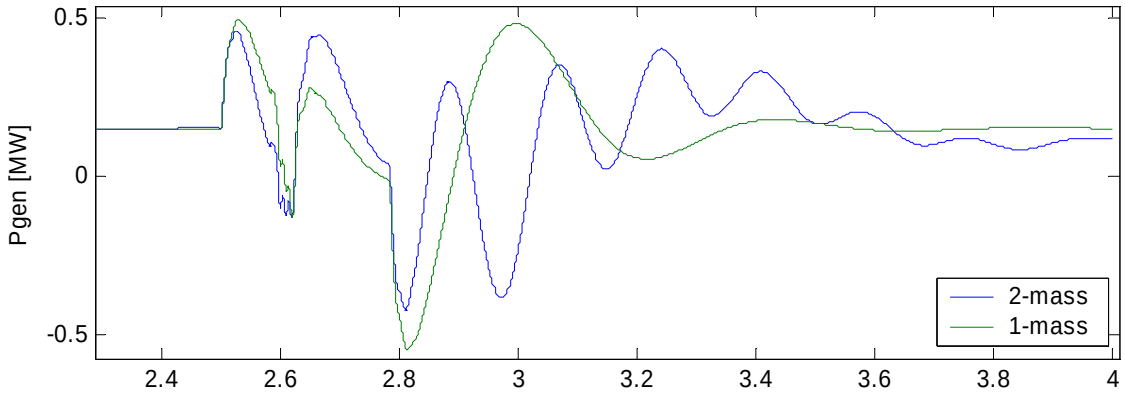

Figure 24. Comparison of two-mass model and single-mass model representation of Olos wind turbne.

The wind turbine mechanical characteristics vary from one turbine type/manufactures/size to another. In [25] is mentioned that typically the torsional resonance frequencies are about 0.5…2 Hz. In that sense also, the above used 0.8 Hz or 0.98 Hz would seem more obvious frequencies to be used for spring constant calculation instead of seemingly too large 5.65 Hz. In the model, K = 300 pu/mech.rad is used due to fact that it seems to be more correct for the simulations. It is not known how in PSCAD/EMTDC the pu-value of spring constant is defined.

The generator inertia used in ADAMS-model described in section 3.1 was mistakenly defined to be 63 kgm^2, when the actual value provided by the generator manufacturer is 16 kgm^2. This was due to guessing the inertia values. Although the actual value of inertia is about fourth of that used in ADAMS, it is purely a mistake, not e.g. a confusion with American software using WR^2 (American system units & equation) instead of GD^2 (SI-system units & equation).

In addition, the high speed shaft (HSS) inertia in ADAMS was defined to be 15 kgm^2. In [12] value of 8 kgm^2 was used for HSS, and it was estimated from the generator inertia value to be half of it by experience. Simulations, however, reveal that the actual HSS inertia must be smaller than 15 kgm^2 but larger than 8 kgm^2.

When using measured voltage as input to simulation, generator and HSS lumped inertia is defined to be 0.5268 s, which corresponds to HSS inertia 12.3 kgm^2. As mentioned earlier in section 3.1, the more parameters in the model, the more there are possible error sources. The incorrect inertia values probably are partly causing the differing simulation results between the combined ADAMS-PSCAD-simulation and only PSCAD-simulation, as well as the measurements shown in section 3.1. The ADAMS-model can be improved also based on results received from the measurements as well as parameter definition based on these PSCAD-simulations.

Definition of the mechanical parameters of the turbine involve first of all finding out the inertia of the generator. The generator inertia is given by the generator manufacture. To the generator inertia also part of the high speed shaft parts should be added in order to come up with high speed lumped mass inertia. The amount of inertia to be added depends on the structure of the turbine and e.g. gearbox, and this information may not be easily available. The turbine inertia may not be an easy task to define, either. There is more discussion on this in connection with DFIG modeling in section 4.2.

Influence of change in high speed lumped mass inertia, low speed lumped mass inertia and in spring constant are shown in Figure 25 – Figure 29. The parameter values are varied in reasonable range (and maybe more) in simulation response to a fault cleared after 250 ms. Active power, in which the oscillation is seen most clearly, is used as the quantity of comparison.

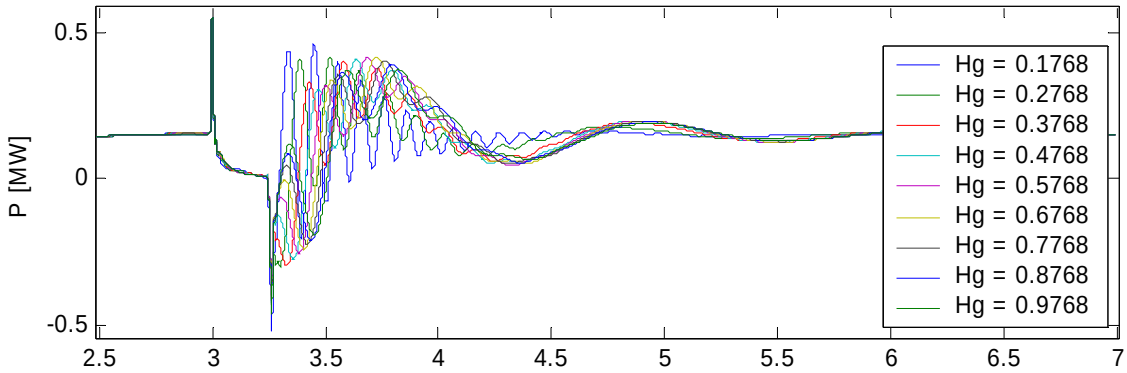

Figure 25. Influence of variation of high speed lumped mass inertia on active power in case of a short circuit of duration of 250 ms starting at 3.0 s.

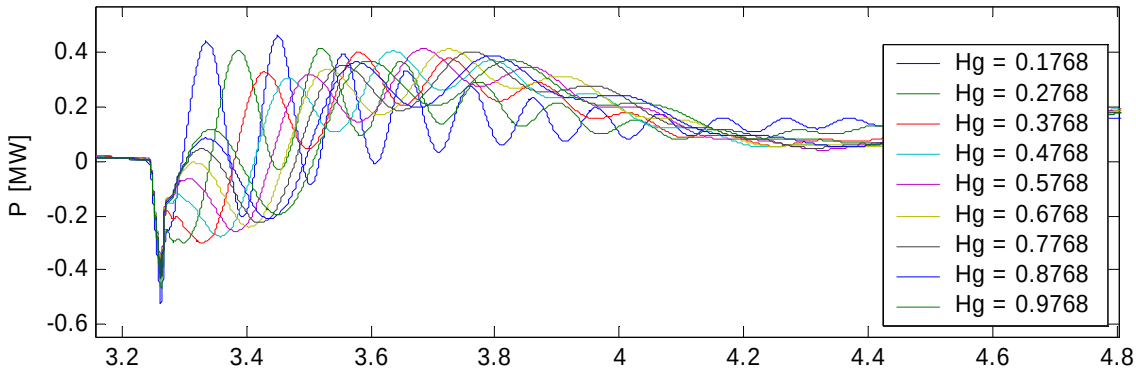

Figure 26. Zoom of previous figure. The first post-fault swing.

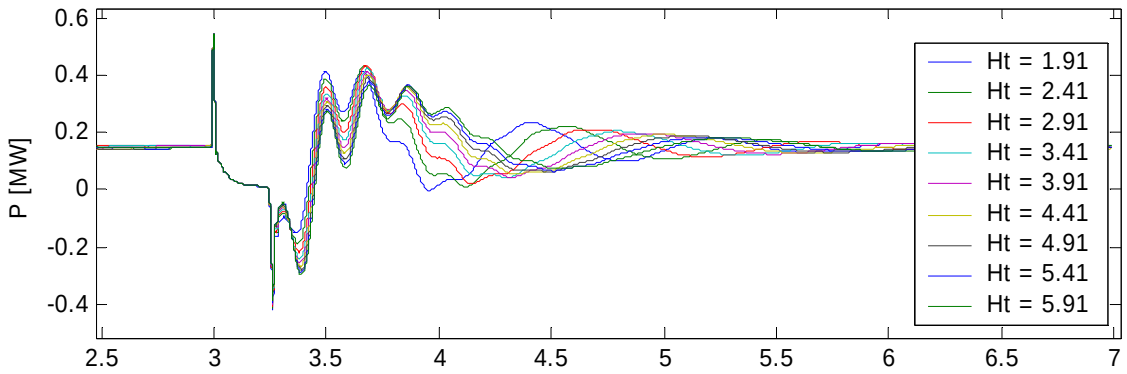

Figure 27. Influence of variation of low speed lumped mass inertia on active power in case of a short circuit of duration of 250 ms starting at 3.0 s.

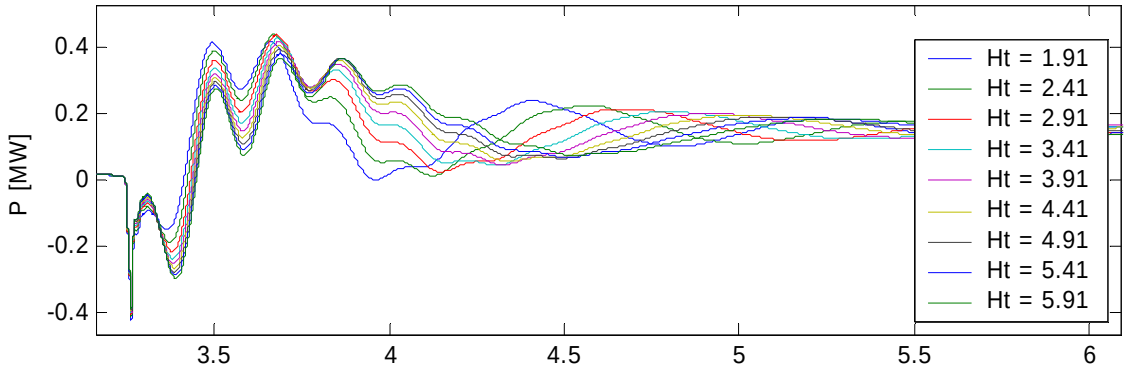

Figure 28. Zoom of previous figure. The first post-fault swings.

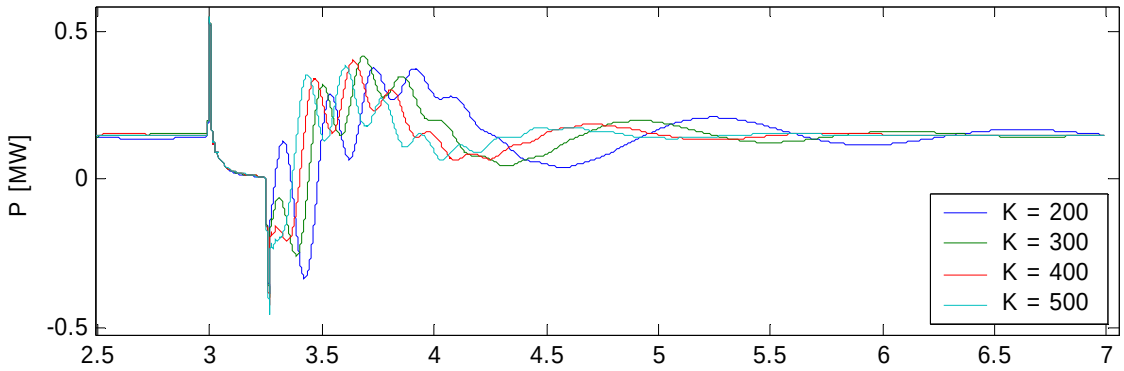

Figure 29. Influence of variation of spring constant on active power in case of a short circuit of duration of 250 ms starting at 3.0 s.

Simulations were also performed by using the measured phase voltages as input to simulations. The model mechanical parameters were checked by simulation result comparison with the measurements. The initial values of mechanical parameters were as earlier approximated and defined analytically, for the 600 kW generator mode to be Hg = 0.5768 s, Ht = 3.91 s, and K = 443 pu/mech.rad, which was calculated by (3.6). As can be concluded of previous figures Figure 25 – Figure 29 where the magnitude of mechanical parameters were changed one by one, the most significant influence on high frequency oscillation frequency is the Hg value. Of Figure 31 can be seen that the two main frequencies existing in both, simulation and measurement, are quite equal to each other.

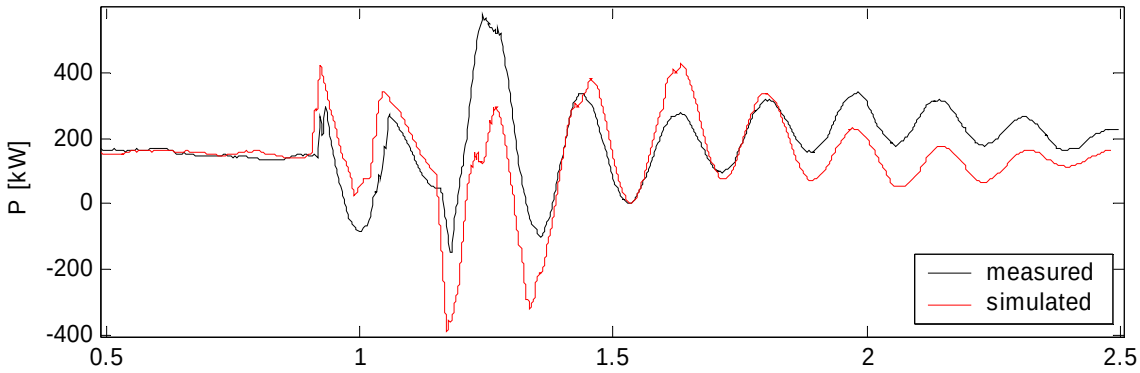

Figure 30. Simulated (with measured voltage as input) active power compared to the measured one. Simulation with Hg = 0.5768 s, Ht = 3.91 s, and K = 443 pu/mech.rad.

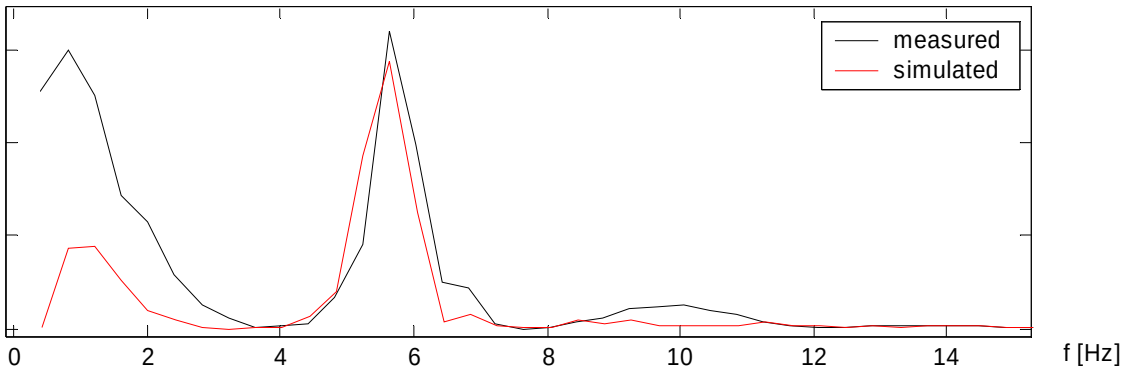

Figure 31. Scaled (simulation scaled by 5 – scaling factor depends on the length of the datasei) frequency spectrum of measured and simulated active power.

As the Hg value was confirmed by the simulation and measurement comparison based on higher frequency oscillation 5.65 Hz, there are Ht and K which could be checked. Equation (3.6) links the parameters and oscillating frequency together, and thus there can be a set of pairs of Ht and K values that could be possible. In figure Figure 32 is shown two extreme Ht, K pairs which could be solutions for equation (3.6), but which values are not likely or even possible considering even large errors possibly done in turbine inertia estimation. The simulation results with these extreme values are such, that it can be stated that when applying equation (3.6) when f_T is known, and when the Hg inertia is fairly accurately defined, small error in Ht estimation are not significant in the model performance. In Figure 33 is plotted the solutions of (3.6) for K = f(Ht) with Hg = 0.5768 s and f_T = 5.65 Hz. At smaller Ht the value of K changes more when increasing Ht, but at larger Ht, K changes rather little when increasing Ht.

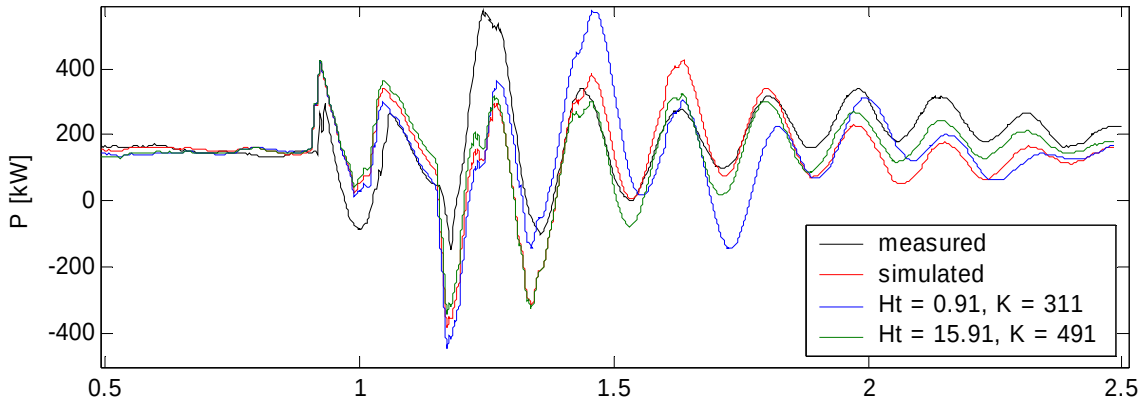

Figure 32. Comparison of extreme Ht, K pair solutions for equation (3.6) compared to the measured and initially defined Ht, K pair simulation solution.

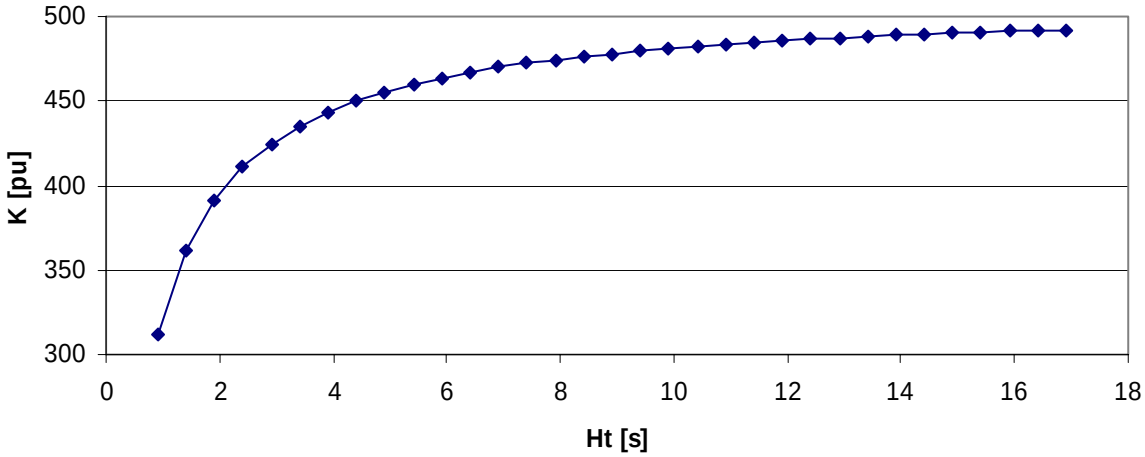

Figure 33. Solutions of equation (3.6) for K = f(Ht) with Hg = 0.5768 s and f_T = 5.65 Hz.

As mentioned earlier the interface between the two masses in two-mass model is usually (almost always in recent studies) in the gearbox. In [26] a study much like the one described in section 3.1 was performed. In the study there was used an ADAMS wind turbine model of 325 degrees of freedom presenting a realistic large scale machine of 1.5 MW turbine. The study case was a three phase short circuit lasting for 100 ms, and the purpose was to analyze the generators shaft response. 4 Hz component was detected in the shaft speed, which magnitude is said to be typical of large scale wind turbines. According to [26] large scale wind turbines usually have first-mode natural mechanical frequency in 0…10 Hz range, and as this range is typical for electromechanical oscillations, it is critical to represent the mechanical oscillations of the turbine as they tend to interact with electromechanical oscillations.

A conclusion, that the model could be represented by a two-mass, single spring-damper system. This assumption is the same as generally used. However, the interface of the masses is done differently in [26]. The mass interface is put on the blades, including only the blade tips on one mass, and all the rest of the blades roots, hub, turbine shaft, gearing, generator shaft, and generator rotor are lumped as the second mass.

3.2.4 Aerodynamics

Aerodynamics of wind turbines are usually represented by Cp-curve in simplified modeling of aerodynamics. In [23] it is stated that the aerodynamics are reported to be quite different from static conditions during stall conditions. Thus the wind turbine control torque based on Cp-curve may not apply, and it fairly represents the turbine torque in wind speeds below stall conditions. Aerodynamic model for fixed speed wind turbine is discussed and PSCAD-model is presented in 3.2.4.2 as well as the wind speed model. Aerodynamics and Cp-curves are further studied later in context of variable speed wind turbines in section 4.5.

3.2.4.1 PSCAD/EMTDC standard library Wind Turbine component

There is a wind turbine component '*Wind Turbine'* in PSCAD/EMTDC standard library, but it does not work properly or as expected. The so called aerodynamic component is based on Cp-equation, but there are some mistakes done in the modeling, as can be seen in Figure 34, where is shown a simulated power curve of the *Wind Turbine* component. The component response to changes in wind speed is immediate, thus the power curve was produced by inputting the simulation time variable as wind speed input to the component. The outputs of the component are turbine torque and power in pu, which are equal to each other in the simulation. The power curve in Figure 34 does not resemble a power curve any wind turbine. The shape may resemble a Cp-curve, but even the scale of the curve is very far from any actual wind turbine power curve or Cp-curve, both in wind speed axis (operation up to about 30 m/s) and torque/power axis (maximum 1.0 pu or slightly above 1.0 p.u. in case of foxed speed wind turbine, and maximum reached usually around at wind speed 13…16 m/s).

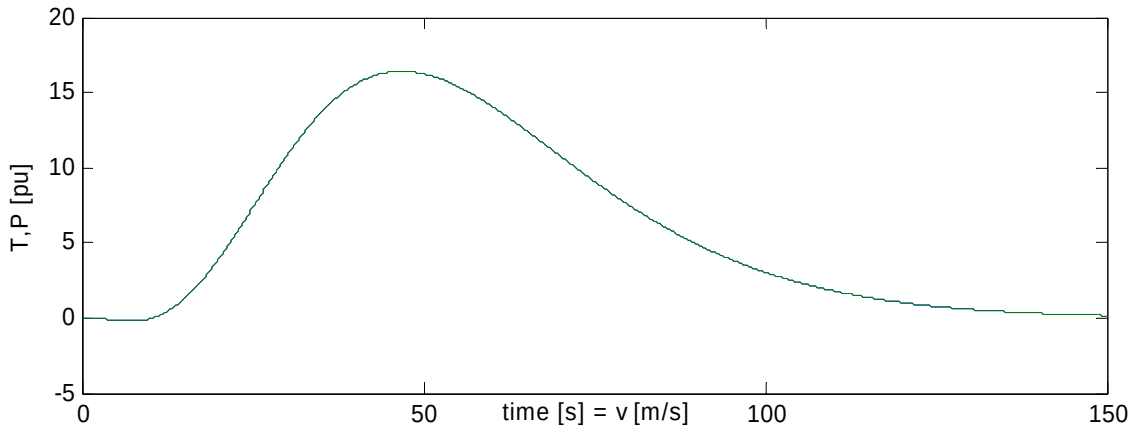

Figure 34. Simulated power curve of the PSCAD Wind Turbine component.

3.2.4.2 User-built wind turbine aerodynamic components for PSCAD/EMTDC

Within this project a couple of PSCAD/EMTDC components were built to represent the aerodynamic behavior of a fixed speed wind turbine. The aerodynamics of the turbine are represented in terms of the Cp-characteristics of the turbine, and thus the *FSWT*-component (Fixed Speed wind Turbine, shown in Figure 35) uses the turbine Cp-characteristics as parameters. The user can input the Cp-curve of the turbine in three ways, i) Cp at fixed wind speed, i.e. at wind speeds 1,2,3…29 m/s, ii) Cp(v_{wind}), 29 data points or iii) Cp(λ), 29 data points. The model calculates internally the Cp(λ) values out of user provided Cp(v_{wind})-values. Default value for data entry points is 0.0, and the data entry points not used, the Cp value must be 0.0, and there must be no 0.0 values in between the first and the last data entry points.

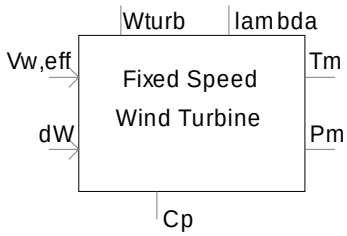

Figure 35. User-built FSWT-component for PSCAD/EMTDC.

There are two more data sheets on which the component parameters are given. On *Generator data*-sheet, are given *System frequency* (default 50.0 Hz), *Generator rated MVA* and *No. of pole pairs in current speed mode*. Usually there are two speed generator modes in fixed speed wind turbines, and the PSCAD-fixed speed wind turbines are most easily constructed by modeling each mode separately (two generator–multi-mass–aerodynamic sets). On *Wind turbine data*-sheet there are *Turbine rated power (info)*, which is only informative parameter and thus not mandatory, *Turbine radius* (this should indeed be the turbine radius for turbine sweep area calculations, not the blade length), *Gear ratio (1:_)*, *Gear box efficiency* (default 1.0), *Air density* (default 1.225 kg/m^3) and *Cp-data* input choice selection. Usually the wind turbine manufacturers provide the parameter information needed for the *FSWT*-component, including the Cp-characteristics, in turbine brochures.

The *FSWT*-component outputs are the turbine speed (Wturb), turbine mechanical power (Pm) and torque (Tm). The torque and power are positive values for production, and in case of a generator, the torque used as input to the generator components, is negative. This needs to be remembered when combining the generator- and *FSWT*-components.

The *FSWT*-component needs the wind speed (Vw,eff) and the difference between the rated speed (generator mechanical rated speed) and the speed of turbine (dW) as inputs. The difference between the rated generator mechanical speed and the turbine speed in generator mechanical speed reference, can be easily obtained from *Multi-Mass*-component on sheet *Internal Output Variable Names – 2*. The wind speed can be given e.g. as a constant, as a data series, or *Wind_Speed*-component can be used.

The *FSWT*-component calculates the turbine speed based on difference from rated speed

$$\omega_{turb} = \frac{\omega_{mech,rat} + d\omega}{GR}, \tag{3.8}$$

where $\omega_{\mathrm{mech,rat}}$ is the generator rotor mechanical rated speed, dω the turbine inertia (in *Multi-Mass*-component) speed difference from rated mechanical speed, and *GR* the gear ratio of the turbine (or in fact the speed factor of generator rotor compared to turbine rotor).

Tip speed ratio is calculated by

$$\lambda = \frac{\omega_{turb} r}{v_{wind}}, \tag{3.9}$$

where r is the turbine rotor radius (notice, the radius may, and usually is, a bit different from the blade length), and v_{wind} the inputted (effective) wind speed.

Based on value of λ, the operating point is detected from the user provided Cp(λ)-table, and Cp-value is interpolated for the above defined tip speed ratio value. In case the operating point (λ) exceeds the λ-range for which there are values given, then Cp will get value of 0.0, which – when Cp is monitored – should give the user a signal of out of range operation.

The Cp-value is used for mechanical power, and further mechanical torque calculation

$$P_m = \frac{0.5\rho A C_p v_{wind}}{S_n}, \tag{3.10}$$

where ρ is the air density and A the turbine sweep area, calculated by the user given rotor radius, and

$$T_m = \frac{P_m}{\omega_{mech,pu}}, \tag{3.11}$$

where $\omega_{\mathrm{mech,pu}}$ is the turbine speed in pu relative to turbine rated speed, and thus the generator rotor speed in pu.

The *Wind_Speed*-component (Wind field to equivalent wind speed, shown in Figure 36) takes into account the variability of the wind field due to wind shear (different wind speed at different altitudes), and rotational sampling – altitude variation due to the rotating blades – in effective wind speed calculation. The *Wind_Speed*-component need as parameters the *Hub height* and *Turbine radius* on *Turbine data*-sheet, and *Turbine siting* selection on *Wind data*-sheet for roughness length value determination. The component inputs are wind speed at hub height (Vw@hbh) and turbine rotating speed (Wturb), which is taken from the *FSWT*-component. The wind speed at hub height can be e.g. a data series or a constant value. The *Wind_Speed*-component output is the effective wind speed, which is used as input to *FSWT*-component.

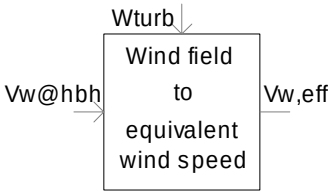

Figure 36. User-built Wind_Speed-*component for PSCAD/EMTDC.*

The component calculated on each time-step of the simulation a now position angle value for each blade

$$\begin{aligned} \alpha_n &= \omega_{turb}\Delta t + \alpha_{n-1} \\ \beta_n &= \alpha + \frac{2\pi}{3} \\ \gamma_n &= \alpha + \frac{2\pi 2}{3} \end{aligned} \tag{3.12}$$

and based on the position angle the height above ground level of the blade tip is calculated by

$$z_\alpha = rh\sin(\alpha), \tag{3.13}$$

where h is the hub height. The wind speed in then calculated at the tips of each blade, although more accurate way would be integration along each blade. The wind speed at tip of the blade is

$$v_\alpha = \frac{\ln(z_\alpha / z_0)}{\ln(h / z_0)} v_h, \tag{3.14}$$

where z_0 is the roughness length of the terrain (user selected) in current wind direction, and v_h the wind speed at hub height. The effective wind speed to the turbine is calculated by these three wind speeds at the tips pf the blades by

$$v_{w,eff} = \sqrt[3]{\frac{v_\alpha^3 + v_\beta^3 + v_\gamma^3}{3}} . \qquad (3.15)$$

The *Wind_Speed* component effective wind speed is fluctuating at triple frequency compared to the turbine speed. This is due to the symmetry of three bladed turbine rotor and its rotation.

Similar test to the one shown in section 3.2.4.1 for PSCAD/EMTDC standard library component, is done here for the used-built components. The simulation time is used as input to *Wind_Speed* component as the wind speed at hub height and the generator speed is kept constant at nominal value (no generator model included). In Figure 37 is shown the output of the component, the effective wind speed which is used as input to the *FSWT*-component. There is some variation of wind speed seen at higher wind speeds even in this figure.

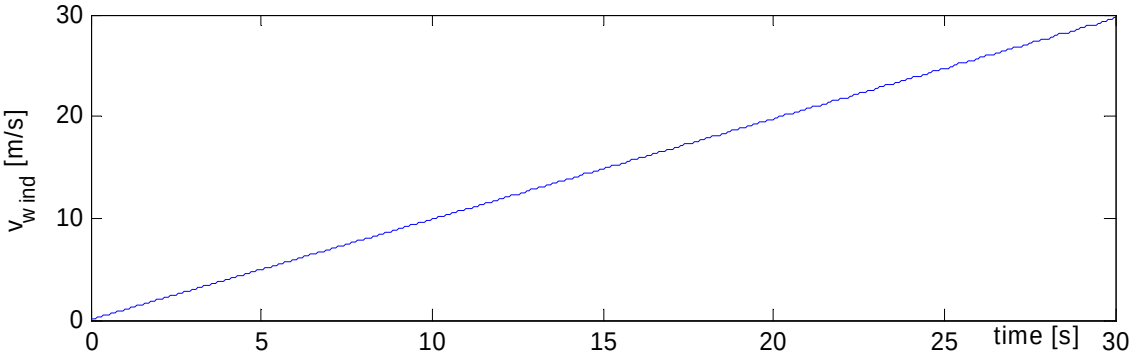

Figure 37. Simulation time used as input, wind speed at hub height, to the Wind_Speed-*component, the component output, effective wind speed, plotted.*

The Cp-curve is given for Bonus 600 kW wind turbine high-speed mode at wind speed range 7…25 m/s. In Figure 38 the Cp-curve, and in Figure 39 the mechanical torque, the outputs of FSWT-component are shown. In this case the Cp(λ)-parameter input option was used.

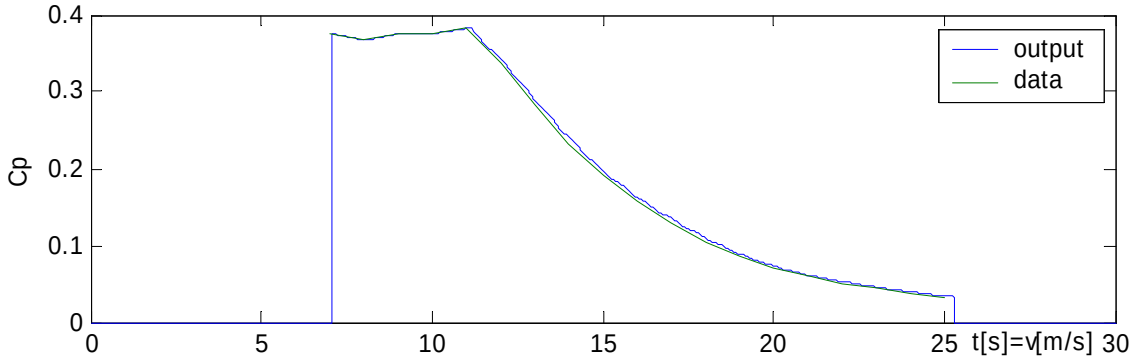

Figure 38. Cp-curve, the output of FSWT-component when the above wind speed is inputted to the component, and the parameter data of the component.

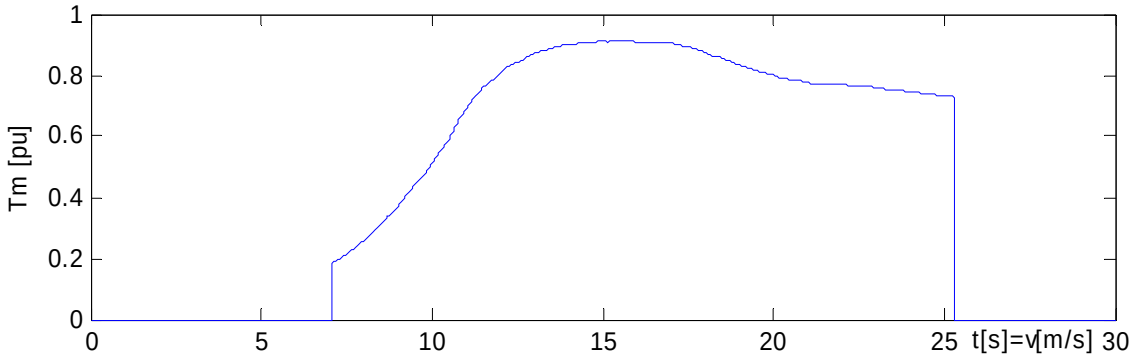

Figure 39. Tm-curve, the output of FSWT-component, when the above wind speed is inputted to the component. Pm-curve is identical in this case as the speed was constant 1.0.

The influence of aerodynamics in case of a grid fault was studied at different operating points. The fault simulations were run with *FSWT*- and *Wind_Speed*-components, as well as without them using constant torque input instead for comparison. The initial operating points at 8...24 m/s wind speed (at hub height), every 2 m/s, were studied. The Cp-curves at different operating points are shown in Figure 40. Mechanical torque of the turbine is shown in Figure 41, the electrical power fed to the grid by the generator in Figure 42 and Figure 43, and the generator speed in Figure 44 and turbine speed in Figure 45. The turbine speed and generator speed (both in pu) are compared in Figure 46.

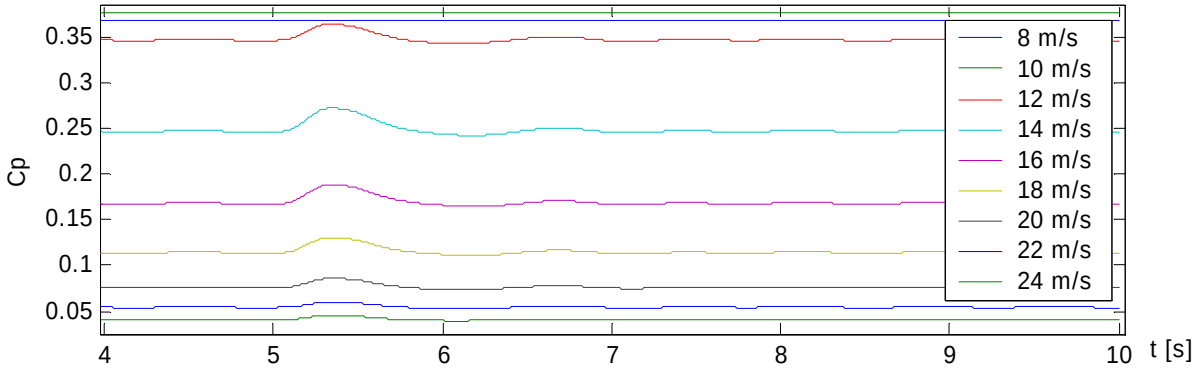

Figure 40. Cp-curves at different initial operating points of the turbine. A grid fault of duration 250 ms takes place at 5 s.

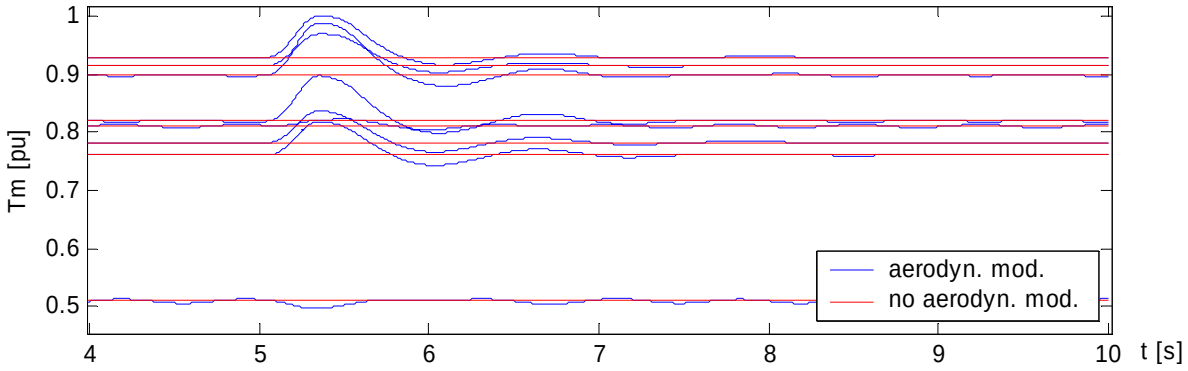

Figure 41. Mechanical torque input to the generator. Initial operating points at wind speeds 10…24 m/s. Comparison of simulations with FSWT- and Wind_Speed-components and constant mechanical torque input to generator.

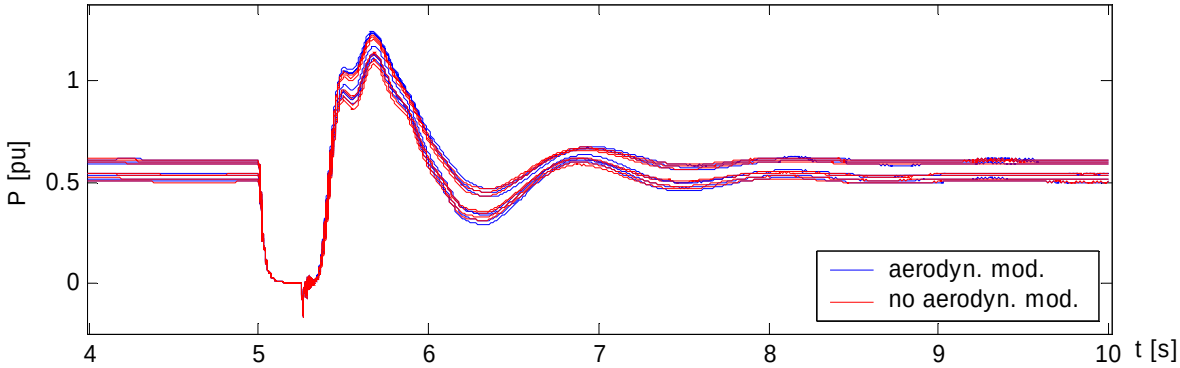

Figure 42. Output electrical power of the turbine generator to the grid. Initial operating points at wind speeds 12…24 m/s. Comparison of simulations with FSWT- and Wind_Speed-components and constant mechanical torque input to generator.

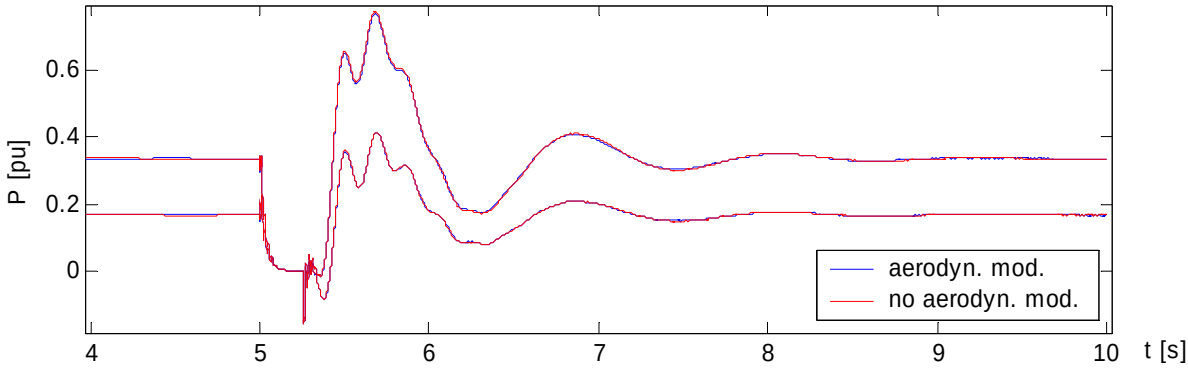

Figure 43. Output electrical power of the turbine generator to the grid. Initial operating points at wind speeds 8 and 10 m/s. Comparison of simulations with FSWT- *and* Wind_Speed-*components and constant mechanical torque input to generator.*

Although there are visible differences in mechanical torque (wind turbine *FSWT*-component output mechanical torque) input to the generator seen in Figure 41, the electrical power during the grid fault of duration 250 ms occurring at 5 s, seems not to differ hardy at all irrespective of if the turbine aerodynamics are being modeled or not, see Figure 42 and Figure 43. It can, thus, be concluded that modeling the aerodynamics of fixed speed wind turbine in dynamic

grid fault studies, is not of importance. In case the turbine behavior (turbine speed, mechanical torque etc.) is intended to study as well, then the aerodynamic model should probably be included. The aerodynamic components can be used and be of significance in simulations of normal operation, flicker analysis, or studies of wind turbine behavior.

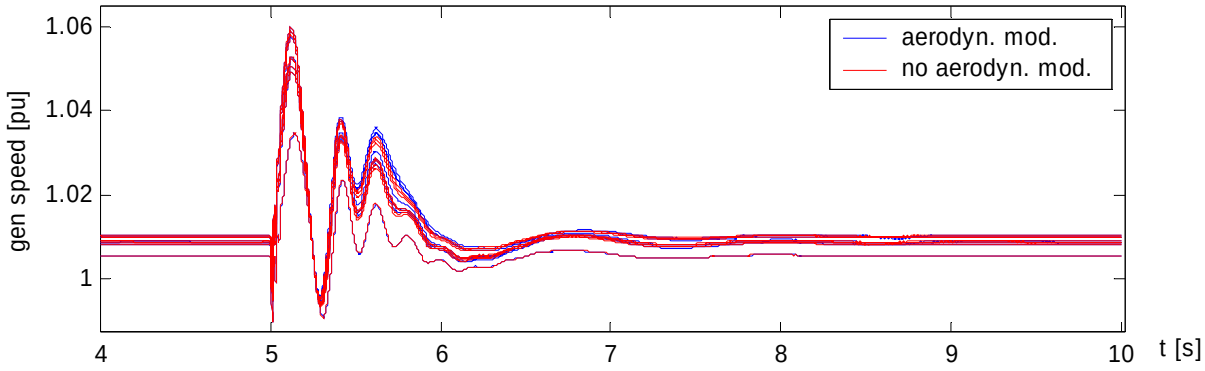

Figure 44. Generator speed. Initial operating points at wind speeds 10…24 m/s. Comparison of simulations with FSWT- *and* Wind_Speed-*components and constant mechanical torque input to generator.*

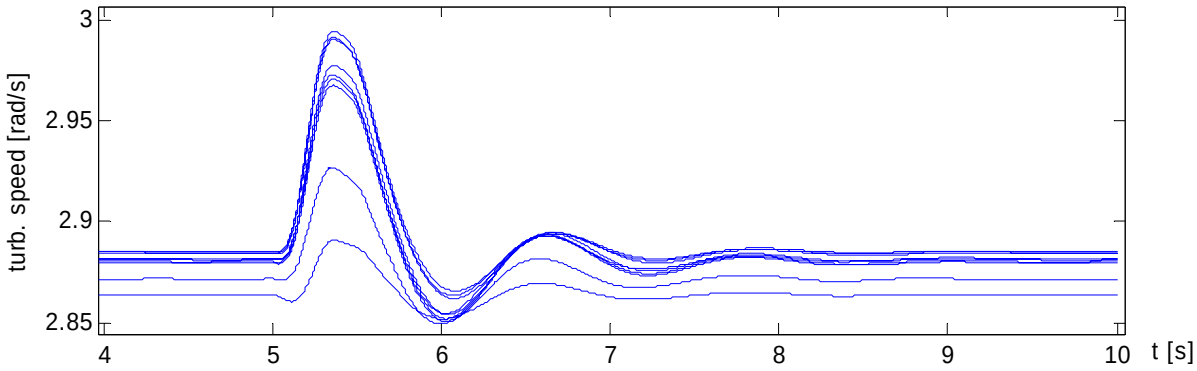

Figure 45. Turbine speed at initial operating points 8…24 m/s.

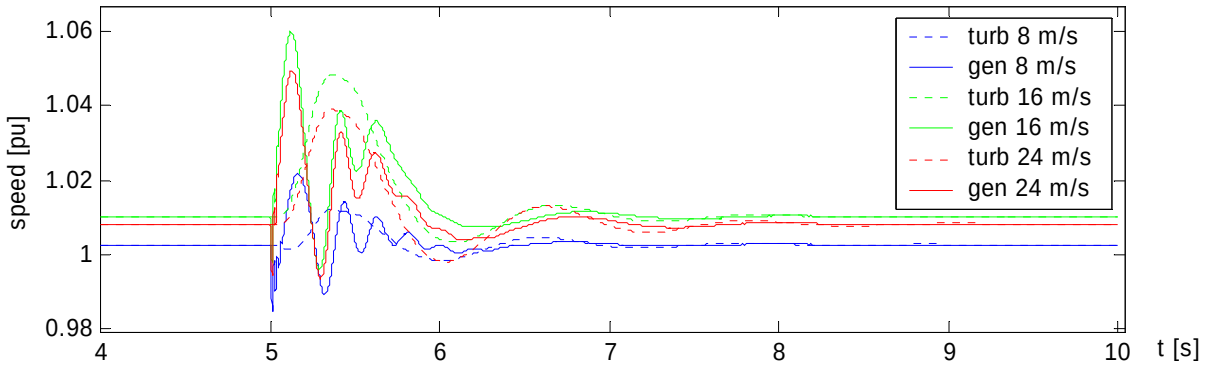

Figure 46. Comparison of generator and turbine speed in pu at wind speeds 8 m/s (lowest wind speed), 16 m/s (highest generator/turbine speed, and thus largest speed deviation) and 24 m/s (highest wind speed).

3.2.5 Transformer

The PSCAD/EMTDC standard library component *3 Phase 2 Winding Transformer* essential input parameters are transformer MVA, system frequency, winding types (delta-wye etc.), lagging/leading of the windings, positive sequence leakage reactance, no load losses, copper losses, and the voltage levels. In *3 Phase 2 Winding Transformer* model the amount of lagging/leading is 30º. In transformer data sheets, usually there are given the short-circuit impedance and resistance in percents and no load losses in watts, or short-circuit impedance in percents, and short-circuit power and no load losses in watts.

3.2.6 Transmission lines

In system simulations the line components are needed. The (transmission) line model component requires the line positive sequence values, as well as the zero sequence values as input. The negative sequence values equal to the positive sequence values for transmission lines because they are static elements. The positive sequence parameters are given for each transmission line type in catalogues/tables, but the zero sequence reactance depends on the mutual location of the phase lines relative to each other, as well as to ground. For example, the zero sequence reactance for a transmission line with three phase conductors arranged in triangle shape in cross-section in such a way that the distance from each conductor to the other two is the same is

$$X^0 = X^1 + 3X_n, \tag{3.16}$$

where

$$X_n = 2\pi f\left(0.2\ln\frac{D_n}{D}\right)\ [\mathrm{m\Omega/km}], \tag{3.17}$$

in which D is the distance between the conductors, and D_n the distance from the line to ground [27].

3.2.7 Soft starter

Induction machine currents are large at starting the machine. In order to reduce the voltage dip the staring large currents would cause, the currents are limited in wind turbine induction machine applications by a soft starter. A user-built soft-starter model as page module for PSCAD/EMTDC is described here. The page module block is shown in Figure 47. The block must be created for the case soft starter is needs to be used. The block has three electrical connections on both sides and it is placed on a three-phase circuit. Two input connections are needed for selected generator nominal power and wind turbine grid connection instant of time. The soft starter model is not validated.

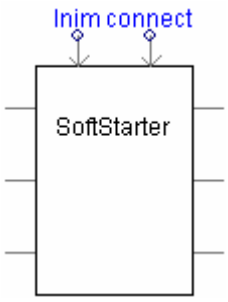

Figure 47. Soft starter page module block with necessary connections, three electrical connections on one side, and three on the other side of the block, and two input data connections for generator (in use) nominal current and wind turbine grid connection instant of time.

3.3 Fixed speed wind turbine model validation

There have been several occations where fixed speed wind turbine model has been validated in this project. These cases include Olos 600 kW wind turbine, Hagesholm 2 MW wind turbine and Alsvik 180 kW wind turbine.

3.3.1 Olos – Bonus 600 /120 kW wind turbine

The Olos wind farm consists of five Bonus 600 kW fixed speed wind turbines. The turbine generators are two-speed squirrel cage induction generators. Each turbine is equipped with capacitor banks of 50+50+62.5 kVAr reactive power supply. Each turbine has its own Dyn-type step-up transformer, and connection cable to the assembly point in the wind farm area. The network which the Olos wind farm is connected to, is transformer star points are isolated from ground. The area of farm location is fairly sparsely populated and there is not much industry connected to the power system nearby, either. Therefore the grid is relatively weak.

The measurement data is taken at one location at the wind farm connection point of the whole wind farm and the single wind turbine located at the connection point (see Figure 48).

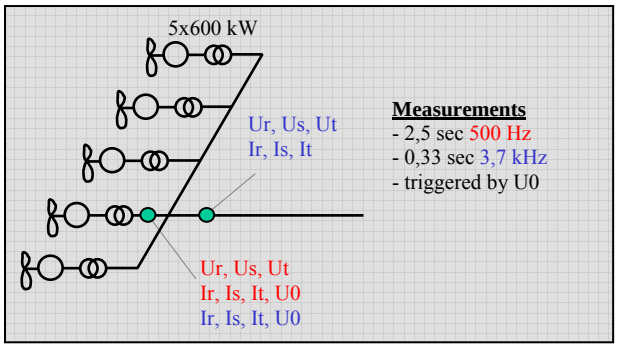

Figure 48. Validation data acquisition lay out from Olos wind farm.

The Olos 600 kW fixed speed wind turbine model implemented in PSCAD/EMTDC consists of *Squirrel Cage Induction Machine*- and *Multi-Mass*- components, capacitor bank, and step-up transformer. The grid is being modeled as a voltage source at wind turbine terminals at high voltage side of the wind turbine step-up transformer. The grid impedance is defined by summing up the calculated short circuit impedance of the grid at the substation, the substation

transformer and the line impedance between the substation and the wind farm. For Olos wind farm this gives Zk = 31.74 /72.64º, which corresponds to short circuit power of 13.9 MVA.

The dataset being used in validation, is restrictedly available in the IEA Annex XXI database. [28] The data is of a changing fault with a 2-phase, 2-phase and ground, and a 3-phase fault components. The particular dataset is described shortly and shown also in [10] and [14].

The measured voltage is used as input to simulations according to what was described in section 2.2.4. Inputting the measured voltage during fault (3.7 kHz measurement of 1250 data points), and comparing the simulated and measured currents of one turbine, there seems to be a slight difference in angles between them at times during fault. Changing the spring constant of the 2-mass turbine model does not really have any affect on the phase shift. Large changes in spring constant value do, however, have slight affect on the current amplitudes, especially on the latter part of the fault. The simulated phase voltages (coming through the voltage source) match quite perfectly to the measured ones, Figure 49.

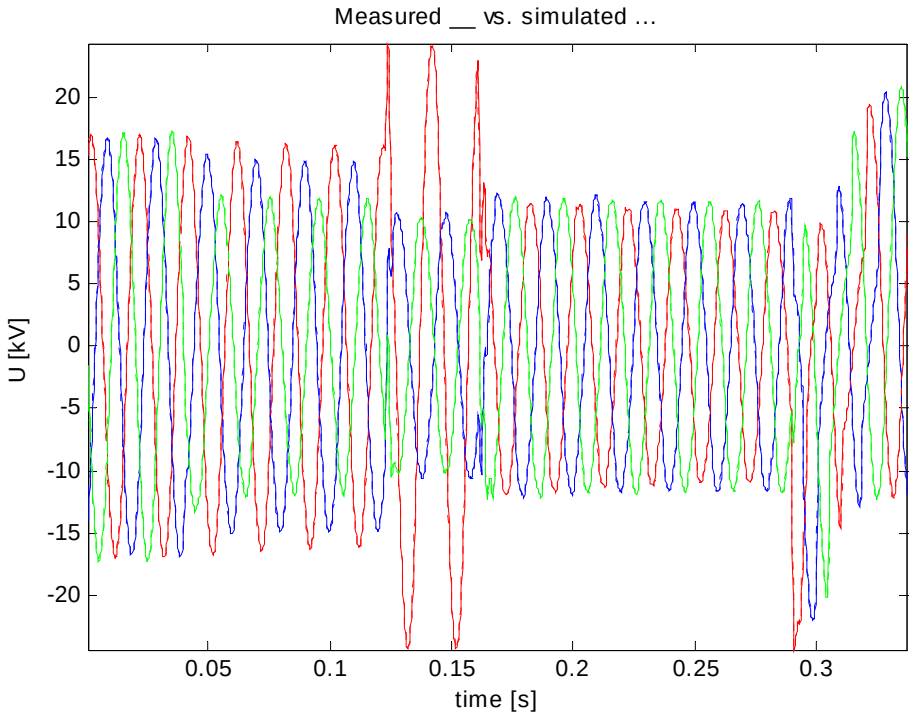

Figure 49. Measured and simulated phase voltages during a fault.

The phase currents of a single turbine simulation are shown in Figure 50. The simulated currents correspond relatively well to the measured ones. The different phases behave differently, and the simulated current of each phase follows the envelope and amplitude of the respective measured current with reasonable accuracy. Besides the slight differences between the simulation and measurement in envelopes and amplitude, there seems to be also a slight difference in phase angles. The simulations were run on the whole farm model of five turbines as well, of which simulation the results are shown in Figure 51.

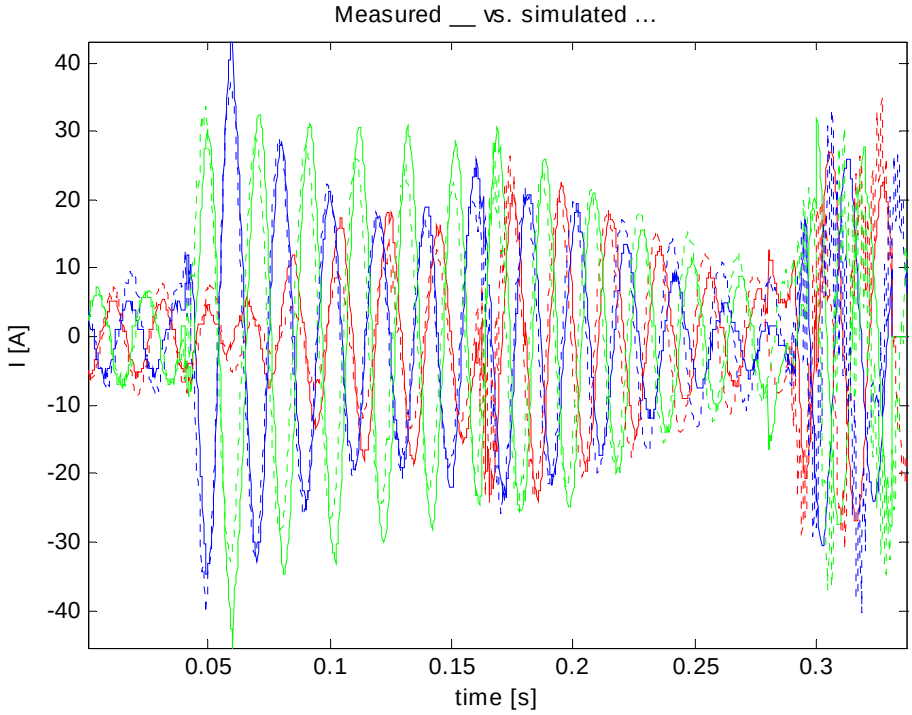

Figure 50. Measured and simulated phase currents of a single turbine when the model consists of a single turbine.

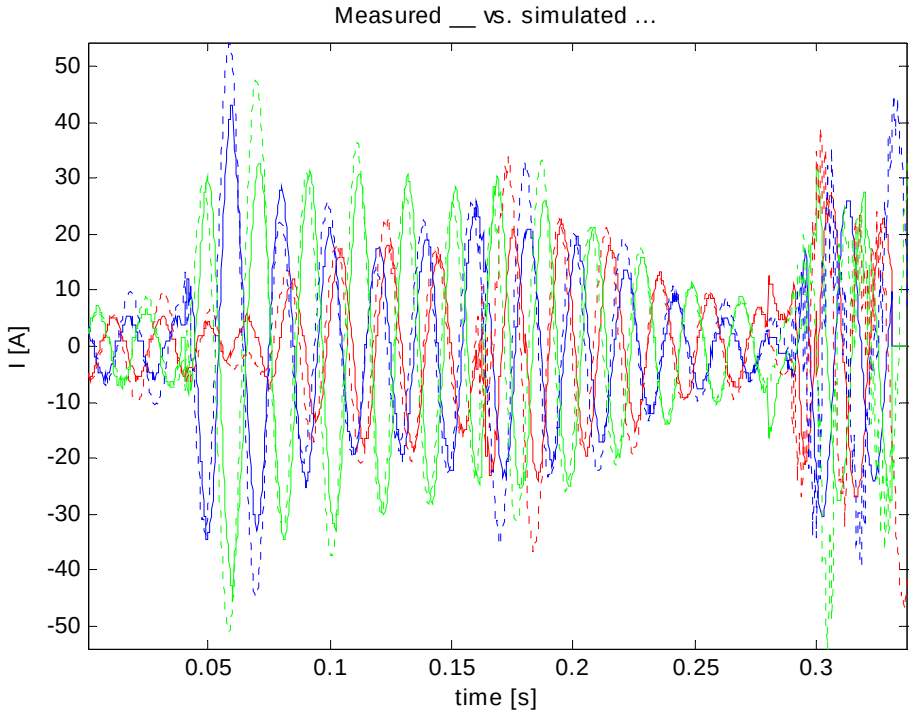

Figure 51. Measured and simulated phase currents of a single turbine when the model consist of the farm of all 5 turbines.

The simulation results shown in Figure 50 and Figure 51 differ slightly from each other. The measuring point of voltage used as input to simulation is taken from a bit different location (the whole wind farm measuring point) than the single wind turbine currents which are

compared to the simulated currents (see Figure 48). It might well be that as the measuring point is not exactly the same although they are in the same building, there is some small difference in voltages between these points.

500 Hz measurement voltages and currents of the previous case are shown in Figure 52 and Figure 53 respectively.

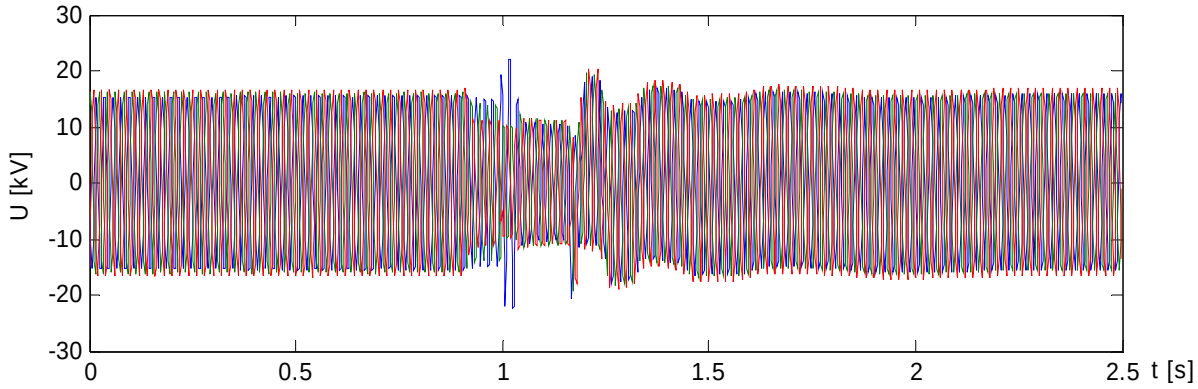

Figure 52. Phase voltages measured at 500 Hz.

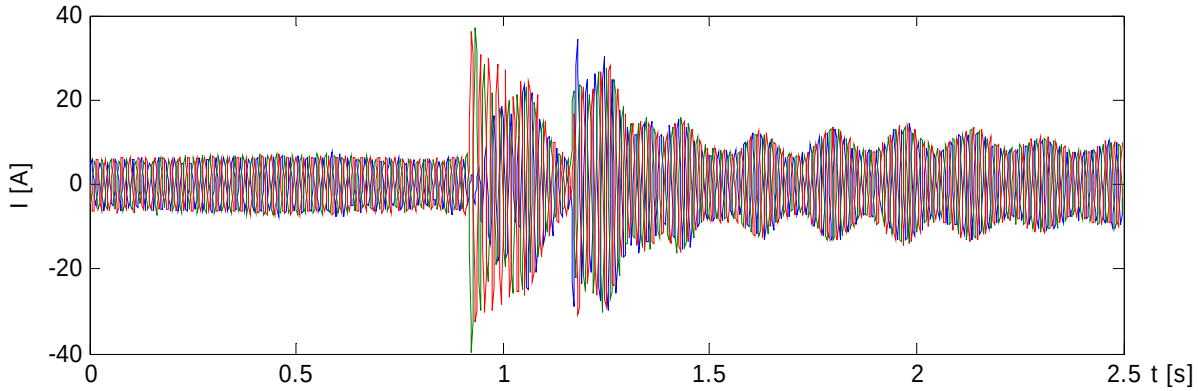

Figure 53. Phase currents measured at 500 Hz.

500 Hz measurement voltage data, shown in Figure 52, was used as input to simulation to see the post fault response of the model. The data set was 2.5 s of length with approximately 0.5 s with pre-fault data. In Figure 54 is shown calculated RMS-voltage from the measurements with positive sequence fundamental frequency method discussed in section 2.1.2. In the following figures the time scale is changed due to simulation technical reasons by adding instant of time by 2.5 s compared to the figures above.

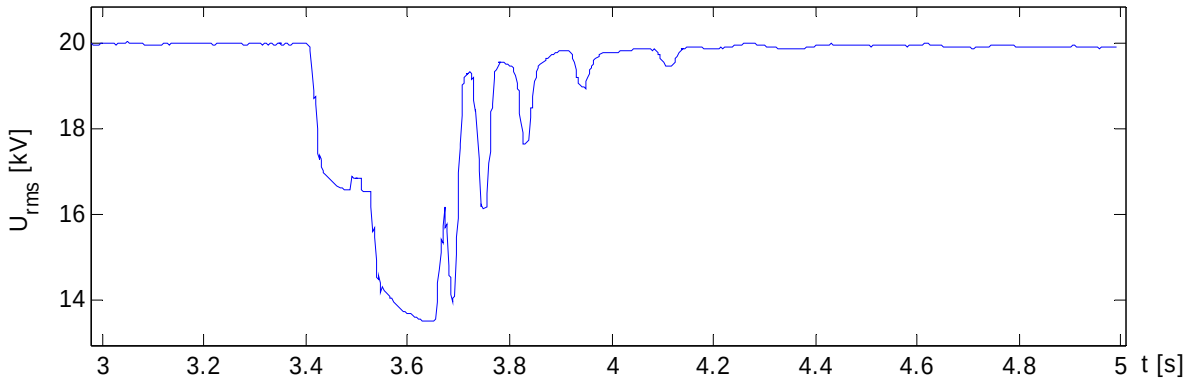

Figure 54. RMS-voltage calculated of the 500 Hz sampling measurement data.

The 500 Hz voltage measurement data was expanded by using spline interpolation method to be suitable to be used as input voltage in simulation. Active and reactive power from simulation are compared to those calculated from measurement data in Figure 55 and Figure 56 respectively.

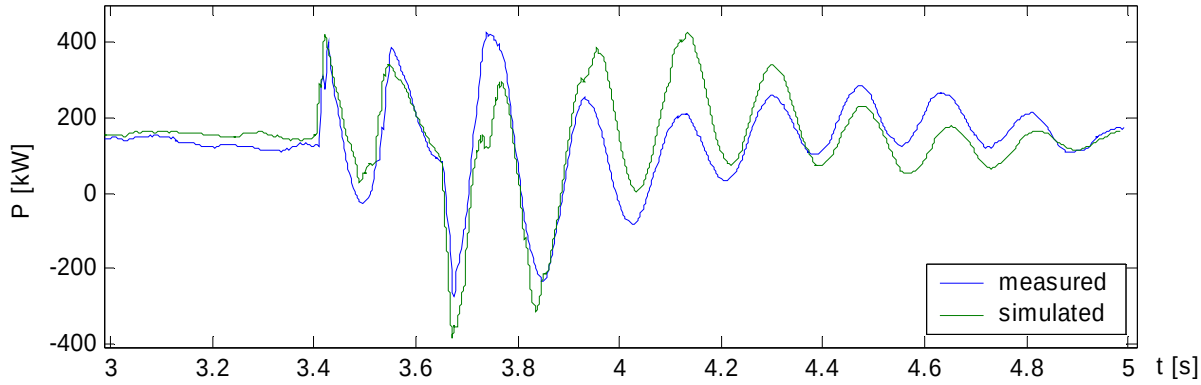

Figure 55. Active power of measurement and simulation, both calculated from phase currents and voltages using positive sequence fundamental frequency phasor based method.

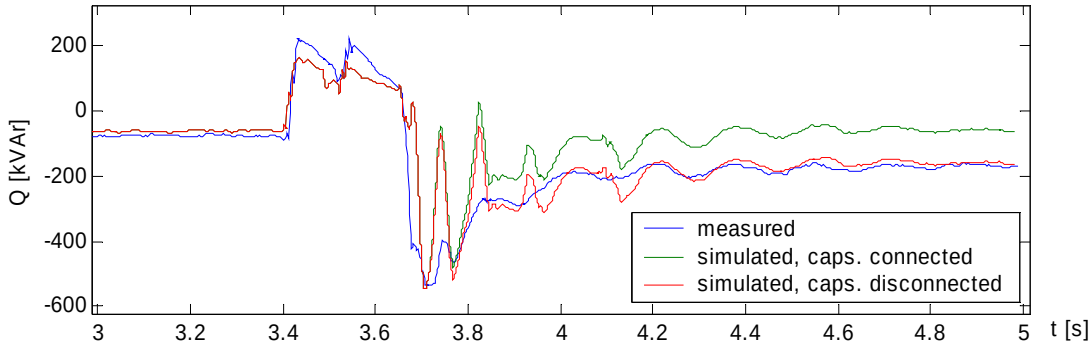

Figure 56. Reactive power of measurement and simulation, both calculated from phase currents and voltages using positive sequence fundamental frequency phasor based method. Two simulation cases presented, one with no disconnection of capacitor bank and the other with disconnecting the connected capacitor bank steps at the end of the fault period.

In case keeping the capacitor bank steps connected during the whole simulation period, there is a large difference of about 100 kVAr in reactive power magnitude in post fault stage

between the simulation and measurement. It is due to difference in capacitor bank usage, as in the measurement case the capacitor bank was automatically disconnected at the end of the fault period. Disconnecting the capacitor bank does not really change the reactive power figure form, but raises the reactive power usage to the level of the measurement.

Active power, as expected, was not affected at all due to different operation of reactive power compensation neither due to different initial reactive power compensation nor disconnection of the capacitor bank or keeping it connected.

3.3.2 Alsvik – IEA Annex XXI validation case

The dataset from Alsvik 180 kW wind turbine used in this validation procedure, is restrictedly available in the IEA Annex XXI database [28]. The Alsvik wind turbine data acquisition is described also in [6].

Alsvik validation case is a common validation assignment of the IEA Annex XXI and the simulation results from all the parties have included in proposed paper [13] about model validation. There are results from 9 different models and validation simulations, which can be compared with each other and against the measurements. In Figure 57 and Figure 58 the active power and reactive power from one simulation model is compared to the measured quantities, or more specifically to P and Q which are calculated from measured voltages and currents. Measured phase voltages were used as input in simulation.

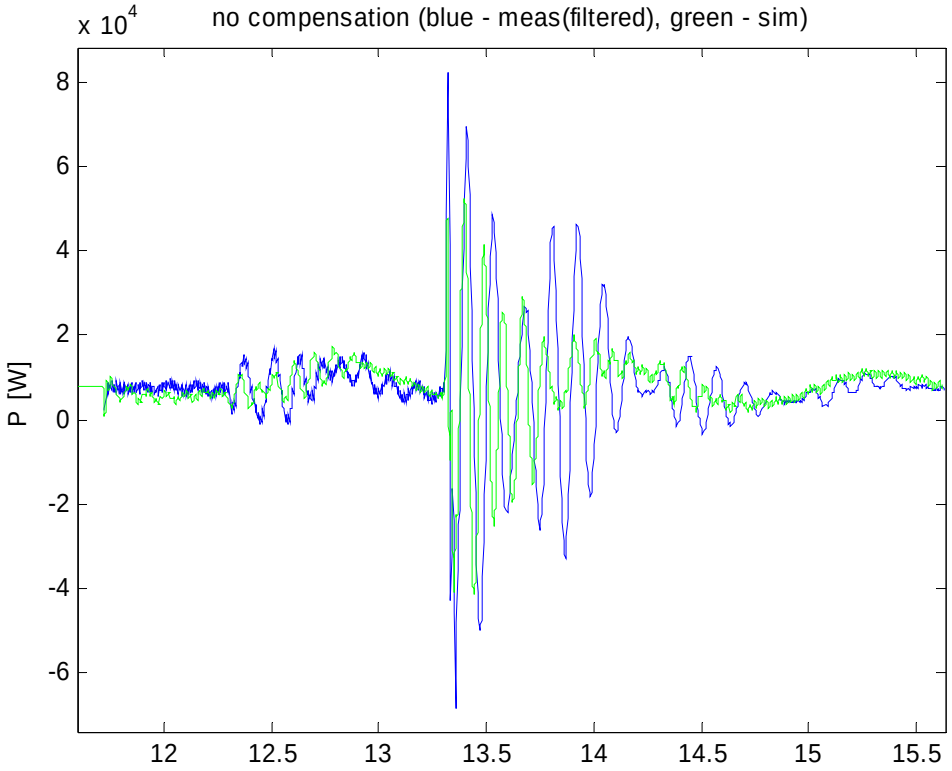

Figure 57. Active power, simulation and measurement comparison. Measurement data was filtered.

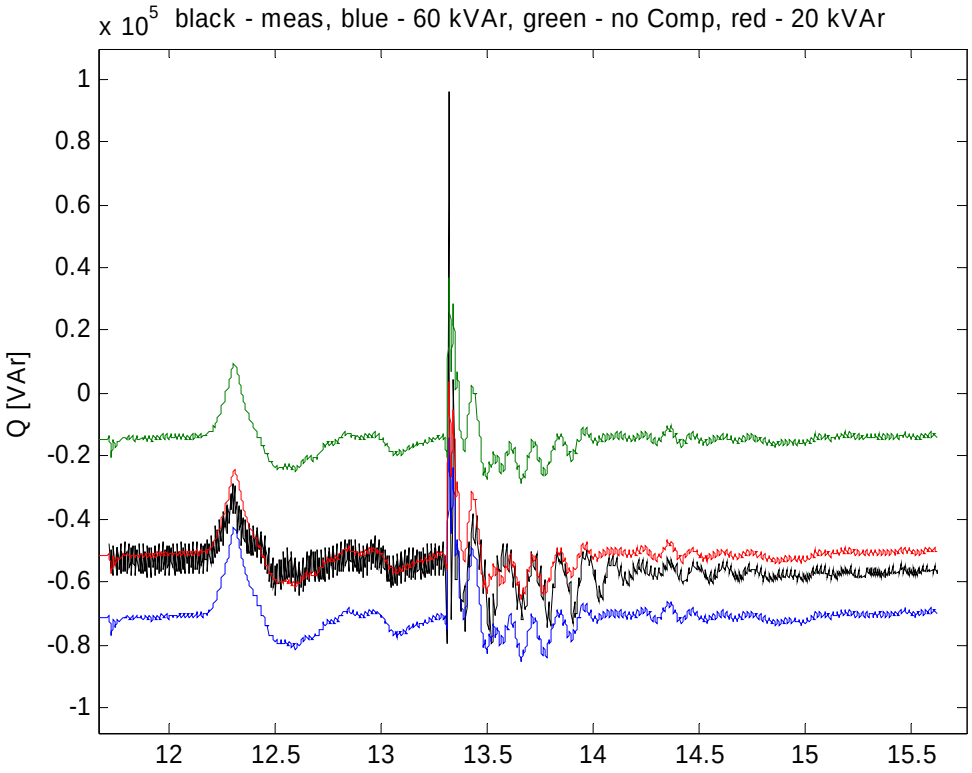

Figure 58. Reactive power, simulation and measurement comparison. There are three simulation results shown, each with different compensation. Measurement data was filtered.

There were told to be capacitor bank of 60 kVAr, but using 16 kVAr gives better correspondence between the simulation and measurements, although the normal operation should be with no capacitors connected. It is not, however, know what was the status of the capacitor bank, nor if there are such steps in the bank enabling 16 kVAr reactive power compensation. Regardless of the size of the compensation, the active power response remains the same. Over all, the correspondence between the simulation and measurement is quite good in case the assumption of 16 kVAr compensation is correct.

3.4 Fixed speed wind turbine aggregation – theory and experiments

A wind farm model implemented in PSCAD/EMTDC is being used to examine how a whole wind farm behaves in comparison to single wind turbines in the farm. The wind farm implemented is the Olos wind farm which consists of 5x600 kW fixed speed wind turbines, which all are equipped with step-up transformers, and a 3-step capacitor banks (50+50+62.5 kVAr). The cables to the wind turbines are modeled, and the connection grid is being modeled as a voltage source with appropriate impedance at the wind farm connection point. The fault response of the farm is being examined by applying a fault at the wind farm connection point.

Five identical wind turbine models with identical production – despite of the production level – produce the total wind farm model response (active and reactive power comparison) to a grid fault being the same as five times scaled up single wind turbine response.

When there is different production at each – or some – turbines, it makes a difference in the whole wind farm response. Wind turbine response to grid fault varies due to the initial

production level before the fault. This is shown below in two ways, first by scaling up a single turbine production by multiplication (Figure 59 and Figure 60), and then by scaling up the production by addition (Figure 61 and Figure 62). There have been two simulations run with identical fault but different production. One simulation is with initial wind turbine production of about 129 kW (which is about at the lover limit of this generator mode of the turbine) and the other with about 593 kW, which is almost nominal production. The smaller production (129 kW case) real power response to the fault is scaled up first by multiplying the power by 4.65 (Figure 59), and then by adding the difference of initial powers (Figure 61).

It is easily noticed that neither of the methods is perfect. Scaling by multiplying makes a huge difference on power response, and displays the situation worse than it in fact is. Of Figure 61 it can be seen that the response of the turbine at different production levels is somewhat similar to each other, but the response to real power does not match in these two cases. At higher production level the phenomena/oscillations are somewhat smoother than in the case with lower production.

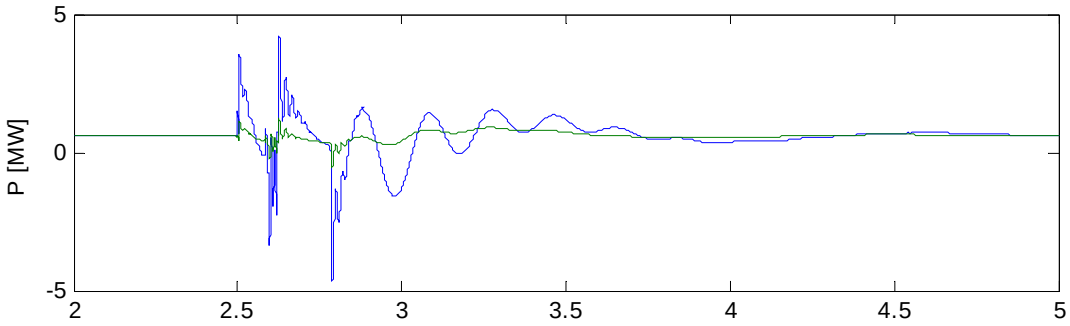

Figure 59. Wind turbine response to grid fault – active power. Initial WT production being 593 kW (green), and 129 kW "scaled up" by multiplying the active power by 4.65 (blue).

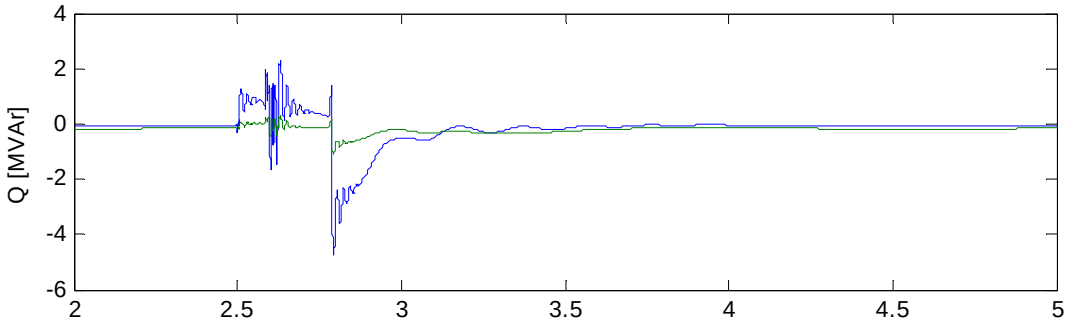

Figure 60. Wind turbine response to grid fault – reactive power. Initial WT production being 593 kW (green), and 129 kW. Reactive power in lower production case "scaled up" by multiplying the reactive power by 4.65 (blue).

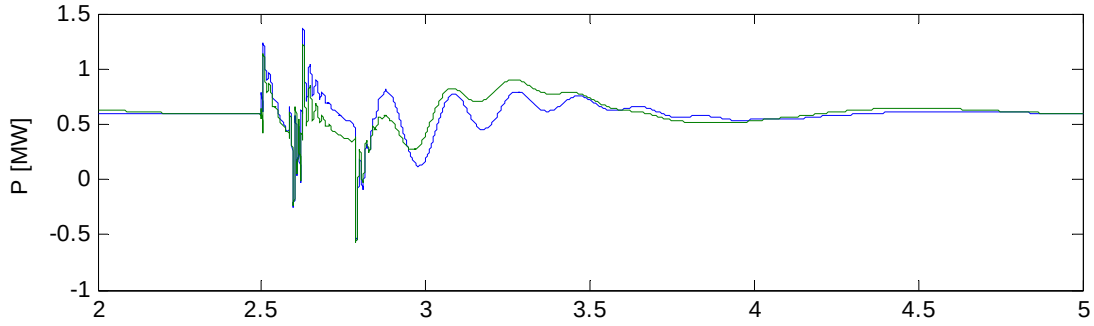

Figure 61. Wind turbine response to grid fault – active power. Initial WT production being 593 kW (green), and 129 kW "scaled up" by adding 464 kW to the active power (blue).

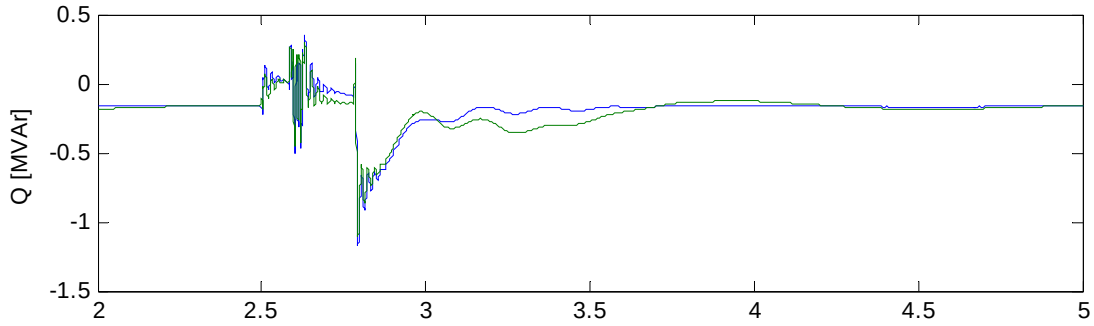

Figure 62. Wind turbine response to grid fault – reactive power. Initial WT productions being 593 kW (green), and 129 kW. Reactive power in lower production case "scaled up" by adding 150 kVAr to the reactive power (blue).

The wind farm aggregate model is scaled up from single wind turbine by multiplying its response, or for simulation purposes, the model itself is scaled up.

3.4.1.1 Different power allocation to turbines

In Figure 63 is shown real power response comparison of wind farm with two different power allocation schemes. In first case four turbines produce 129 kW (rather low production) and a single turbine almost nominal power, 593 kW. In the second case total production of the farm is equal to previous case, and it is allocated among the turbines equally. The two simulations give very good correspondence in real power response. However, in reactive power there are larger differences (Figure 64) in post- and during-fault time scale, as well as in the pre-fault period. The PQ-dependency is not quite linear, but instead, as the active power of the turbine increases, the reactive power need increases even more than linear relationship between active and reactive power would presume. However, the error in reactive power is not very large in this simulation although this case may not be the extreme case. Making comparison of similar simulations on production allocation with four turbines on 593 kW and one turbine on 129 kW against simulation with total production allocated equally, 500 kW, to each turbine, gives similar correlation between different production allocation as the case with 4 x 129 kW + 593 kW.

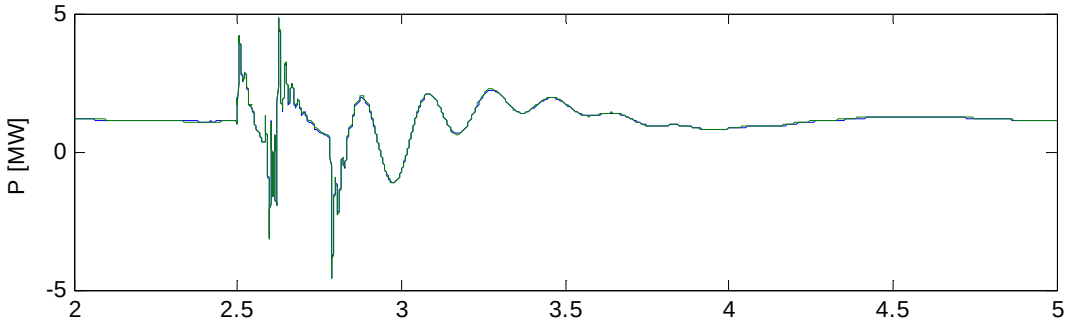

Figure 63. Response of wind farm active power to grid fault with two production allocation schemes. 4 turbines with 129 kW and one with 593 kW production (blue) compared to identical production of 221 kW at each turbine (green).

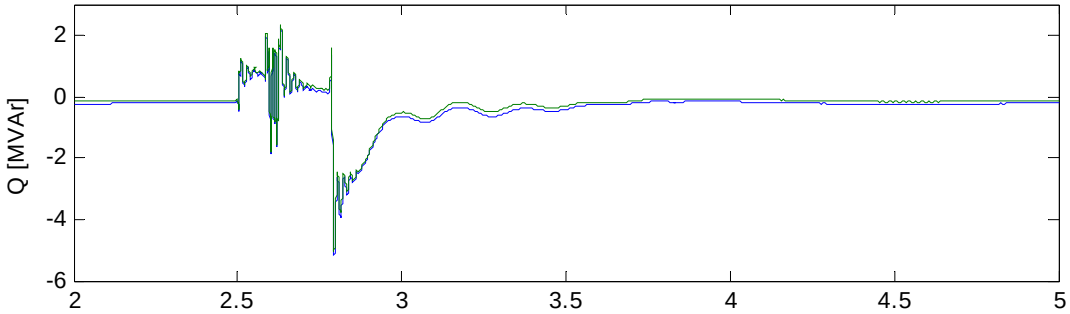

Figure 64. Response of wind farm reactive power to grid fault with two production allocation schemes. 4 turbines with 129 kW and one with 593 kW production (blue) compared to identical production of 221 kW at each turbine (green).

The maximum reactive power consumption of Bonus 600 turbine – when the capacitor bank compensation is already taken into consideration – at maximum production of 600 kW is 110 kVAr at nominal voltage. In the wind farm model simulation the reactive power consumption at different production levels of a turbine are about 14 kVAr at 129 kW, 28 kVAr at 221 kW, 112 kVAr at 500 kW and 160 kVAr at 600 kW. Larger reactive power consumption is due to a slightly lower voltage than nominal – the 21 kV grid voltage being 20 kV at wind farm assembly point. Lower voltage causes lower reactive power production of the capacitor banks.

When using a wind farm aggregate model for simulations, the N turbines composing the wind farm, are usually presented as one equivalent, scaled up, turbine with production equal to the wind farm production. This assumption leads to the question, if all the turbines in the wind farm can be included to equivalent turbine, regardless of their true operating state. This is discussed below.

The generator PQ-relationship of Bonus 600 (the larger generator mode), is shown in Figure 65 based on the generator data sheet. In Figure 65 is also drawn linear PQ-relationship if defined by the no load and nominal points. In case of a wind farm with several turbines, the production of the turbines very likely differs from each other. It is probable, however, that the production of all the turbines in a wind farm is in a smaller range than ranging from (almost) no load to nominal production. This means that there is a group of PQ-points located somewhere on the generator characteristic PQ-curve that ought to be summed up to get the whole wind farm active and reactive power. The average of all of the turbines' active and

reactive power PQ-point falls slightly out of the generator PQ-characteristic curve – which the aggregation model follow. Thus there becomes an error in aggregate model reactive power value.

The local extreme cases of reactive power error would take place when about half of the N turbines in the wind farm operate at power P1,Q1, and the other half at power P2,Q2 (P1 < P2). When taking an average of P for a single turbine operation point, the resulting PQ-point would lie on the linear line intersecting points P1,Q1 and P2,Q2, about in the middle between the values P1 and P2. In this case the aggregation assumption (using a scaled up single turbine model) would give slightly erroneous reactive power consumption on generator PQ-characteristic curve instead of the point on the linear curve intersecting points P1 and P2.

The largest error occurs when the difference of production of turbines is largest, and just about half of the turbines is producing the minimum power and the other half the maximum power (either locally, with for example productions P1 and P2, or globally with zero production and maximum production). The largest difference (=error) between the linearized, i.e. true average, and the generator PQ-curve point, i.e. the aggregation turbine, is not necessarily exactly in the middle of the line between the points P1 and P2, but is, however, in the middle section. In case some turbines' production is between P1 and P2, then the operation point of these turbines is closer to the average turbine, i.e. aggregation turbine, operation point and then the aggregation model is closer to reality.

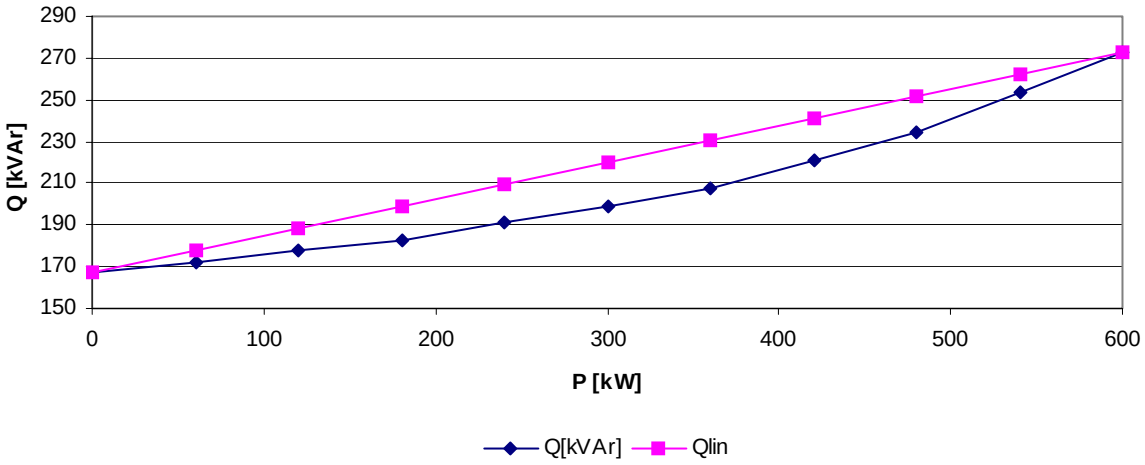

Figure 65. The Bonus 600 kW larger generator mode PQ-curve [29]

If a wind farm consists of N Bonus 600 wind turbines and the production of all the turbines is in 120 kW range – and half of them operate at P1 and the other half at P2 – the maximum error in Q of the aggregation model is about 1.3 % (when about P1 = 300 kW and P2 = 420 kW). This is not very significant in percentage, but may be an issue when considering large wind farms where the absolute reactive power values become larger. In case of a large wind farm, also the production range of the turbines may be larger.

The extreme hypothetical case is where a little less than half of the turbines operate at no load, or almost at no load, and over half of the turbines at full power, the maximum error in aggregation model reactive power consumption may become even 10 %. Considering this, it is of importance to exclude the wind turbines not connected to the grid the moment of the

study. Wind turbines at no load, but connected to the grid, are, however, significant to be included in studies where, e.g. inertia plays a role, such as dynamic fault studies.

It ought to be remembered that in this case example only one specific turbine type and model was used in calculating the possible aggregation model error regarding reactive power modeling. Also, the comparison only concerned the generator, and capacitor banks were not included. As mentioned above, the compensation power of the capacitor banks depend quite a lot on the voltage, and the wind turbine (consisting of the capacitors as well) reactive power may vary easily 10 % by only 5 pu change in voltage (change from 1 pu to 0.95 pu). In addition, only the larger generator mode of the turbine was considered. Normally in this wind turbine, there is another generator mode operating on small production up to about 120 kW.

The PQ-relationship on the two modes is shown in Figure 66. As can be seen, the turbine PQ-curves of different generator modes do not overlap. Combining the operation of these two generator modes in aggregation model may cause larger errors than the ones concerning only larger generator mode (even on operation are 0…120 kW where this mode does not usually operate). It could be considered to have two separate aggregated turbine models, one with smaller generator mode and another with the larger generator mode.

Also the capacitor bank operation depends on the generator mode, and handling compensation would also become easier. With the smaller generator mode there is only one capacitor bank in operation, and with larger generator mode all three capacitor banks are in operation. In some turbine types with capacitor banks, the capacitor banks may even be switched on or off depending on the production increase or decrease over certain limit during one generator mode operation.

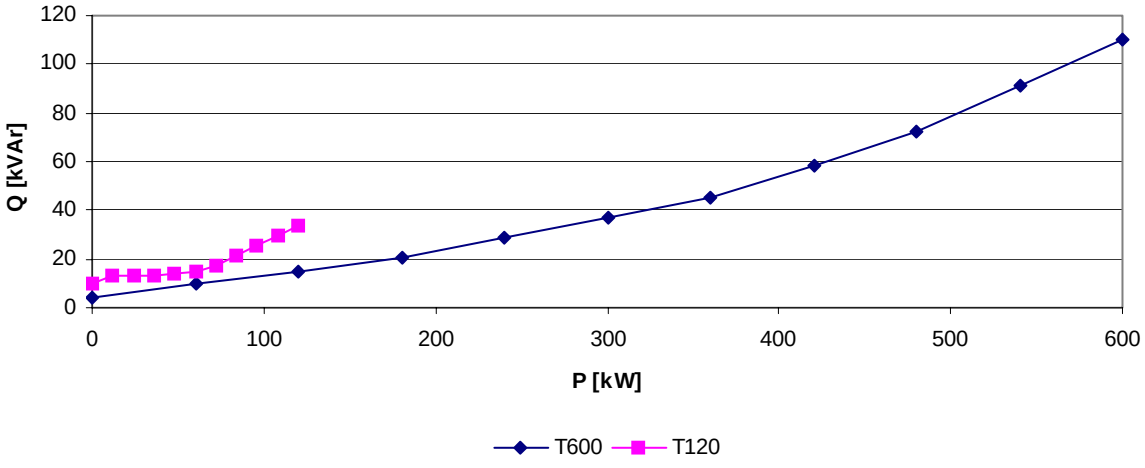

Figure 66. Bonus 600 wind turbine PQ-relationship at nominal voltage. Generator modes 120 kW and 600 kW with appropriate compensation.

As proved that the whole wind farm (consisting of identical turbines and identical turbine operation) response is identical to scaled-up single wind turbine response, these investigations with different actual operation state on different turbines compared to identical average operation on each turbine, are to examine the error this assumption may cause. Also, it was noticed that the response of a turbine to a grid fault varies due to the operating state of the turbine.

Thus, the aggregate fixed speed wind turbine model can be implemented by replacing the single turbine rating by the sum of the farm turbine ratings

$$S_{agg} = \sum_{i=1}^{n} S_i \ . \qquad (3.18)$$

Some conditions should be taken into account, e.g. that there might be some turbines not connected to the grid, and thus these should be excluded from the aggregate model as well. In addition, if the turbines are equipped with two-speed generators and the operating conditions are in the area where some turbines might be operating on different generator mode than some others, these two groups of turbines should be presented each by their own aggregate model with suitable parameters and appropriate aggregate model ratings.

The generator and multi-mass parameters are given in pu-values in PSCAD/ENTDC-models, so changing the single turbine models to aggregate model is quite easy; only the ratings need to be changed in generator- and multi-mass-component parameter entries.

3.5 Wind farm aggregation – simulations with measured voltage input

Essential in composing a wind farm model, is the information on which, or how many, of the wind turbines of the farm are on-line. It is not that important, if the turbines are producing power, or not, but more significant is if they are connected to the grid. A simulation was performed on wind farm model consisting of 5 identical turbines and their individual production was varied. The total wind farm production was kept constant. It's not always presumable that all the turbines are generating power somewhat equal to the other units within the farm. The turbines are located closer together in a small farm, but they still may be spaced by tens or hundreds of meters from each other. Also the terrain contours, wind direction and wind shadow may cause different wind conditions for individual turbines. Especially in arctic location the icing in turbine blades may cause different production of a turbine.

First the production of all the turbines was assumed equal, being 151.8 kW each. The simulated currents are shown in Figure 69 and compared to actual measurements. Then the wind farm production was divided to each turbine in such a way, that the total farm production remained the same, and each turbine had production proportional to the normal operation measurements just before the fault. Compared to 5 x 151.8 kW turbine simulation, the currents are very accurately identical.

The role of inertia and very unbalanced production between the turbines was examined. One turbine was producing 151.8 kW, and another one the rest, 607.2 kW (the rated power of the turbine is 600 kW, and 660 kVA, and this a bit overgenerating power was obtained, because the model uses torque as input, which is 0.92 p.u.) to still keep the farm production same. Other three turbines were producing zero power, but were connected to the grid. In Figure 67 are compared the simulation currents with simulation currents from 5 x 151.8 kW farm total production currents. The difference in currents is quite small between the two production distributions.

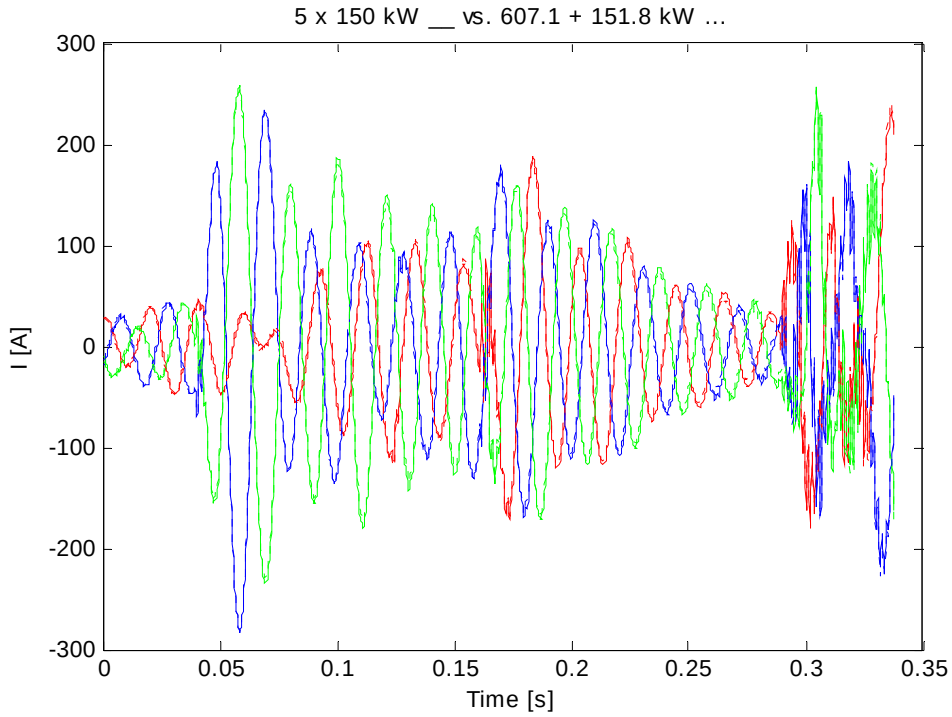

Figure 67. Comparison of farm currents in case of three turbines at zero power and two turbines producing 151.8 kW and 607.2 kW vs. 5 x 151.8 kW. In both cases the farm total production is the same, and in first mentioned case also the three zero power producing turbines are connected to the grid.

The zero production units were switched offline, and a simulation was performed with two turbines online, one with 151.8 kW and another with 607.2 kW production as in previous simulation. The Figure 68 shows the current comparison with 5 x 151.8 kW farm simulation.

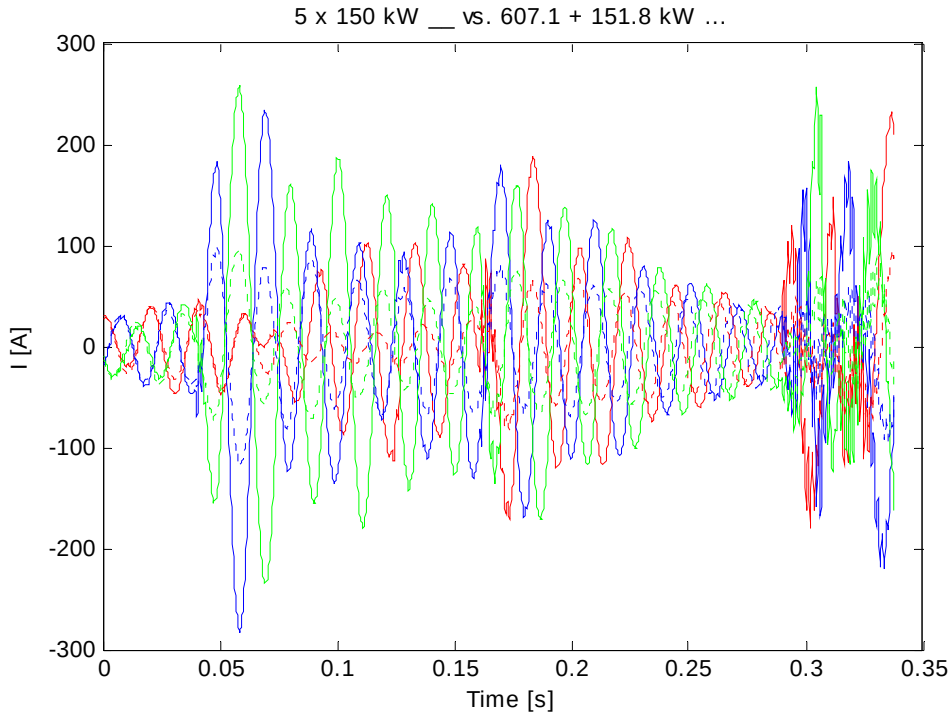

Figure 68. Comparison of farm currents in case of three turbines at offline and two turbines producing 151.8 kW and 607.2 kW vs. 5 x 151.8 kW. In both cases the farm total production is the same.

It can be noticed that the change in inertia connected to the grid makes a big difference in wind farm output currents during fault.

3.6 Fixed speed wind farm model validation

Wind farm consists of five identical Bonus 600 kW turbines. The turbines are distributed from collection point after different lengths of cables. Each turbine has its own collection cable. The measured turbine is the one with least length of cable between the collection or measuring point, and the turbine generator. These turbines may not, however, be operating identically at the same time e.g. due to the different location of them, or icing in the blades etc. It was first assumed that all the turbines are operating identically. The phase currents of this simulation are shown in Figure 69.

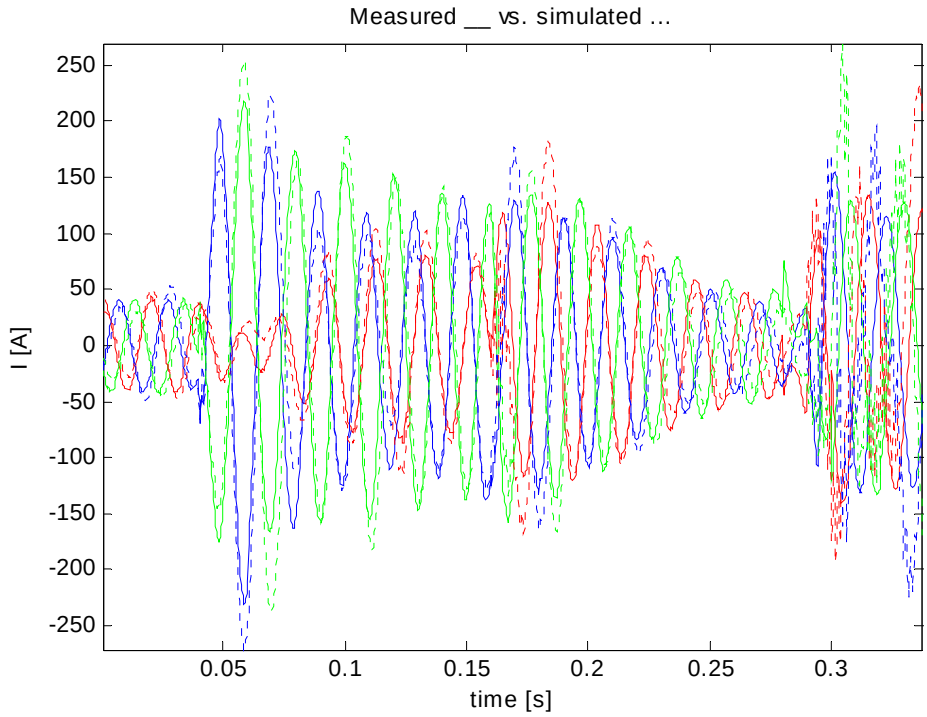

Figure 69. Measured and simulated phase currents of a farm model consisting of 5 turbines.

3.7 Wind farm aggregation – measurement data analysis of a medium size farm

In IEA Annex XXI database there is some data from Smøla wind farm phase 1 (20 x 2 MW) in Norway. The turbines are 2 MW induction generator equipped fixed speed wind turbines. The individual turbines are equipped with thyristor controlled capacitors (522 kVAr) and the whole wind farm with a two-step capacitor bank (8 + 6 MVAr).

The voltage dip measurements are taken from a single wind turbine at 690 V level, and from the whole farm of 20 turbines at the wind farm 20/66 kV transformer high voltage side. The phase voltages measured at these two locations are shown in Figure 70 over period of 10 seconds, and in Figure 71 more closely over 5 seconds. The voltage dip is larger at the wind farm transformer station than at the individual measured wind turbine. The fault is probably a two-phase short circuit somewhere up-stream main grid [30]. It is not known what causes the notch in voltage at 295.7 s.

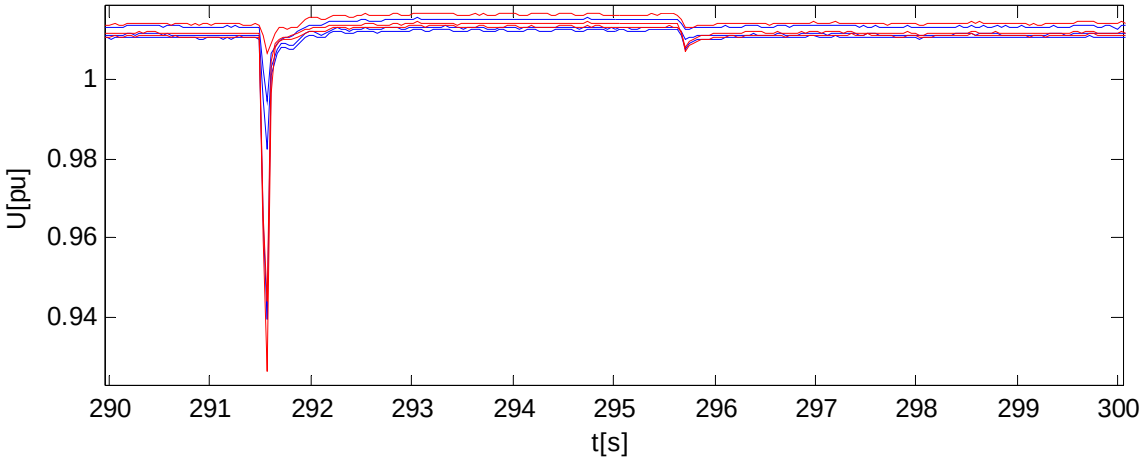

Figure 70. Phase voltages measured at wind turbine terminals (blue) and wind farms connection point (red).

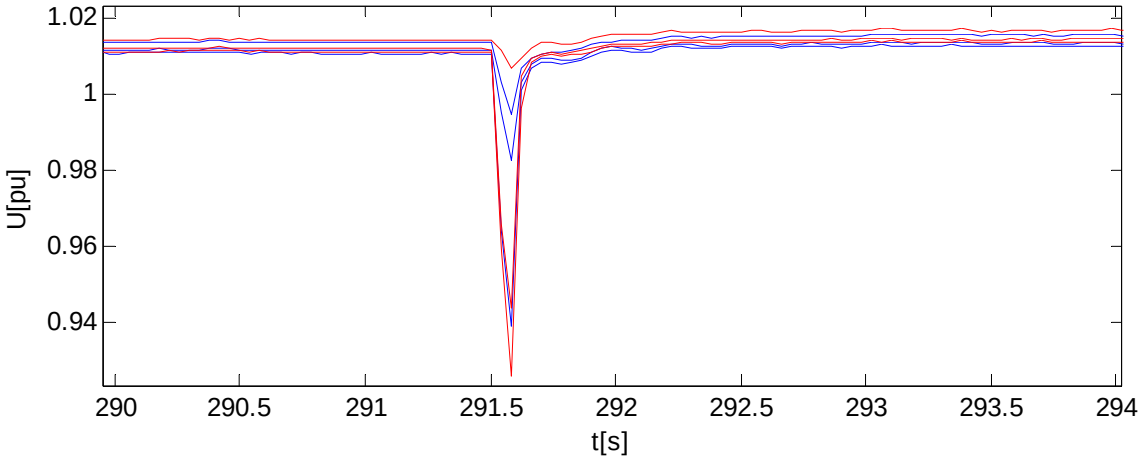

Figure 71. Phase voltages measured at wind turbine terminals (blue) and wind farms connection point (red).

The phase voltages in wind farm connection point are slightly higher than at the single wind turbine terminals. The voltages at each phase differ from each other as well. In Figure 72 and Figure 73 the wind farm and single turbine active and reactive power are shown respectively in per unit values. The active power fluctuates both in single wind turbine, and on whole wind farm, although the whole wind farm active power is a bit smoother than the single wind turbine power due to balancing effect of multiple wind turbines. The voltage dip is seen in active power as power fluctuations during the dip. This can be observed more closely in Figure 74. The fluctuation is very much in phase in the measured single turbine and the whole wind farm. In farm aggregation studies it therefore may be justified to take the simple and more conservative approach by using multiple of the single wind turbine behavior, as the actual farm response is most likely a bit smoother and more damped.

The reactive power of both single wind turbine and the whole farm is very smooth, and small, compared to the active power. However, it seems that the whole wind farm is producing reactive power, whereas the measured wind turbine is consuming reactive power. There is a spike, of duration about that of the voltage dip, in reactive power as the voltage dip occurs. After this first spike, there is another smaller and slower decaying spike to the other direction

after the voltage recovery. There is also a small reactive power spike after 0.5 s the voltage dip. It is not clear what has happened here, but the same incident was seen also in the voltages in Figure 70.

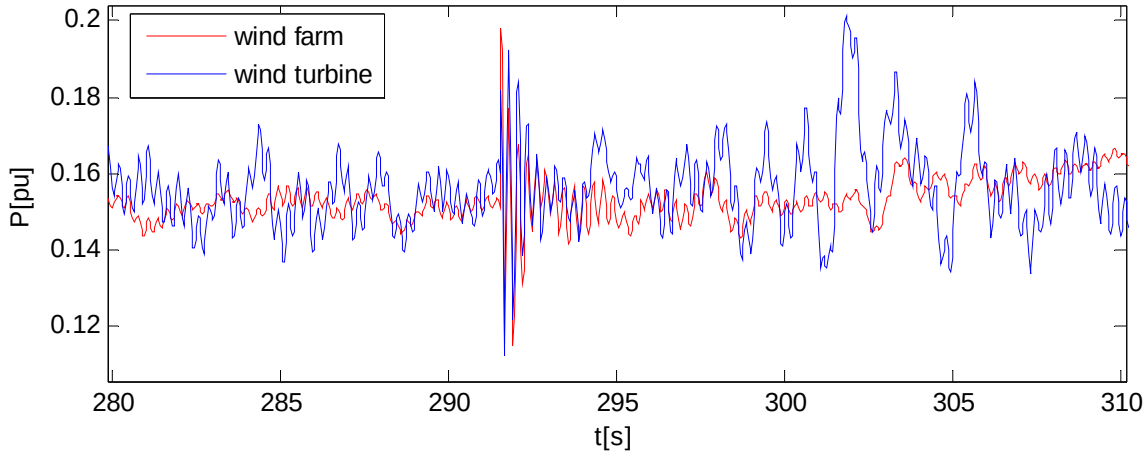

Figure 72. Wind farm and a single wind turbine active power measurements in pu during 20 s around the voltage dip. Dip at t = 291.5 s.

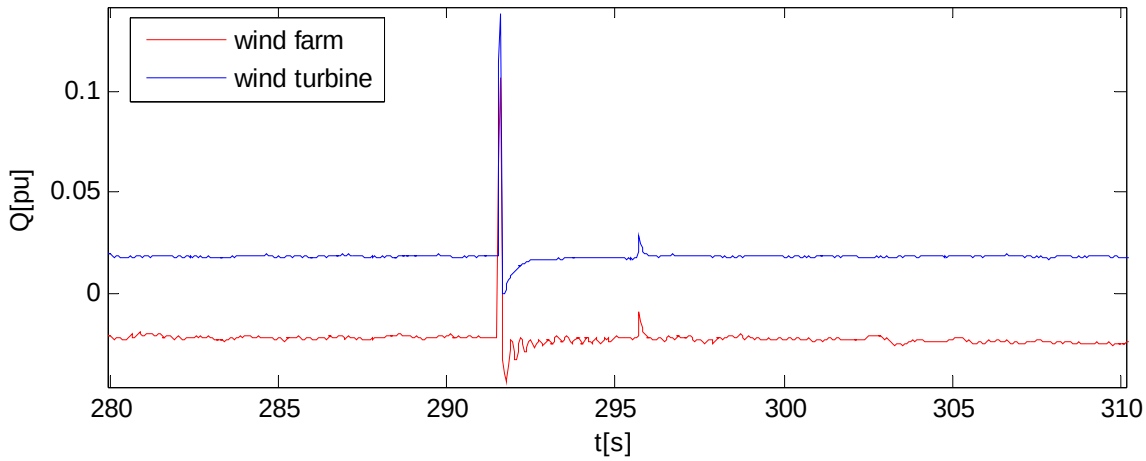

Figure 73. Wind farm and a single wind turbine reactive power measurements in pu during 20 s around the voltage dip. Dip at t = 291.5 s.

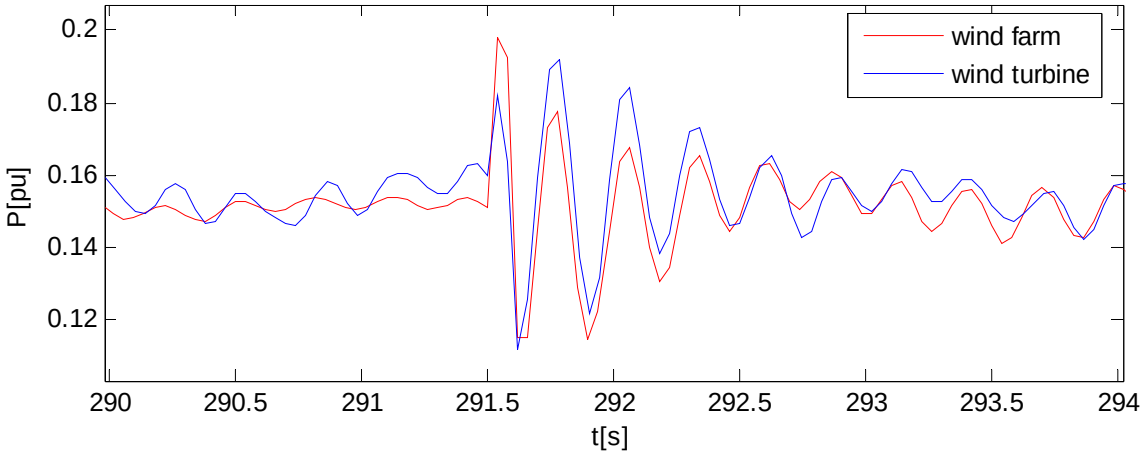

Figure 74. Wind farm and a single wind turbine active power measurements in pu during the voltage dip.

Due to the different sign (and magnitude) of measured reactive power of the wind farm and the wind turbine, it is not directly possible to make a conclusion of how the reactive power should be presented in aggregate model. The difference in reactive power is partly due to the presence of the whole find farm capacitor banks, and possibly partly due to the internal farm earth cable influence.

What is seen on the reactive power response to the voltage dip, in case of a wind farm compared to a single turbine, a conclusion of using multiplication in reactive power as well, can be drawn. In this case also, this approach is more conservative and pessimistic due to the smoothing effect of multiple turbines. It is, however, seen that the direction of reactive power does not make an error, as long as it is remembered to apply the changes in the same direction (independently of the actual sign of reactive power – no multiplication), and the initial level of reactive power of the farm is known.

4 DFIG

A purpose in this project was to test available DFIG models. There has been a lot of DFIG equipped wind turbine model development during the recent years in the world, and of different types of models. In some models the mechanical side of the wind turbine is omitted, either by arguing that the mechanical and aerodynamical parts of the wind turbine do not affect on the electrical behavior of the wind turbine when the study is concentrated on the interaction between the grid and the wind turbine, or that the study period is so short that the turbine mechanics have no influence during that time on e.g. the generator behavior during the electrical transients.

4.1 Overview

When talking only about the DFIG machine regardless of what kind of a model or the turbine is presented, there still are different modeling approaches. The DFIG rotor circuit is equipped with a power electronic converter, consisting of network-side and rotor-side converters.

The fifth, third and first order models were described in [31] (single mass representation – 2-mass representation adds the order of the model by two, compare to group of eq. (3.3)). The

fifth order model consists of five differential equations; two voltage equations, two flux linkage equations, and one mechanical equation

$$\underline{u}_s = r_s \underline{i}_s + \frac{d\underline{\psi}_s}{\omega_n dt} + j\frac{\omega_{ref}}{\omega_n}\underline{\psi}_s, \tag{4.1}$$

$$\underline{u}_r = r_r \underline{i}_r + \frac{d\underline{\psi}_r}{\omega_n dt} + j\frac{\omega_{ref} - \omega_g}{\omega_n}\underline{\psi}_r, \tag{4.2}$$

$$\underline{\psi}_s = (x_s + x_m)\underline{i}_s + x_m \underline{i}_r, \tag{4.3}$$

$$\underline{\psi}_r = x_m \underline{i}_s + (x_m + x_r)\underline{i}_r, \tag{4.4}$$

$$J\frac{d\omega_g}{dt} = t_m + t_{el}. \tag{4.5}$$

Neglecting the stator transients and reducing the model to third order, the group of equations simplify to

$$\underline{u}_s = r_s \underline{i}_s + j\frac{\omega_{ref}}{\omega_n}\underline{\psi}_s, \tag{4.6}$$

$$\underline{u}_r = r_r \underline{i}_r + \frac{d\underline{\psi}_r}{\omega_n dt} + j\frac{\omega_{ref} - \omega_g}{\omega_n}\underline{\psi}_r, \tag{4.7}$$

$$J\frac{d\omega_g}{dt} = T_m + T_e. \tag{4.8}$$

In [32] the third order and fifth order models are compared, and it is shown that the stator transients can be neglected and the third order model be used in transient stability studies. The conclusion was that the simulation results are quite similar to each other in that point of view, and the rotor speed response is conservative for the safety when using third order model instead of fifth order model.

The first order model consists of two steady state voltage equations, and the mechanical differential equation

$$\underline{u}_s = r_s \underline{i}_s + j\frac{\omega_{ref}}{\omega_n}\underline{\psi}_s, \tag{4.9}$$

$$\underline{u}_r = r_r \underline{i}_r + j\frac{\omega_{ref} - \omega_g}{\omega_n}\underline{\psi}_r, \tag{4.10}$$

$$J\frac{d\omega_g}{dt} = t_m + t_{el}. \tag{4.11}$$

The DFIG model for PSCAD/EMTDC developed by the University of Vaasa for HELib-library in Simulointiympäristö-project discussed and analyzed in section 4.7.3, is a single mass model.

The drive train in variable speed wind turbines is not directly coupled to the grid by the generator, as the rectifier-inverter combination on the rotor circuit of the generator fed from the grid permits the rotor to rotate at any speed of the generation unit [33]. A grid fault causes also voltage fluctuation at natural frequency because of the torsional shaft mode [9]. As seen earlier in Figure 23, the short-circuit impedance at the wind turbine connection point has a small influence on the power oscillations. In a weak grid where the voltage may fluctuate (because of other reasons also), a DFIG equipped wind turbine may be advantageous, as it can

produce or absorb reactive power to or from the grid, and thus be used to control the grid voltage [34].

The bi-directional rotor circuit converter enables the DFIG to operate as a generator in both, sub-synchronous (positive slip s > 0) and super-synchronous (negative slip s < 0) operating state area. If neglecting the stator and rotor losses, the slip power of the rotor circuit through the converter, can be approximated with the slip and the stator circuit power

$$P_{rotor} \approx sP_{stator}, \tag{4.12}$$

and the stator power can be approximated with slip and grid power

$$P_{stator} \approx \frac{P_{grid}}{1-s}. \tag{4.13}$$

The stator circuit is always feeding power to the grid, but the rotor circuit may either be feeding power to the grid or absorbing power from the grid depending on the drive operating conditions [34], [35]. Thus, the needed converter rating can be defined along with the machine operating speed range.

$$P_{conv} = P_{rotor} \approx \left(\frac{s}{1-s}\right)_{\max}. \tag{4.14}$$

Usual converter size of doubly fed induction machine is 20…30 % of the machine rated power.

In [36] comparison of DFIG model of Vestas V80 was compared to the measurements taken at site. The model was implemented by Vestas in PSCAD/EMTDC, and it consisted of 2-mass representation of the shaft, blade pitching, the generator, rotor-side and grid-side converters and the DC-link in between, as well as the transformer. The electrical components used, were from the standard library of PSCAD/EMTDC. The model was intended to electrical interface analysis between the wind turbine generator and the grid. This model, however, was not described in any details, due to proprietary information reasons.

4.2 Multi-mass

The DFIG model requires a two-mass representation of the turbine in a similar way as shown necessary for a fixed speed wind turbine model. This has been marked in e.g. [37], [38] and [25]. In [36] a four-mass system, i.e. including lumped gearbox, braking disc, generator and turbine as separate masses, simulations showed that higher frequencies produced by this mass division are strongly damped, and have no influence on the electrical system. In [25] was stated that under normal operating conditions the variable speed generator is decoupled from the grid, and thus the torsional shaft oscillations are filtered out by the converters, but in case of e.g. severe grid faults, the generator and turbine acceleration can be simulated with sufficient accuracy only if the shaft oscillations are included in the model.

According to [9], a common argumentation to use single lumped mass representation for variable-speed wind turbines in voltage stability investigations is the fact that the generator rotor speed and the voltage dynamic behavior are de-coupled. In addition it is suggested to use a two mass model because the electric power fluctuations will follow the generator rotor speed oscillations, at natural frequency of

$$f_T = \frac{1}{2\pi}\sqrt{\frac{\omega_0 K_S\left(H_M + H_G\right)}{2H_M H_G}}. \tag{4.15}$$

Usually the natural frequency is from one to few Hz, which is relatively close to large (conventional) power plant synchronous generator natural frequencies. Thus there might be a risk of mutual oscillations between the large (conventional) power plants and wind farms consisting of variable-speed wind turbines. There are gearboxes with large gear ratios in DFIG equipped wind turbines as the generator stator is connected directly to the grid, and thus the turbine low speed must be raised to the grid speed [9]. Use of power electronic link to the grid and its control, controls the electrical power generated, and thus the generator reaction torque (electrical torque), which again influences the rotor speed [33].

In many models where the turbine is modeled beyond the generator and converters, both, the blade pitching and the mechanics (at least as two-mass model) are being modeled [39][40]. And on the other hand there are those DFIG equipped wind turbine models represented in publications, where the mechanical and aerodynamical representation is omitted [41].

The DFIG mechanics should be modeled in a similar manner as in case of a fixed speed wind turbine, with at least two masses model with damping and spring constant (3.3). Active and reactive power control are de-coupled in the DFIG, which means that the shaft torsional oscillations are seen as speed fluctuation, but they do not affect the voltage. Thus, for short-term voltage stability studies, a lumped mass model is sufficient. The generator rotor current follows the generator rotor speed fluctuations, which the converter protection system monitors. Thus, during (and after) a grid fault, the converter is usually blocked by short circuiting the rotor, and then the DFIG is quite like a squirrel cage generator which is also used in wind turbines. [9]

Due to a grid disturbance, for DFIGs there is a risk of excitation of shaft system, which may be fatal to turbine operation. In case the damping in the shaft system is poor, the shaft oscillations may increase. This behavior sets requirements to the converter control. Insufficient damping of shaft oscillations may lead the DFIG to disconnect. Based on these facts, the mechanics of a DFIG equipped wind turbine must be represented with two-mass model and (3.3). [9]

The needed mechanical parameters in simulation model may not be known. Estimates for inertias can be calculated of the given geometrical data and the masses, and using available information of mechanical parts of the turbine. Here the inertia constants for a 850 kW variable speed wind turbine were defined by approximation and calculations.

Blade LM 25.1 P [42]:

Rotor diameter (max.)	52 m
Generator	800 kW
Turbine control	Pitch
Blade length, nominal	25.1 m
Weight	2950 kg
Bolt circle diameter	1250 mm

In [43] a small wind turbine blades' center of mass was given for a blade of about 5 m long to be at 1.7 m from pitch shaft. On this blade the center of mass is located at 0.34 (pu). In [44] the center of mass was measured and calculated for a similar size and type turbine. The center of mass was defined for a 23.3 m long 2951 kg weighing wind turbine blade of a pitch controlled wind turbine. The measured span-wise center of mass was at 8.451 m, and this distance is used in the following calculations.

The inertia of a uniform rotating bar of mass m and length l is

$$J = \frac{1}{3} m l^2 , \tag{4.16}$$

and the inertia of a point of mass m rotating about an axis at distance r is

$$J = m r^2 . \tag{4.17}$$

If representing the bar as a point off mass rotating about the axis at distance of its center off mass ($0.5l$), the inertia is

$$J = m\left(\frac{1}{2} l\right)^2 = \frac{1}{4} m l^2 , \tag{4.18}$$

which signifies that the estimated inertia calculated with equation (4.18) is only 75 % of its actual value calculated with equation (4.16). Wind turbine blade is not uniform by its length, but instead more solid at its base than its tip. Thus, it is often done that the wind turbine blades in more detailed modeling are represented as several segments and the mass of each segment is located at the center of gravity of each segment. As further information about the blades is not available, the inertia of blades is calculated with equation (4.17) by placing the whole blade mass in its center of gravity.

In place in the turbine, the center of gravity is of distance $l_{cog} + r_{navel}$ from the axis of rotation. The inertia of one blade of 2950 kg is about 257 952 kgm^2 and of 1500 kg blade 131 162 kgm^2. The inertia of navel with 0.9 m radius weighing 1 150 kg is 466 kgm^2, and of 5 500 kg 2 228 kgm^2. Thus, the inertia of the rotor J_t is with heavier blades 774 322 kgm^2 and with lighter blades 395 713 kgm^2. Hereby it can be seen that, firstly, the turbine inertia is very sensitive to defined mechanical parameters, and secondly, as the mass distribution is not known when calculating the rotor/blade inertia, it may cause rather large errors in the result.

When using the *Multi-Mass*-component in PSCAD, the inertia values of both turbine and the generator (the low speed components and the high speed components) are inputted as mechanical values, i.e. the pu-value [s] for them is calculated by using the rated power as the base value. It is not really clear if the rated power used is the rated active power, or the rated apparent power of the turbine. It should probably be active power, but may well be, that in electrical simulation tool where apparent power is normally the base rated power, in this case it is used as well. In case omitting the *Multi-Mass*-component, the generator inertia is given for the machine component as pu-value [MWs/MVA] calculated with the apparent power apparently as the base value. Using the active nominal power as base value for *Multi-Mass*-component parameters, the inertia in pu-value is calculated as

$$H = \frac{\frac{1}{2} J \omega^2}{P_n} . \tag{4.19}$$

The generator inertia is calculated for ABB generator. There may be small differences in inertias of different generator manufacturers, which there may be several for one wind turbines manufacturer. Inertia in pu calculated with equation (4.19) is 0.653 s. In the high speed side lumped mass the gearbox inertia needs to be included in addition to the generator inertia. The gearbox inertia is not easily found. Considering that the gearbox inertia adds to the high speed lumped mass inertia, the inertia is larger than the generator inertia 0.653 s.

4.3 Converters

There are only few publications (e.g. [45]) where the control of the DFIG is described as a control diagram instead of equations, and even less those in which also the control circuit parameters would be given (e.g. time constants and gains etc.).

4.3.1 Grid-side converter

The purpose of the grid-side converter is to keep the DC-link voltage constant irrespective of both magnitude and direction of the rotor power [45]. Another task of the grid-side converter mentioned in [34] is to guarantee converter operation at unity power factor, i.e. to transmit active power only. Thus the reactive power is transmitted only via stator. DC-link voltage and reactive power (keeping it at zero) are controlled indirectly by grid side converter current control. [34]

According to [3] the network-side converter usually is represented by a simplified model, which is based on generic control scheme composed of a set of PI-controllers. The PI-controllers produce two-axis (in d, q-reference frame) voltage values of set or required active and reactive power values. Such scheme is employed e.g. in [31], [9] and [45]. The control scheme neglects the switching dynamics of the converter as ideal control is assumed, and thus the controller is capable of following the set/control value at any time [9].

The grid-side converter control scheme is represented in detail in [45], but no parameter values are given. The converter is current regulated and uses a standard asymmetric sampling PWM (pulse width modulation) scheme. This vector control control-scheme allows independent active and reactive power flow between the grid-side converter and the grid. Another control scheme for the grid-side converter is DTC (direct torque control). [3]

Akhmatov mentions in [9] that often DFIG system is represented with only one converter, neglecting the grid-side converter, in transient voltage stability studies because it is considered very fast. It is also shown why both the converters with DC-circuit between them should be modeled, and concern of a wind turbine manufacturer was also bought up regarding the issue of neglecting the grid-side converter model. The single converter model may give inaccurate results in rotor current as well as in DC-voltage compared to the model with both converters, and further more pessimistic overall results. [9] This is a good observation, in case there is only a simpler model of one converter to perform simulations with, i.e. due to simplification the results should not be too optimistic. In [3] there was used a simplified grid-side converter model represented as a discrete transfer function.

Tuning the control loop parameters may be difficult. In [9] help was received from a wind turbine manufacturer for a generic control system parameter tuning for the grid-side converter as well as for rotor-side converter in order to get realistic results.

4.3.2 Rotor-side converter

Rotor-side converter can be modeled in number of different ways, as well as the grid-side converter. The most common approach is the stator flux oriented vector control scheme. The switching dynamics can be included by using a PWM modulator in the model [3]. In [45] is also shown a detailed rotor-side converter model. DTC can also be used in rotor-side converter, and it actually is even more simple than the vector control method. [3]

4.4 Crowbar

The power electronics in DFIG converter are very delegate components, which are vulnerable and can brake in case of a grid fault – voltage dip causing larger currents than normal operation currents. The converters are also costly, and thus they are protected short circuiting the DFIG-machine rotor circuit (bypassing the converters) in case of a fault.

Crowbar can be implemented in a number of ways. E.g. the rotor short-circuiting can be realized by two pairs of anti-parallel connected thyristors connected between the phases, or by a diode bridge to rectify the phase currents with a single thyristor controlling the shorting [4], see Figure 75.

There are passive and active crowbars. The passive crowbar operates in case of a fault short-circuiting the rotor circuit, and remains in operation until the machine stator circuit is disconnected from the grid [46]. The active crowbar is used in fault ride-through [4]. The short-circuit made by crowbar needs to be removed before the converter can start again after the fault. Removing the short-circuit is not a trivial task regardless of the crowbar implementation type due to the flowing current. An active crowbar can cut the current when ever needed. The active crowbar operation is apparently quite fast, as can be observed from measurements shown in [4] of full-scale DFIG-test setup where the crowbar conducted only once (for about 10 ms), and the rotor side converter started again about 75 ms after the beginning of the dip (about 65 ms after disconnection of the crowbar).

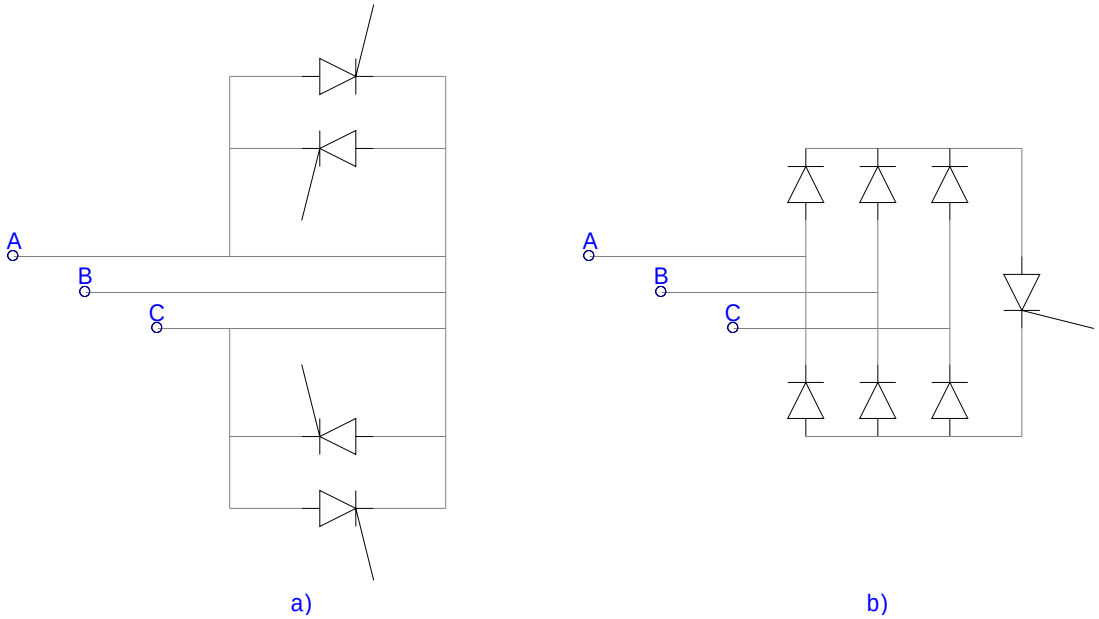

Figure 75. Two crowbar implementation strategies. a) two pairs of antiparallel connected thyristors and b) diode bridge and shorting controlled by thyristor. [4]

Operation level examples of active crowbar are given in [47]. The operation of crowbar can rely either on the rotor current or the DC-voltage, and the crowbar operates in case the control quantity reaches its instantaneous limit $I_{r,max}$ or $V_{dc,max}$. The limit values given in [47] are $I_{r,max}$ = 1.5 pu and $V_{dc,max}$ = 1.5 pu. It is not clear, however, on what these example limits are based on. Also in [48] 1.5 pu limit was used in simulations for both maximum rotor current and DC-voltage, where exceeding either limit was to activate the converter protection. It was also mentioned that the limits are dependent on the wind turbine capacity and converter rating. Wind turbine manufacturers do not seem to give the rotor current or DC-circuit voltage limits

for converter protection in their turbine brochures along with other information. It is not known if the voltage and current limit values are fixed and independent or dependent from the turbine rating or manufacturer, or in case the limits are set for each case individually based e.g. on connection grid characteristics.

4.5 Aerodynamics – Cp-characteristics

In section 3.2.4.2 it was concluded that the aerodynamic model of a fixed speed wind turbine is not necessary for power system dynamic studies in grid fault simulations. In case a pitch controlled wind turbine blade pitch is frozen during a grid fault taking place, the same aerodynamic model components can be used for variable speed wind turbines as used and presented in section 3.2.4.2. The variable speed wind turbine aerodynamic model can be based on the fixed speed wind turbine aerodynamic model described in section 3.2.4.2 with improvements. What makes the aerodynamic models for pitch controlled (or active stall controlled) wind turbines different, is the blade pitching, and its control. Also the initial operating point – or actually the Cp(β)-curves for those operating points are not as easily defined as for fixed speed wind turbines.

An important question is, how much the blade pitching can make a difference during and after a grid fault. If the pitching is very slow and insignificant, the fixed speed wind turbine aerodynamic model could be applied for variable speed wind turbines for a short enough time frame. In case the pitching is relatively quick considering the time frame being observed, the Cp-characteristics and thus the aerodynamic model of the variable speed wind turbine need to modeled more accurately. For normal operation studies the variable speed wind turbine aerodynamic model ought to be modeled properly.

The manufactures do not usually provide the pitch rate information on the turbine brochures. In scientific papers written by research parties, there are mentioned and /or used some pitch rates, such as +4 °/s and -0.7 °/s in [49], ±10 °/s in [50], 15 °/s in [51], ±5 °/s in [48], and in [52] is mentioned the maximum rate of change of the pitch angle to be in the order of 3 to 10 °/s depending on the turbine size. However, there are mentioned no sources of these figures. Manufacturer informs the pitch rate at safety shut-down to be 15 °/s for REpower MM82 2 MW pitch controlled wind turbine [53]. In [54] is stated that the physical limitation of pitch system is maximum pitch rate, which typical value is 8 °/s for an active stall wind turbine. In [54] a pitch rate of 15 °/s was also used along an argument that this value is deemed technically possible, and higher pitch rates seem unrealistic. [51] and [54] base their argument of using 15 °/s on [53], and the safety shut-down pitch rate limit. In [55] pitch rates from 4 °/s to 10 °/s were used in simulations. In a patent [56] for variable speed wind turbine generator the pitch rate is limited to 1 °/s. For FL 1500-70/65 1.5 MW wind turbine, the maximum pitch rate is 16 °/s [57].

Vestas OPTITIP (i.e. power optimization below the rated power) pitch system is capable of feathering the blades at even rate of 15 °/s depending on the turbine rotor speed [58]. Vestas OPTISLIP system at rated power allows the turbine speed to increase even 10 % before blade pitching. As gusts increase the turbine speed, OPTISLIP changes the generator rotor resistance, thus decreasing the torque and keeping the power constant [59].

Obviously wind turbine normal pitch rate is a quantity that is not easily revealed by the turbine manufacturers. Some manufacturers have provided maximum values for pitch rate, e.g. at safety shut-down, but these values most likely are not of magnitude of normal operation pitch rate. In addition to the fact that there is only some information regarding the

pitch rate of the turbines, it is not clear in what order of magnitude the turbine Cp value, or power, is to change by a degree change in pitch angle, or if that even is linear and independent of the turbine type/manufacturer.

In many more detailed models of DFIG equipped wind turbine model, the blade pitching is being modeled. Usually the turbine blade pitching characteristics are not known, and they vary from one turbine manufacturer to another, and also in terms of the turbine size. The manufacturer usually provides the turbine Cp-characteristics as function of wind speed, and this characteristic also vary from turbine to turbine. In Figure 76 is shown a collection of manufacturer provided Cp-curves of 1 MW size and larger variable speed wind turbines. [60][61]

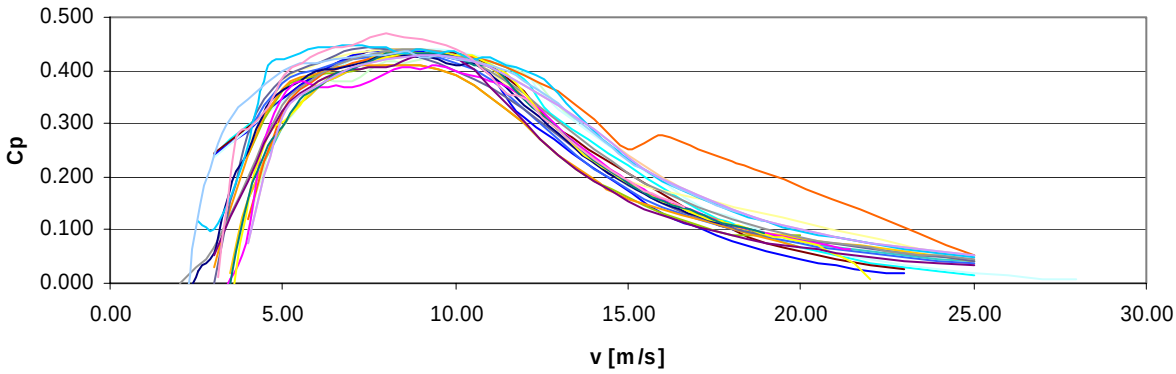

Figure 76. A collection of manufacturer provided Cp(v)-curves of variable speed wind turbines.

The Cp(v)-curves seem to be mainly in a tight group, but still not very tight considering that variable speed wind turbines are sensitive, first regarding their turbine speed control at lower wind speeds, and secondly the blade pitch control on nominal power at higher wind speeds. The provided Cp(v)-values are a set of operating points of the turbine, and no knowledge of the blade pitch angle – a function of which the Cp-value also is – is provided. Usually the Cp-curves, however, are roughly similar to each other, as can bee noticed from Figure 76. In case of a fixed speed wind turbine these manufacturer provided Cp-curves may be used (almost) as they are, as there is no blade pitching or speed control involved and the blade angle is constant.

In Figure 77 is shown the theoretical operating curves of fixed speed (passive stall and active stall) and variable speed wind turbines. Control strategy of variable speed wind turbines is turbine speed control and blade pitch control in order to obtain the optimal operating point at prevailing wind speed. The turbine speed is controlled at operating area before the nominal power, whereas the pitch control is not used and thus the turbine is operating at fixed pitch and variable speed. At low wind speeds providing $Cp(\omega,\beta_{const}) < Cp,max(\omega,\beta_{const})$, the speed is controlled to keep the tip speed ratio constant, and at higher wind speeds than providing Cp,max, the speed is controlled to maintain Cp,max and nominal power on as high wind speeds as possible until the maximum turbine speed. When operating at wind speeds corresponding to the nominal power and maximum turbine speed (constant), the turbine is controlled by blade pitching. The operation is then at fixed speed and variable pitch.

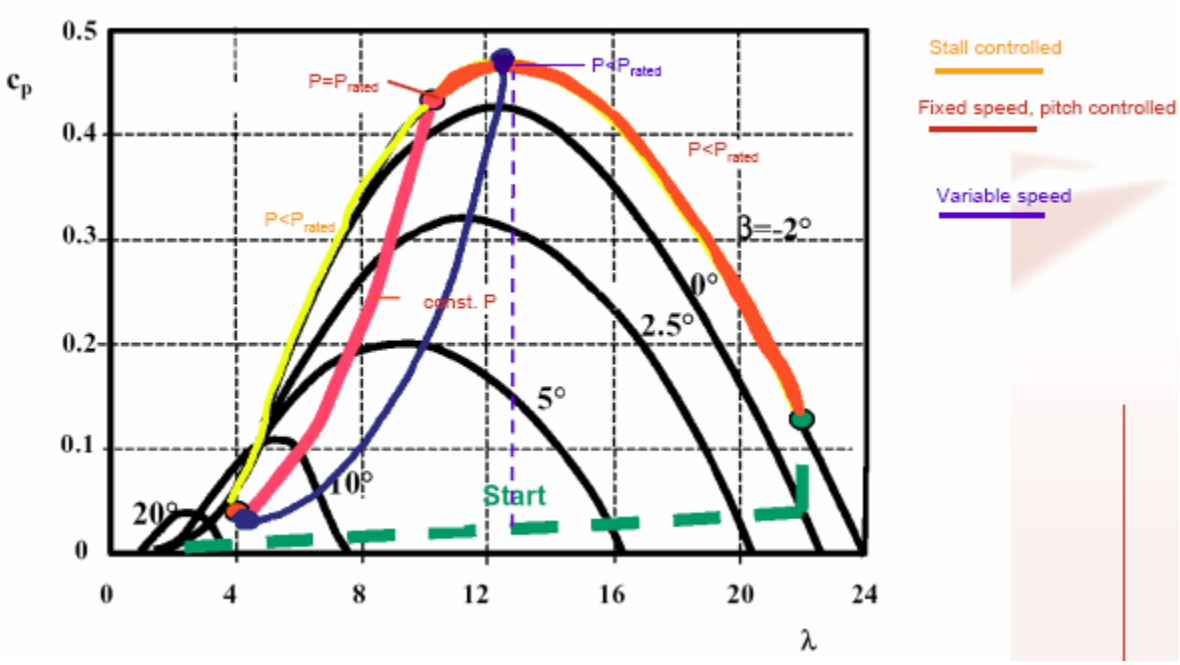

Figure 77. Wind turbine operation on Cp-characteristic curves – theoretical diagram. [62]

There are several methods how to define the generic Cp-characteristics for a turbine. The bases of wind turbine model in PSCAD/EMTDC is the equation [63]

$$Cp(\omega,\beta)=\frac{1}{2}\left(\gamma(\omega)-0.022\beta^2-5.6\right)e^{-0.17\gamma(\omega)}. \tag{4.20}$$

In [64] and [39] is used equation

$$C_p(\lambda,\beta)=\frac{1}{2}\left(\frac{RC_f}{\lambda}-0.022\beta-2\right)e^{-0.255\frac{RC_f}{\lambda}}, \tag{4.21}$$

where β is the pitch angle, λ tip speed ratio, R the turbine rotor radius and C_f the wind turbine blade design constant.

In [65] is used equation from [66]

$$C_p(\lambda,\beta)=0.22\left(\frac{116}{\lambda_i}-0.4\beta-5\right)\cdot e^{\frac{-12.5}{\lambda_i}}, \tag{4.22}$$

where, and λ_i is defined as function of blade pitch angle and tip speed ratio as

$$\frac{1}{\lambda_i}=\frac{1}{\lambda+0.08\beta}-\frac{0.035}{\beta^3+1}. \tag{4.23}$$

In [52], [2] some changes in coefficients in equation (4.22) have been done in order to match the manufacturer data better. The improved equation is

$$C_p=0.73\left(\frac{151}{\lambda_i}-0.58\beta-0.002\beta^{2.14}-13.2\right)e^{-\frac{18.4}{\lambda_i}}, \tag{4.24}$$

where

$$\frac{1}{\lambda_i}=\frac{1}{\lambda-0.02\beta}+\frac{0.003}{\beta^3+1}. \tag{4.25}$$

In [52] is also stated that it is not considered necessary to develop different approximations for the Cp(λ,θ) for different wind turbine types, as the differences between the wind turbine

types are rather small, and can be neglected in dynamic simulations. In case the Cp-curve estimation is needed to be done for fixed speed wind turbine, in [2] changes were done to the coefficients, and the above equation for fixed speed is given as

$$C_p = 0.44\left(\frac{125}{\lambda_i} - 6.94\right)e^{-\frac{16.5}{\lambda_i}}, \tag{4.26}$$

where

$$\frac{1}{\lambda_i} = \frac{1}{\lambda} + \frac{0.002}{\beta^3 + 1}. \tag{4.27}$$

Although there is the blade (pitch) angle in the above, it practically has no influence on the Cp-curve. Cp-curves calculated with equations (4.21), (4.22) and (4.26) for a certain fixed speed wind turbine are shown in Figure 78. The turbine has two operating modes, of which the low speed mode operates up to 250 kW production and the high-speed mode up to 1.3 MW. Fixed speed wind turbine is used as example case here as the Cp-curve is unambiguous compared to the provided Cp-curves of variable speed turbines.

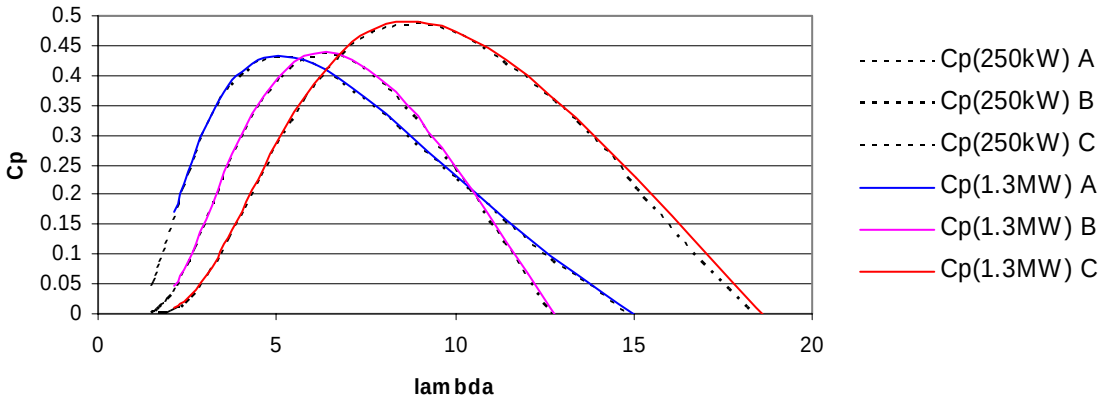

Figure 78. Cp-curves calculated with equations (4.21), A, (4.22), B and (4.26), C. The curves are calculated for both low speed and high speed operation modes.

In Figure 79 the equations and provided Cp-characteristics from three different sources [60][61][67] of the wind turbine are compared. As seen of previous Figure 78, the low-speed and high-speed modes produce overlapping Cp(λ)-curve when calculated by equations, and thus a single Cp(λ)-curve can be calculated of the provided turbine information (usually the Cp and active power data is given as a function of a set of wind speed points) and compared to either mode calculated Cp(λ)-curve.

In Figure 79 there is seen a difference in Cp-curves of the two speed-modes, as the left-hand side portion of a Cp-curve shape is the high speed-mode operation Cp-curve at the turbine high-speed operation range, and the right-hand side Cp-curve shape is the low speed operation mode characteristic. The "abnormality" at left-side of the low speed Cp-characteristic curve (it raises instead of falling at $\lambda \approx 8\ldots6$), which is the operating area just below the low speed-mode nominal power, can be explained to be due to the method of the Cp-characteristic value determination. The Cp-curves are determined for wind turbines as an average of multiple operating points calculated over 10 min operating average. During these 10 min periods at operating range close to the mode-switching area, there are most probably data points of both operating modes. If the left-most data points of the low speed-mode curve in Figure 79 were

calculated for the high-speed mode instead, the data points would line up nicely as expected continuing the high speed-mode Cp-curve to the right.

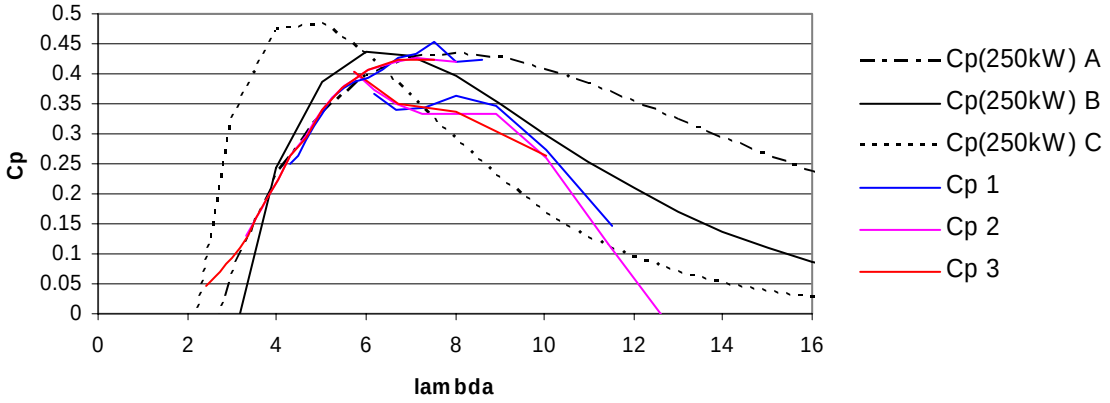

Figure 79. The calculated Cp-curves with equations (4.21), A, (4.22), B and (4.26), C compared to the provided Cp-data of a certain wind turbine from three different sources. There is seen a difference in Cp-curves of the two speed-modes, as the left-hand side portion of a Cp-curve shape is the high speed-mode operation Cp-curve at the turbine high-speed operation range, and the right-hand side Cp-curve shape is the low speed operation mode characteristic.

The Cp(λ)-curves calculated of the provided Cp-data are not smooth. This is because of the two-speed modes. As the Cp(λ)-curves calculated with the equations at both modes overlap, is was assumed that the provided data operating at <250 kW and >250 kW could be put on the same curve. Figure 80 shows that equation (4.22) i.e. curve B, gives the best correspondence. However, the tip speed ratio range (λ-range) over which the different wind turbines (regardless of the magnitude of the turbine rated power and more or less even the wind turbine control type) operate, varies a great deal from turbine to turbine. This can be seen in Figure 81 where the turbine operating λ-range of a selection of wind turbines from 11 manufacturers is plotted. The turbine rated power varies from 500 kW to 2.5 MW and the plots are in order of magnitude of the turbine rated power.

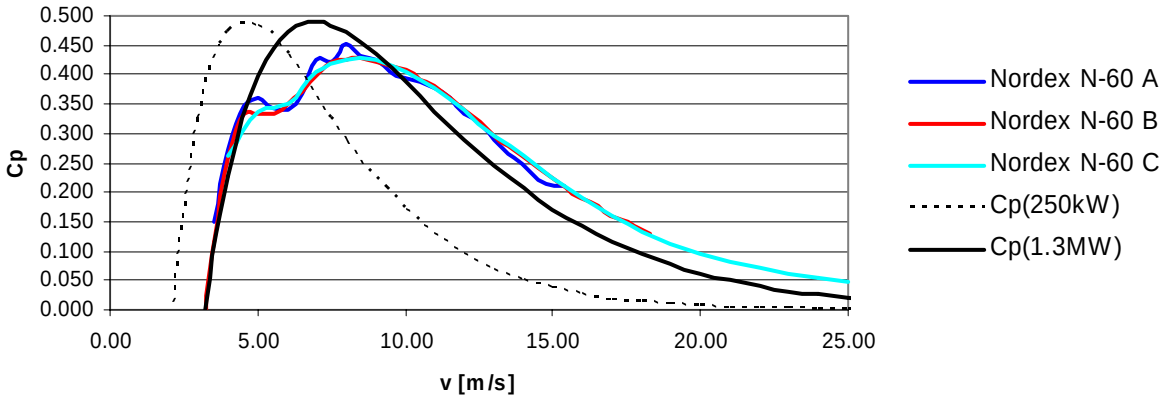

Figure 80. Cp(v)-correspondence of equation (4.22) with provided turbine Cp-data.

The λ-range shown in Figure 81 is defined based on the manufacturer provided information on their turbines and some catalogues [60][61]. All of the fixed speed wind turbines, i.e. (passive) stall and active stall control, shown in the figure have two speed-modes, of which low speed-mode characteristics (turbine speed) λ_{max} is calculated at smallest operating wind speed, and λ_{min} at high speed-mode at the highest wind speed. For variable speed wind turbines λ_{max} is calculated at minimum value of turbine speed range at the lowest operating wind speed, and λ_{min} at the maximum value of the turbine speed range at the maximum operating wind speed. These are just assumptions, as it is not certain if the turbines actually are programmed to be working at the maximum speed, as there might be left some safety margin and/or operating allowance needed by relatively slow pitch control [68].

In case of the fixed speed turbine, it seems to be justified to consider extreme λ-values calculated as above mentioned, as λ_{min} of the low speed-mode and the λ_{max} of high speed-mode are in between the values λ_{max} of the low speed mode and λ_{min} of the high speed mode as can be seen e.g. in Figure 79. The minimum tip speed ratio values of the turbines settle between values 2.41…5.06 regardless of the turbine control type or nominal power of the wind turbine. This is expected, as the limiting factor of the turbine blade tip speed is turbulence and noise. The maximum λ-values, however, are not as evenly distributed, ranging from 7.76 to 29.50. There seems to be no correlation between λ_{max} and either turbine nominal power or the turbine control strategy. However, the cut-in wind speed varies from turbine to turbine at which the λ_{max} are calculated. In Figure 82 the λ_{max}-values are plotted as function of cut-in wind speed, and a correlation is naturally seen there.

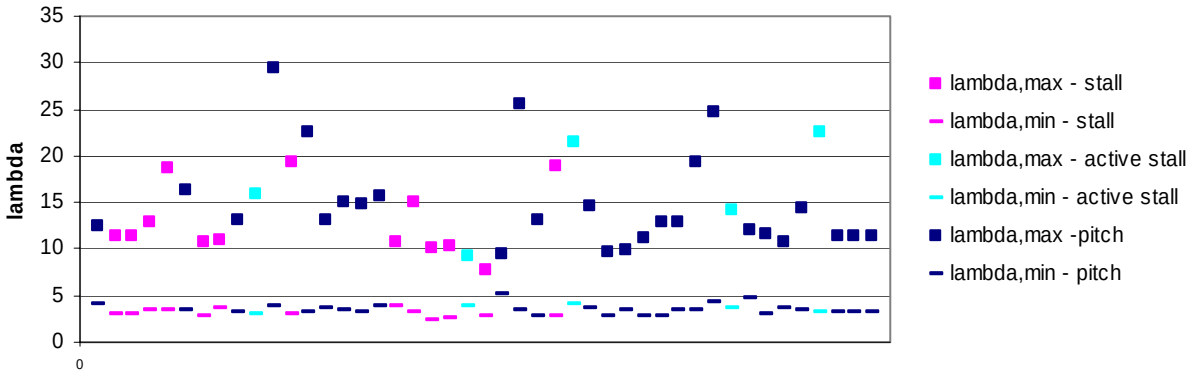

Figure 81. Tip-speed ratio (λ) calculated for a selection of different wind turbines sizing from 500 kW (the left-most data point) to 2.5 MW (the right-most data point, as the plots are in order of magnitude of the turbine rated power). For the (passive) stall controlled turbine the min and max values correspond to the smaller and higher speed modes of the two speed-modes of the fixed speed wind turbine.

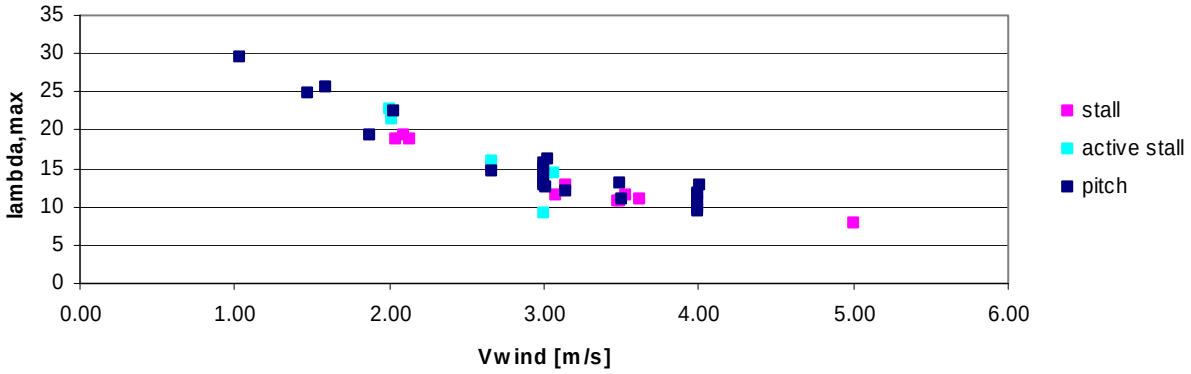

Figure 82. λ_{max}-values plotted as function of cut-in wind speed.

It ought to be remembered (see Figure 77) that the maximum tip speed ratio values of pitch controlled wind turbines are at Cp(λ_{max})=Cp,max, thus being located somewhere in the midsection of the largest Cp(β)-curve λ-span. The fixed speed wind turbine maximum tip speed ratio values are further close to the right-hand side end of the Cp-curve. In Figure 83 the maximum tip speed ratios of turbines are transposed to wind speed 1 m/s for comparison of the curves.

Variable speed wind turbine tip speed ratio is constant at small wind speeds, thus the data points in Figure 81 and Figure 83 are the same for pitch controlled, i.e. variable speed, wind turbines. Refer these variable speed plots as the λ-point of point Cp,max(λ, β). Fixed speed wind turbine, i.e. passive stall and active stall controlled wind turbines, tip speed ratio depends on the turbine speed, which is constant, and the wind speed. Fixed speed plots in Figure 83 are at the far right hand side of the Cp-curve at wind speed 1 m/s (refer to Figure 77).

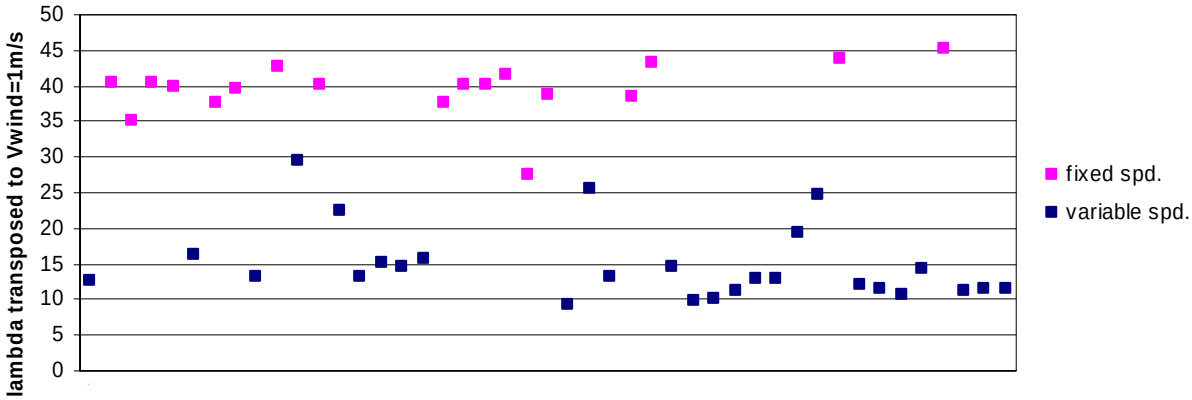

Figure 83. Tip speed ratio values of the turbines transposed to wind speed 1 m/s for comparison.

The plots in Figure 83 are in order of turbine nominal power, thus the most divergent plots not dependent on the turbine size, nor they are dependent on the manufacturer. Of Figure 83 can be concluded that not all wind turbines – not even if considered by their control strategy – can be characterized by a single one Cp-curve characteristic. This should be remembered especially in wind turbine model validation against measurements, but in generic wind turbine models a single Cp-characteristic could probably be used after defining it.

4.6 Control strategies

The control strategies of variable speed wind turbines vary by the turbine manufacturer and are business secrets. In [2] the operation principle of variable-speed wind turbine speed control is describes. The set point of power is derived using characteristic relationship between rotor speed (measured at sampling frequency of order of 20 Hz) and power. The torque set point is defined by power and rotor speed, of which again the current set point is derived. In most cases the speed is controlled to obtain the optimal energy. In Figure 3 shown earlier, the solid line represents the $P(\omega)$-curve of optimal energy.

At low wind speeds the generator torque is adjusted and the speed is kept in minimum value. At some higher wind speeds the tip speed ratio is kept constant/optimum and thus the speed varies. As the speed has reached its nominal value, at high wind speeds the rotor speed is kept at its maximum value and when the nominal power has been reached as well, it also is kept in nominal value (by blade pitching). The practical problem here is according to [2] that the speed may experience slight changes, and if it chances from operation point slightly above nominal speed to slightly below, or from slightly above minimum speed to slightly below it, the changes in power are very large. In [2], a control characteristic that leads to optimal energy capture, is used and shown as dotted line in Figure 3. The area in which the used control characteristic deviates from the optimal solid characteristic line, is a design choice. Under the above mentioned circumstances, it is probable that the variable speed wind turbine characteristics are not strictly based on optimum energy capture, but more or less a variety of different modifications of the optimal energy capture characteristics.

As mentioned earlier, it is not clear how much a degree change in pitch angle makes difference in the Cp value, or the power output. In Figure 84 the relationship between the wind speed and DFIG wind turbine pitch angle is shown. The source of the curve was not mentioned in [48] or if the relationship applies to all the turbine types/manufacturers and turbine sizes, or for which ones it applies to.

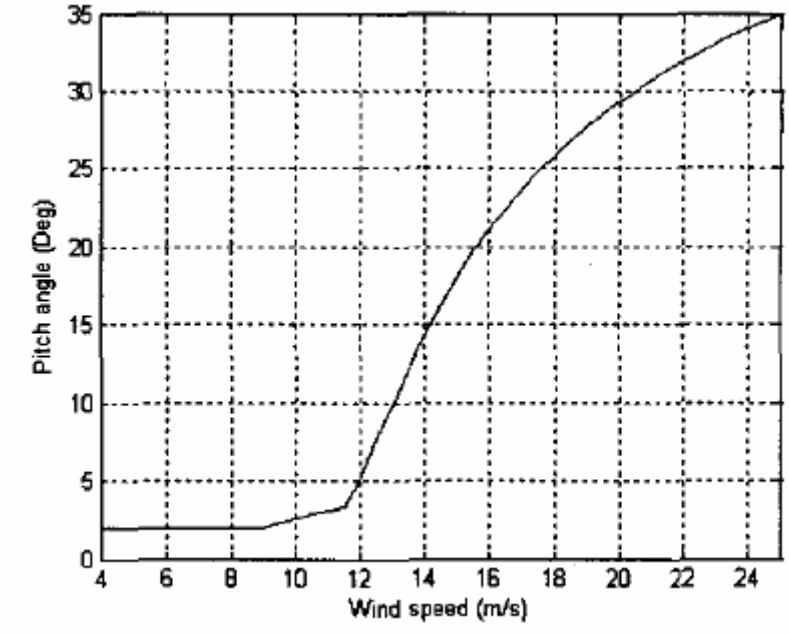

Figure 84. The relationship between pitch angle and wind speed of the DFIG wind turbine. [48]

The *Fixed Speed Wind Turbine*-component could probably be extended to variable speed wind turbine component by making some modifications. The approach which should be taken in most correct Cp-characteristic representation in the component is not very clear.

Earlier it was seen that there are several Cp-equations, which differ from each other, as well as do the actual variable speed wind turbine Cp-operational curves provided by the turbine manufactures. Thus, a single equation can not be used universally. And as the manufacturer provided Cp-curves are operational curves of which even the blade pitch angle is not known in each operation point, it is not possible to employ these curves directly as for fixed speed wind turbines.

The blade pitch would need to be modeled separately as well, instead of letting it be included in the Cp-characteristic curve. In case of fast changes, e.g. a grid fault, the turbine will experience a rapid change in speed, for which the blade pitch may not be fast enough to respond. Thus, the turbine should follow the Cp-curve of constant blade pitch angle at this operating point.

The fixed speed wind turbine aerodynamic modeling with a Cp-curve studied in section 3.2.4.2 did not give any additional value to simulation results. The speed range of DFIG equipped turbines is much larger than that of fixed speed wind turbine. It should therefore at least be investigated, if modeling the aerodynamics would make more difference in variable speed wind turbines than in fixed speed turbines.

4.7 DFIG-models for PSCAD/EMTDC

There are no DFIG models in PSCAD/EMTDC standard component library. Nor there are many other publicly available models (for PSCAD/EMTDC) either. In UMIST webpages there has been available a DFIG model for both Matlab/Simulink and PSCAD/EMTDC [69]. In the Finnish research project Simulointiympäristö, there was developed also a DFIG model for PSCAD/EMTDC [70]. The DFIG model is in HElib-model library [71], which VTT has access and partial ownership to.

4.7.1 Literature on DFIG-modeling for PSCAD/EMTDC

In [48] simulations on a PSCAD/EMTDC-DFIG-model were analyzed. The model used was built using the standard electrical-components from PSCAE/EMTDC component library, and the wind speed, aerodynamic and mechanical models as well as the control components were built with custom components developed in PSCAD.

The wind model in [48] is a two layer model with first park scale wind model simulating the wind speed at hub height at each wind turbine, and secondly a rotor wind model which includes the influence of rotational sampling and integration of along the wind turbine blades as the blades are rotating. The wind model provides an equivalent wind speed for each turbine to be used as input to a simplified aerodynamic model of the turbine. The aerodynamic model is based on the same power equation as the aerodynamic component described in section 3.2.4.2. The Cp-curve is defined in the model by equation (4.22). The wind speed- and aerodynamic-models seem to be quite alike with the models developed and described in section 3.2.4.2 for a fixed speed wind turbine.

Modeling of the mechanics in [48] is done by a single mass model swing equation. The generator is modeled using a standard library wound rotor induction machine component, and

the back-to-back PWM voltage source converter is “an ideal model based on energy conservation principle” described in [72]. Both control stages, speed control and pitch control, of DFIG-turbine are modeled. Also active crowbar is implemented in the model.

4.7.2 UMIST-model

The DFIG-model released at UMIST (University of Manchester) website (described in [73], and model itself in [69]) consists of *Wound Rotor Induction Machine*-component, of which the rotor circuit is fed by three *Single Phase Voltage Source*-components. (See Figure 85) The rotor circuit voltage sources are controlled. This modeling configuration is rather simplified. There are no power converters of rotor circuit modeled, nor there is any connection from rotor circuit to the grid, and instead all the power transmitted to (and from) the grid is via stator circuit.

In an actual DFIG machine up to some 30 % of the power is fed through the rotor circuit as discussed earlier in chapter 3.2. The power fed through the rotor circuit is dependent on the slip and stator circuit power. A question is, thus, is it, and how it is, possible for the model to operate correctly, corresponding to an actual DFIG-machine without connection from rotor circuit to the grid.

The PSCAD/EMTDC simulations are usually started flat, or they at least need to be initialized (simulated) to a certain point of which a snapshot can be taken that would be used as initial situation in further simulations. The UMIST-model needs about 50 s simulation period to reach a somewhat stable operating point. Although the model itself does not include very heavy calculations, it could take quite a while to initialize the simulation when the model is connected to e.g. system model consisting of more complex and multiple components, and thus heavier calculations.

The UMIST-model is shown in Figure 85. The control scheme in the model is a bit different than illustrated in [73]. There is in the model, for example, a *Rotor Crowbar*-component which is not mentioned in [73].

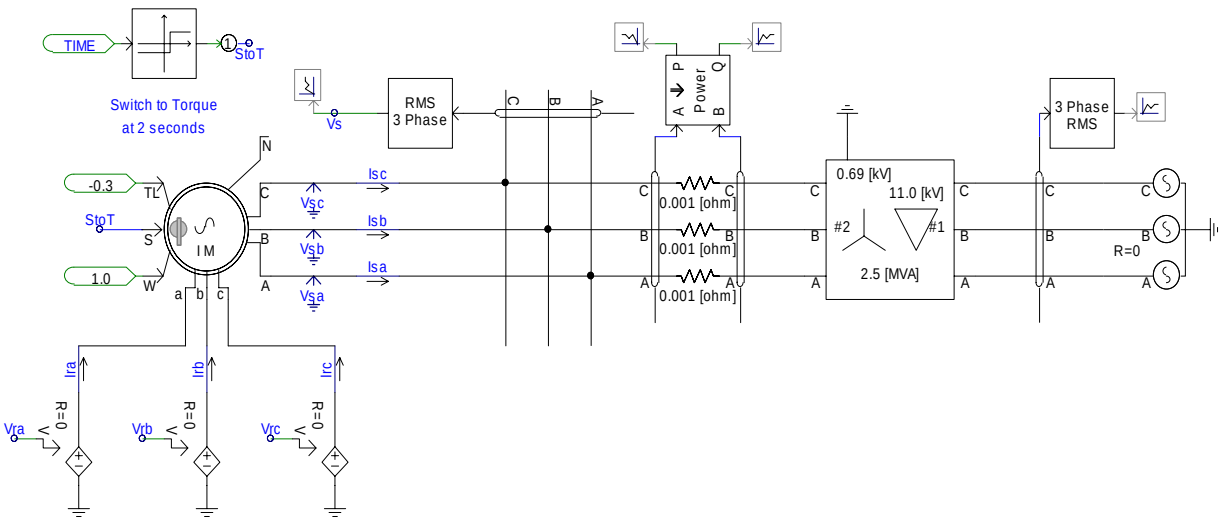

Figure 85. The UMISD-DFIG-model.

A similar simulation to what was described and graphs provided of in [73] was performed. The generator was first run at torque 0.3 pu and at t = 40 s, the torque was changed to 0.8 pu. At t = 60 s a fault occurred. Somewhat similar results were obtained, although not all the used

parameters were known. In this simulation case the crowbar did not operate. When producing a fault with smaller fault resistance and thus a larger voltage dip at generator terminals, the model crowbar operates. Although the fault duration is 100 ms, the generator terminal voltage remains on a low level for several seconds (see Figure 86). The crowbar in the model is obviously of passive type – remaining in operation for the rest of the simulation period although not disconnecting the generator from the grid.

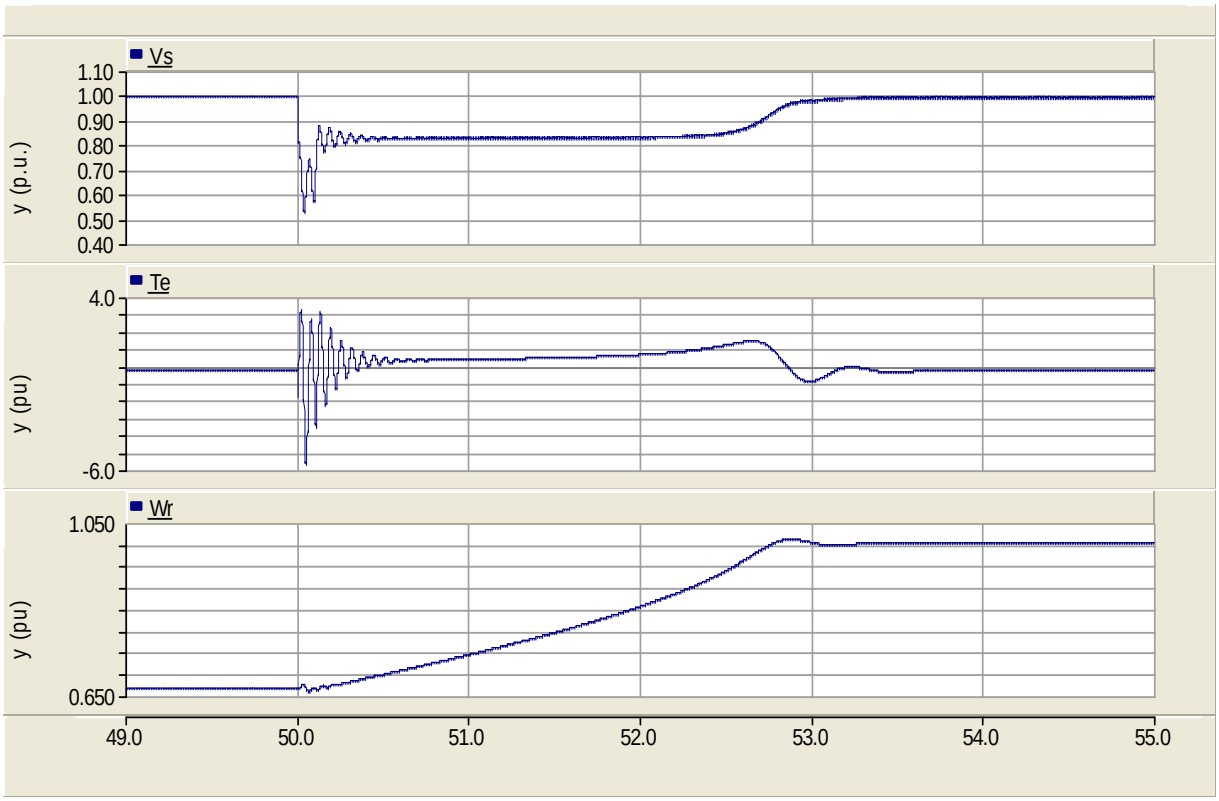

Figure 86. UMIST-model simulation of a fault of 100 ms duration. Generator terminal voltage, electrical torque and rotor speed response.

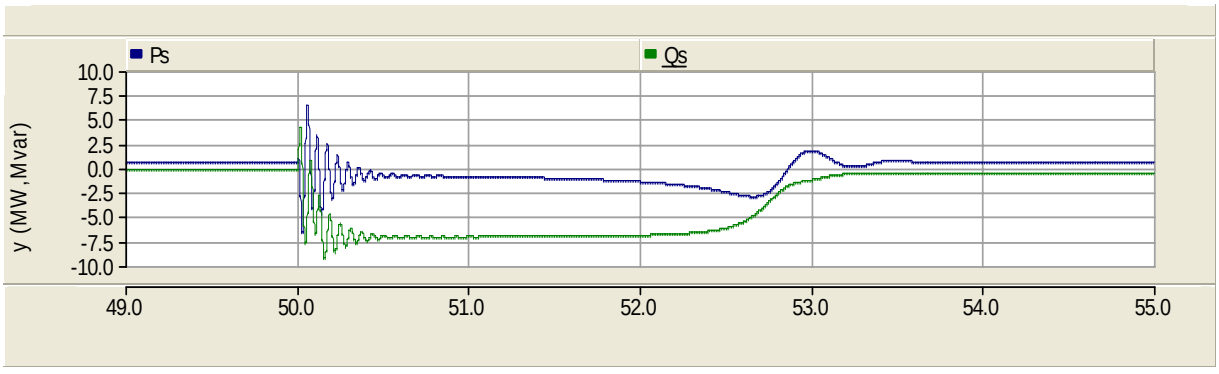

Figure 87. UMIST-model simulation of a fault of 100 ms duration. Generator (stator) active and reactive power response.

The model does not have a *Multi-Mass*-component, and it is a single mass model. Adding multi-mass with flexible shaft to the model makes the rotor speed increase constantly without reaching a stable operating point. Thus multi-mass was not added and included in the simulation studies.

The low voltage at generator terminals and other variable exceptional values after the fault are probably due to the crowbar operation and rotor short circuiting, as no similar response was seen in case of a milder fault when the crowbar did not operate. In simulations in [48] somewhat similar curve forms were inspected, especially those of voltage and reactive power. The low voltage and large negative value of reactive power after the fault clearing was explained to be caused by high inrush current which is drawn from the grid by the turbine trying to recover the air-gap flux. The lowered voltage and large reactive power absorption lasted about 4 s.

In the *Rotor Crowbar*-component, there is *Current Limit* as a parameter which can be changed in order to change the crowbar operation sensitivity. In Figure 88 and Figure 89 are shown simulation results of the same fault as above, but the crowbar current limit was increased in such a value that the crowbar does not operate. It is not, however, desired for the DFIG converters to operate during large voltage dips (refer to section 4.4).

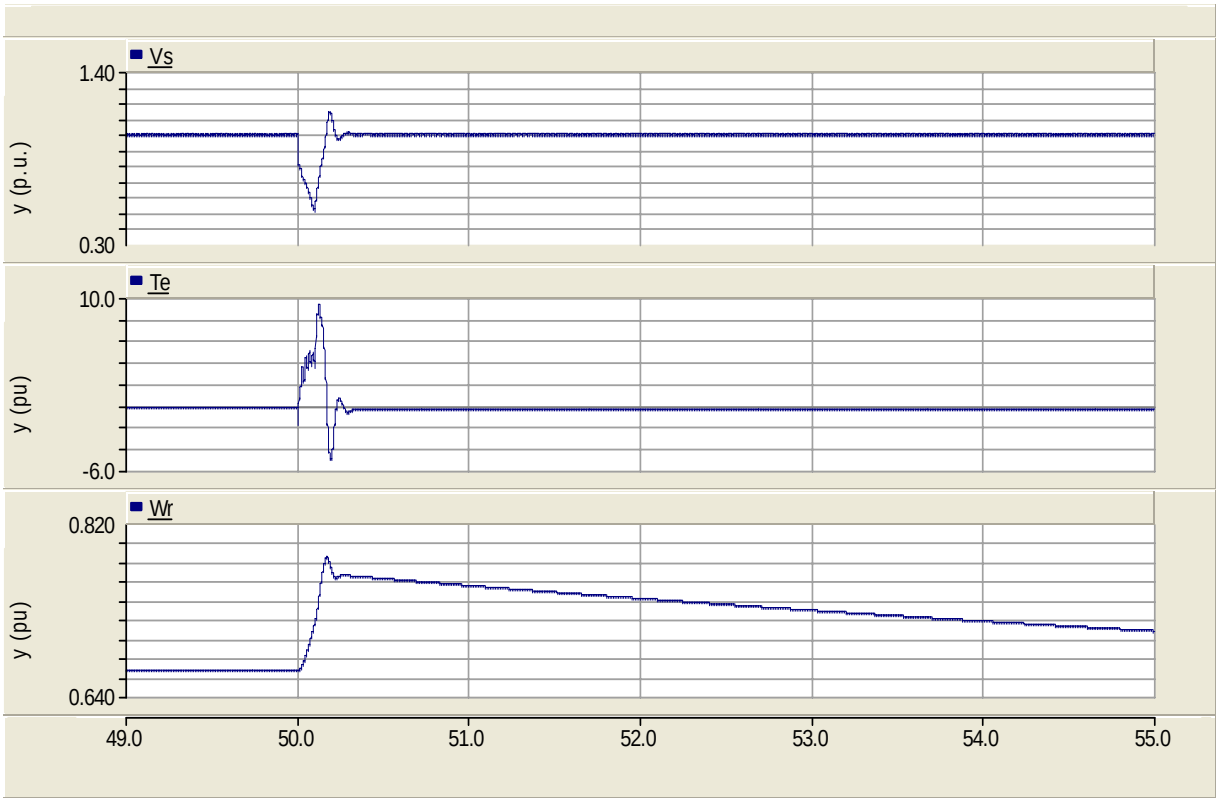

Figure 88. UMIST-model simulation of a fault of 100 ms duration, crowbar current limit increased, thus preventing crowbar operation. Generator terminal voltage, electrical torque and rotor speed response.

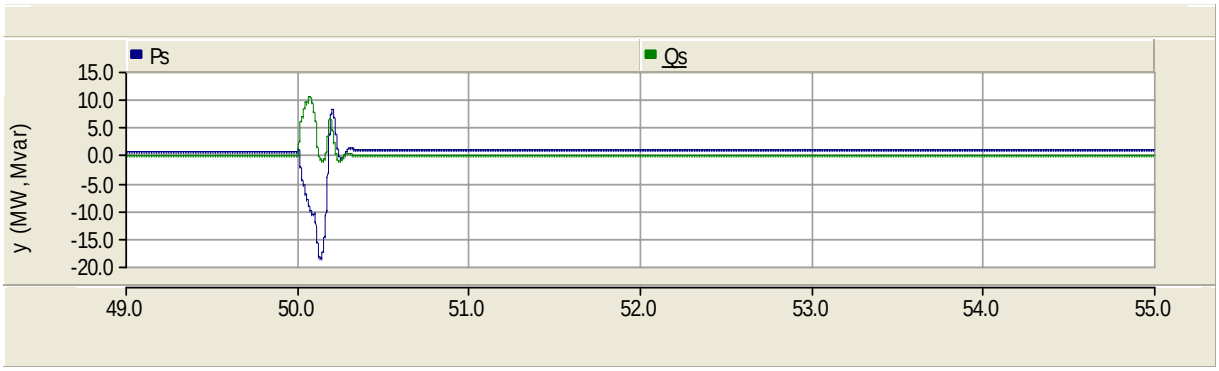

Figure 89. UMIST-model simulation of a fault of 100 ms duration, crowbar current limit increased, thus preventing crowbar operation. Generator (stator) active and reactive power response.

In [69] there is also a Matlab/Simulink model available that provides similar kind of results with the PSCAD/EMTDC model [73]. A Matlab/Simulink model of DFIG is also available in [74].

4.7.3 The HElib-model

The model being validated is based on the DFIG-model in the HElib-library. The library is available to Finnish institutions and companies through licensing and a fee. The HElib-model library administrator is the University of Vaasa.

The HElib-library DFIG-model has not been validated against measurements. The DFIG-model with parameters is provided at two power levels, at 1 MW and 2 MW [75]. It is not mentioned in the model documentation if the models and their parameter values are based on some actual wind turbines. The model consists of the wound rotor induction generator component, the converter bridge and the controls for the converters. The model is a single mass model with no *Multi-Mass*-component included, and it assumes constant torque, and the blade pitching is not modeled. The model can be run either speed control or torque control mode. In the model, the user must set also the active and reactive power control values. The model is described in more detail in [75].

The DFIG-model converter control schemes according to project leader were based on DigSILENT DFIG-model. The control is a scheme consisting of PI-controllers which produce d,q-reference frame voltage values of controlling (set/desired) active and reactive power values.

In the HElib-model there are Pset and Qset-values which the user defines. Also the torque to the generator is determined separately. There is one more 1 MW DFIG-model where the torque and active power reference value are defined based on the user defined wind speed.

Some modifications, were done or were tried with the original DFIG-model;

- *Multi-Mass*-component was added, and the turbine mechanics were presented as a two-mass model, as recommended in [9]. The aerodynamics were still omitted by assuming a constant torque.
- The parameters of a 850 kW turbine were used for the 1 MW turbine model.
- For validation purposes, the voltage source component was replaced with measured voltage input components in order to be able to perform model validation simulations.

The control scheme parameter value tuning was mentioned above to be possibly difficult. When changing the 1 MW model to 850 kW model, the model performance was not the same as with 1 MW model, although the only parameters apparently, that should be needed to be changed, were the generator rating and possibly the converter circuit component (capacitances, inductance and resistances given in SI-units) values.

The model is controlled either by speed or torque. The DFIG is used in variable speed wind turbines, where the generator speed varies firstly by the operating point, and secondly by letting the speed vary, the output power (active and reactive) can be kept smoother and closer to constant. The DFIG operating speed range is in addition very large from sub-synchronous to super-synchronous as mentioned in section. Thus, rotor speed control, either constant speed of somehow controlled, seems to make some of the DFIG machine characteristics to disappear.

Also adding multi-mass confused the simulations. In simulations with multi-mass modeled with flexible shaft, the rotor circuit speed did not find a stable operating level and instead increased.

4.8 Model validation

4.8.1 HElib-model – measured voltage input

Using measured voltage as input in DFIG simulation seems to be a bit more challenging than in case of a fixed speed wind turbine due to the presence of the power electronics and their control.

The model was expanded to 2-mass model with appropriate estimated parameter values. It seems, however, that the single-mass representation gives better correspondence to measurements. This, on the other hand, does not prove that the model is more correct as a single-mass representation with no aerodynamic properties modeled, nor that its control is correct as will be demonstrated ahead.

It is suggested, that in order to perform a reliable validation for a model, measurements should be available also on rotor circuit of the generator, behind the converters. The power electronic converter model controls are set such that they will absorb from or feed to the rotor circuit a certain power – active and/or reactive – according to its control strategy. Thus the rotor circuit phenomena are kind of in a black box. If the model is validated at some operation point of which measurements are available, due to the blackbox nature, one can not be certain that the model operates correctly at another operation point – as it is not known if the rotor circuit operated correctly even in the validation operation point.

Measured voltage was used as input to simulation. In Figure 90 a single phase rms-voltage at the generator terminal of measurement and simulation are shown in case of a symmetrical fault. The voltages of 2-mass and 1-mass simulations are overlapping. The reason for ripple in calculated rms-voltage of measurement not known. In Figure 91 and Figure 92 the active and reactive power of simulations are compared to the ones calculates of the measurements.

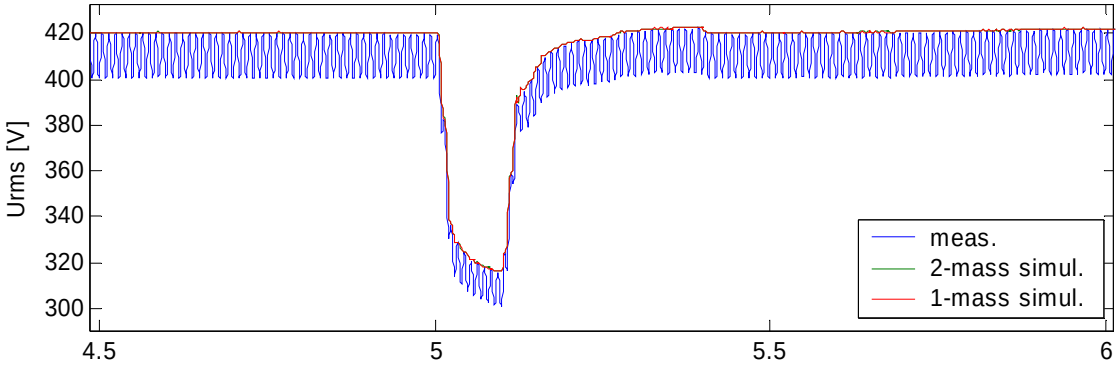

Figure 90. Calculated rms-values of a phase voltage. Measured voltages were used as input to simulation. Comparison of 2-mass model and 1-mass model simulation to measurement.

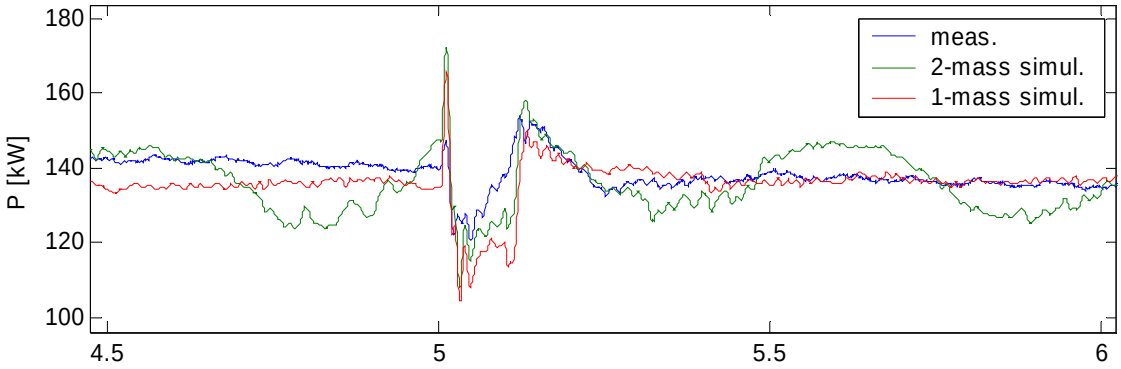

Figure 91. Active power of 2-mass and 1-mass model simulations compared to the active power calculated of measurement.

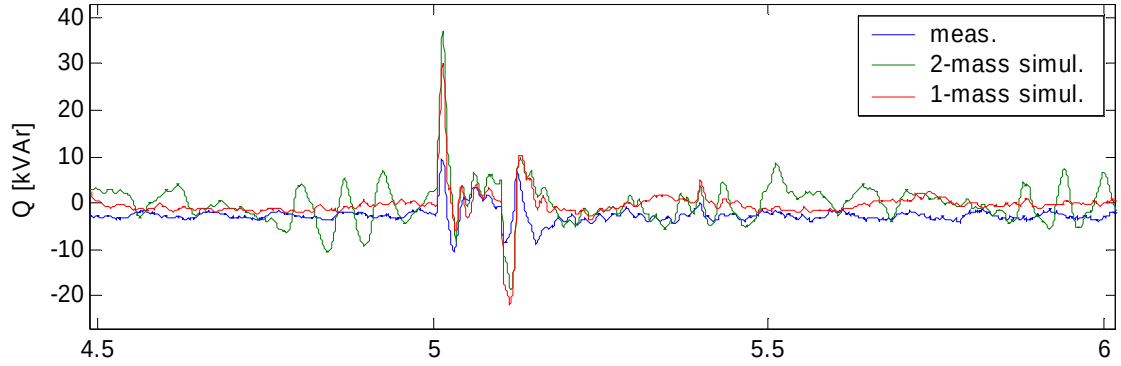

Figure 92. Reactive power of 2-mass and 1-mass model simulations compared to the reactive power calculated of measurement.

Based on simulation results in Figure 91 and Figure 92, it seems that the single mass model gives better correspondence. What is happening behind the rotor circuit is not included in the measurements. Thus, accuracy of the models can not be fully evaluated. Therefore, the model is proven, in some extent, to be suitable for power system studies for this particular wind turbine and for the area of operation of approximately 0.14 pu. No analysis of the generator variable behavior beyond the generator terminal voltage, and output active and reactive power to grid, should be done without further knowledge of actual DFIG behavior regarding the issues wished to be analyzed. Thus, as the behavior of the generator is sort of black-box type

at this stage, it could be that the model behaves differently at different operating stages than the one simulated here, e.g. close to nominal power when the machine is operating very close to its limits.

The DFIG-model simulation starts without rotor converter operation as the simulation starts always from flat, and the rotor side converters are turned on e.g. 1 s after the beginning of the simulation run. After switching on the converters, it takes about one more second to reach the set P and Q values (so called stable operating point).

The events or phenomenon taking place on the rotor circuit of the DFIG-model during simulation are not very assuring of the overall operation of the model although from the grid side it seems good. In Figure 93 is shown rotor speed from simulation with measured voltage used as input on the same observation period as a phase voltage at machine terminal, and active and reactive power output to the grid. In Figure 94 the generator rotor speed over the whole simulation period is shown. The frequency of rotor speed oscillation is 50 Hz. The rotor speed variation in this manner does not seem correct or reasonable. The rotor speed should probably also have obtained a steady state operation point.

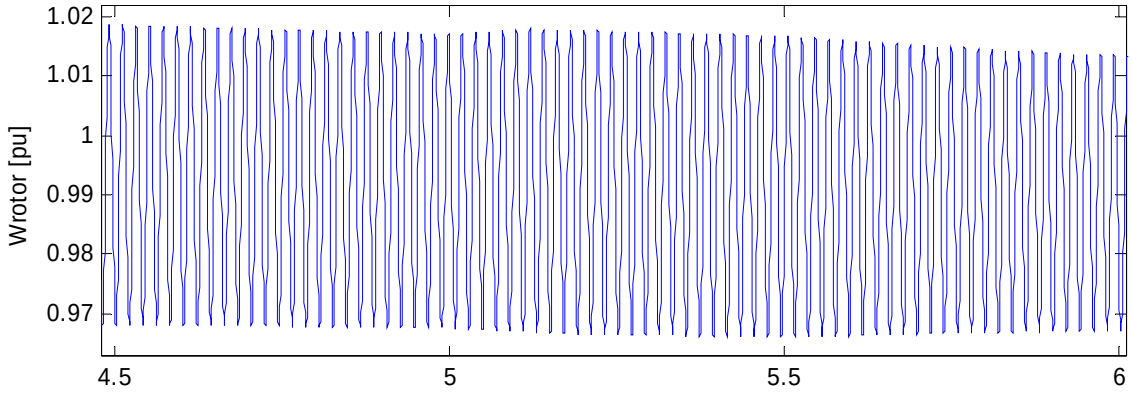

Figure 93. The generator rotor speed output of 1-mass model with measured voltage input used in simulation. Corresponds to the simulation and timeframe of which the previous V, P and Q curves above are taken.

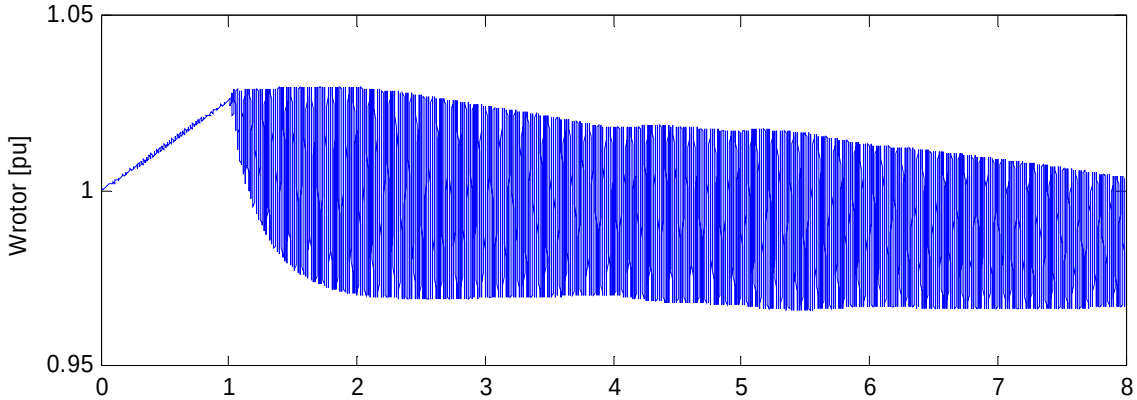

Figure 94. The generator rotor speed output of 1-mass model with measured voltage input used in simulation. Corresponds to the simulation of which the previous V, P and Q curves above are taken, and showing the whole simulation period.

Simulations were done also with a voltage source and an artificial fault creating a voltage dip. In Figure 95 is shown the active power of simulation and measurement, and in Figure 96 the reactive power of simulation and measurement. The generator speed is shown in Figure 97.

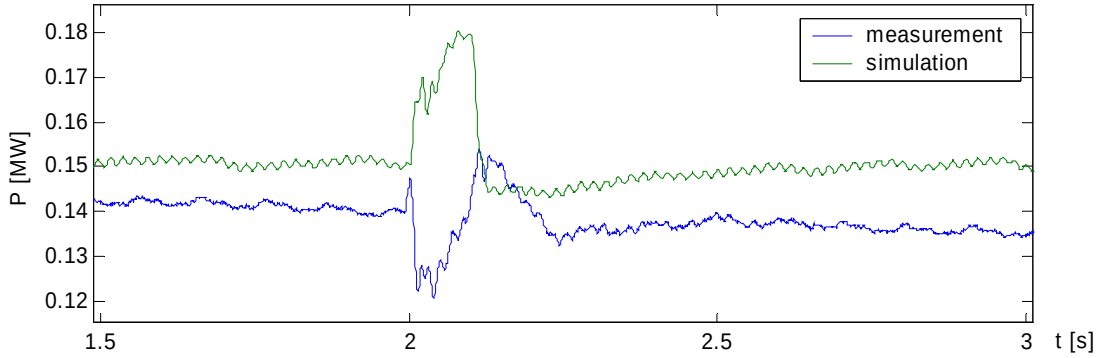

Figure 95. Active power comparison of simulation with 1-mass model with voltage source used in simulation. The input mechanical torque corresponds to the same value as used in above simulation with measured voltage used as input.

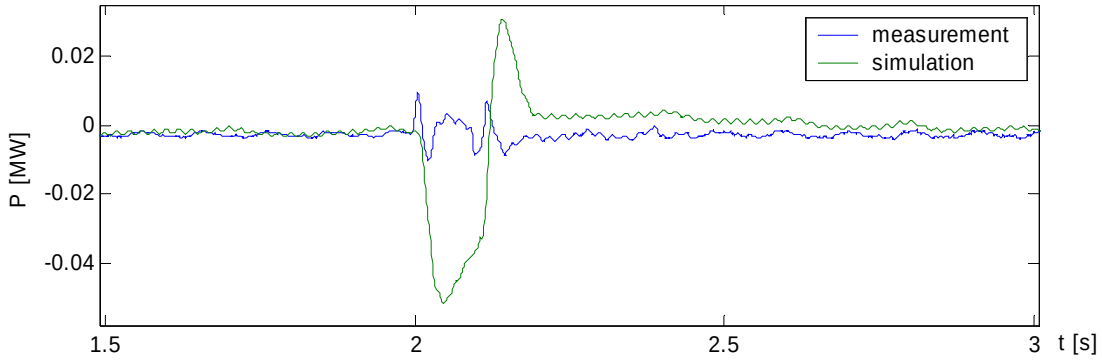

Figure 96. Reactive power comparison of simulation with 1-mass model with voltage source used in simulation. The input mechanical torque corresponds to the same value as used in above simulation with measured voltage used as input.

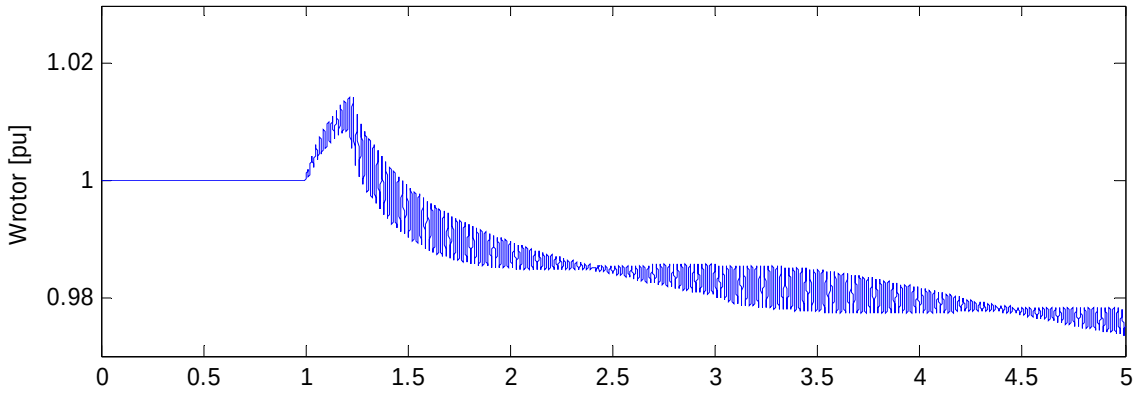

Figure 97. The generator rotor speed output of 1-mass model with voltage source used in simulation. The simulation corresponds to the same power output as in above simulation with measured voltage used as input.

The above shown figures of active power and reactive power in the voltage source simulations differ from measurement much more than in the simulation with measured voltage used as input to simulation. This might be due to the fact, that the DFIG model includes active control of the converters, and thus the power output. In case of a fixed speed wind turbine, there were no active parameters or controls, and thus the measured voltage could easily be used as input to simulation, and the model was forced to adjust to the voltage. I.e. if the generator would have wanted to change the voltage, current instead must change as the voltage cannot. In case of a DFIG model, there is the converter control circuit that does control actions based on the situation. Thus it might not be valid to use measured voltage as input to simulation of a DFIG machine. The same conclusion on the same bases can be done for full converter models.

The above simulations were done on modified model (generator parameters changed, multi-mass, although with stiff shaft, added and crowbar removed etc.). When performing a simulation with original model with no changes, and running the simulation with moment control, the generator speed does not necessarily behave like above and instead shows much nicer curves and reaches constant value in normal operation. The active power, however, may not reach, or even exceeds the active power without returning to set value. It seems that the reactive power is more likely to reach set value (very small) than active power. Active power of a turbine depends on mechanical torque. Thus, it might be good idea to control the active power control value of the model by the value of the mechanical torque. Three controllable parameters seem to be quite much, as they are not even independent from each other.

Identical simulations on original model with only slightly differing torque show the interdependency and the need of linking the torque and active power. In case the torque is slightly too large compared to desired active power (or apparent power), speed of the generator will increase. In an opposite case with slightly too small torque, the rotor speed increases. It is not easy to obtain the absolute correct value to maintain speed constant.

In the simulations the P_{set} was 0.5 MW, Q_{set} 0.0 MVAr and the mechanical torque was 0.49, 0.50 and 0.51 pu. On Figure 98 and Figure 99 are shown the active and reactive power output of the generator. After the first second of simulation when the rotor side converter is turned on, the reactive power reaches, and remains in the set value, but the active power kind of breaks to a new value after a couple of seconds. This is explained by generator speed shown in Figure 100. The speed does not reach a stable point in any of the three simulation cases. Instead, the speed in simulations where torque is 0.50 and 0.51 pu, increases until some point and the increase is faster with the larger torque. In simulation with 0.49 pu torque, the speed decreases until some point. The active power “breaks” to a new value at the same time as the speed stops increasing or decreasing. The model is somewhat unstable, and the torque control, and active power control needs to be linked together somehow, although they are really constant set values even in these simulations. Correlation between torque, active power and speed is

$$T = \frac{P}{\omega}. \tag{4.28}$$

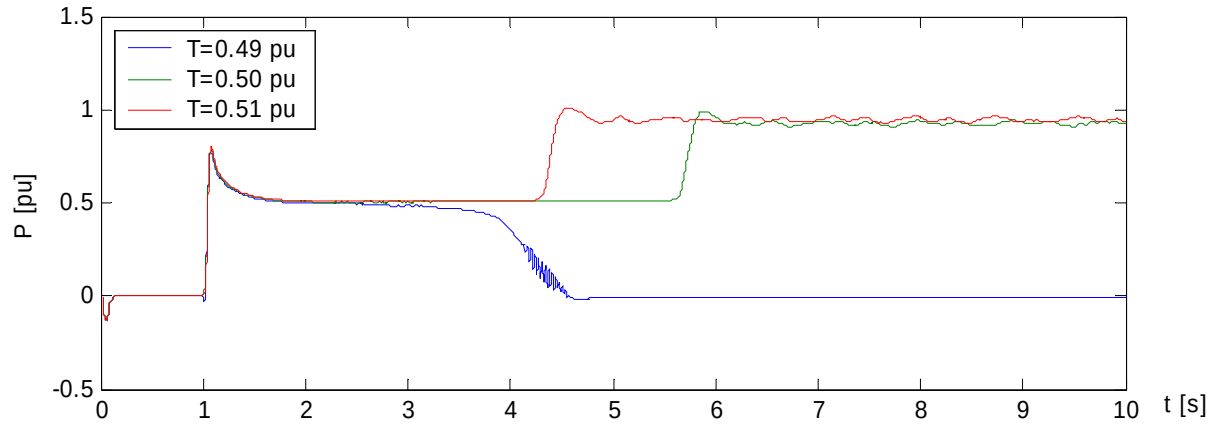

Figure 98. Active power of three normal operation simulations with slightly differing mechanical torque. Rotor side converter turned on after 1 s.

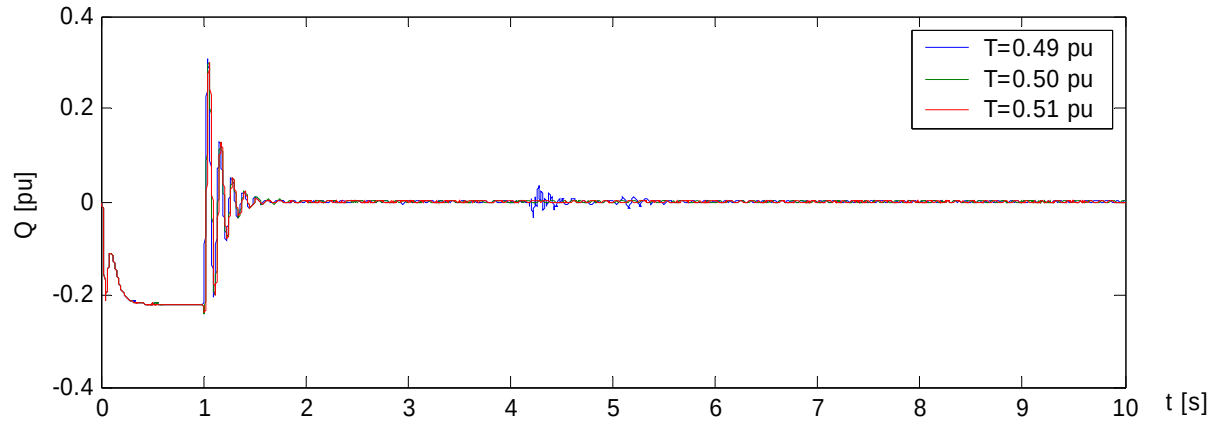

Figure 99. Reactive power of three normal operation simulations with slightly differing mechanical torque. Rotor side converter turned on after 1 s.

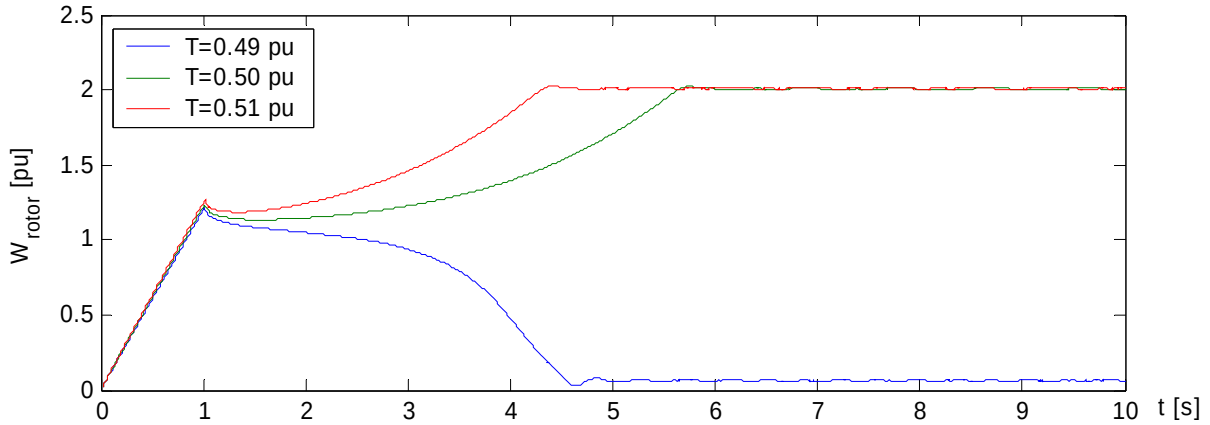

Figure 100. Rotor speed of three normal operation simulations with slightly differing mechanical torque. Rotor side converter turned on after 1 s.

In one model named *pscadvindmodel.psc*, P_{set} is eliminated as the wind power is modeled as a function of wind speed and turbine characteristic (rotor radius and $T\omega$- and $P\omega$-relationship), and a constant Cp-value. *pscadvindmodel.psc* is also a model in the HELib-library. It was

stated in [75] that the simulations with the wind model are not realistic, as the inertia is not included. It was also stated about the models in general, that it is difficult to get the control parameters tuned, and that the grid impedance has a great influence on controller operation and when changing the grid impedance, the control parameter tuning musty be done again. Simulation results with constant wind speed on model *pscadvindmodel.psc* are shown in Figure 101, Figure 102 and Figure 103. The converters are connected from the beginning of the simulation. Both, the active and reactive power seem to reach and maintain the steady state value quite nicely, as does the rotor speed as well.

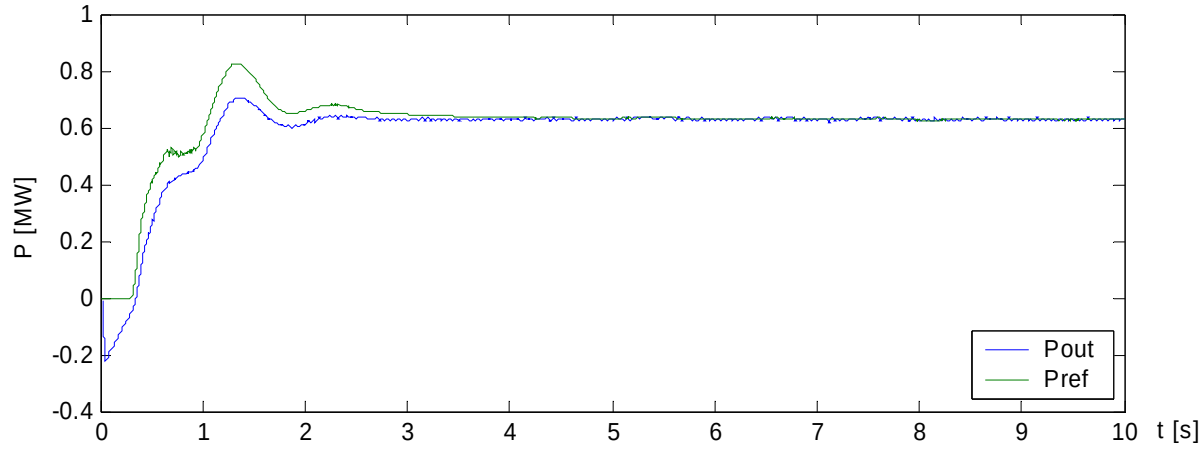

Figure 101. Active power output and reference value in simulation with constant wind speed to wind power equation.

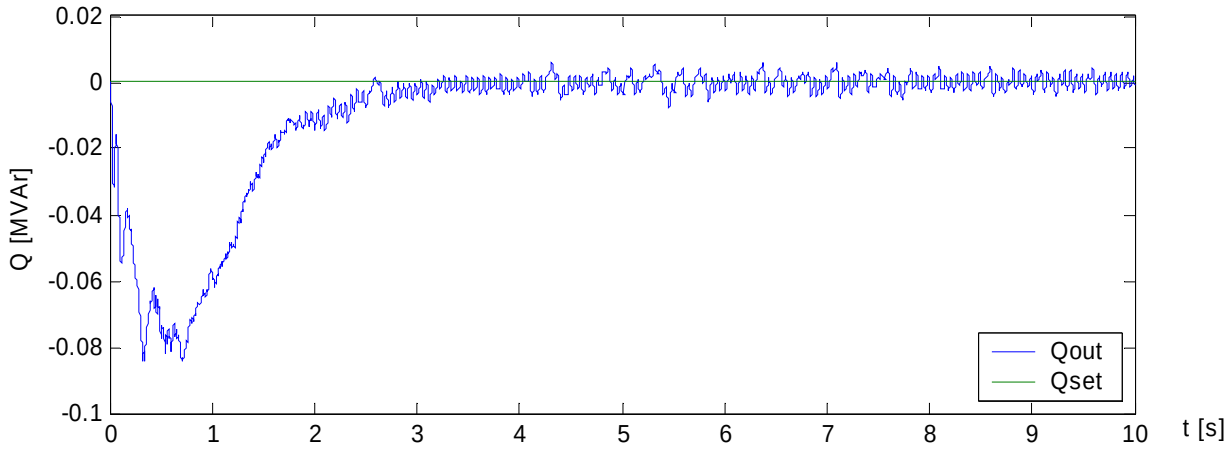

Figure 102. Reactive power output and reference value in simulation with constant wind speed to wind power equation.

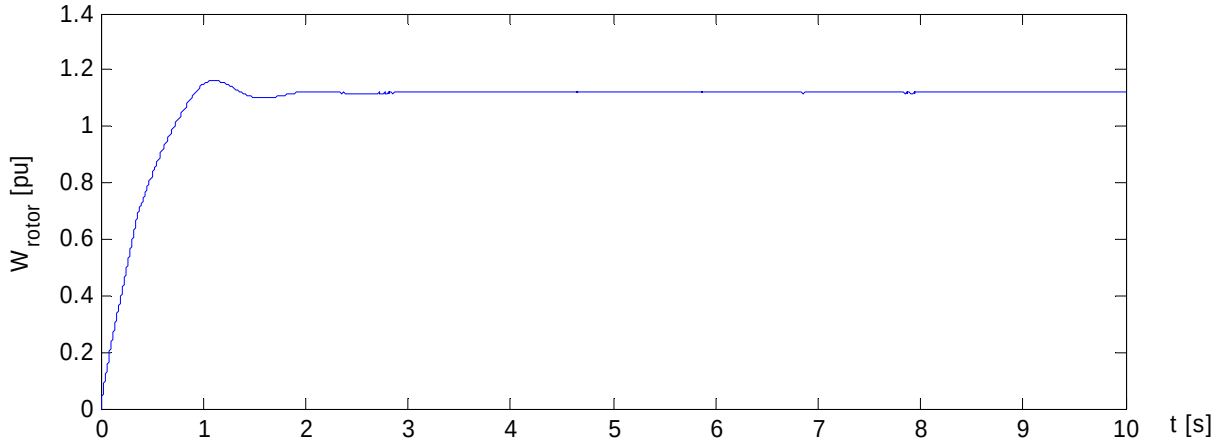

Figure 103. Rotor speed in simulation with constant wind speed to wind power equation.

4.8.2 UMIST-model – voltage source-artificial fault simulation

The measured voltage input simulation did not make any sense, even when using symmetrical artificial ideal voltage data before inputting the actual measured data. The simulation was very disturbed, and thus the validation simulation was decided to be performed with an ordinary voltage source component in the model and a user-created grid fault causing a voltage dip reasonably similar to the measured dip.

Model validation simulations were performed on the UMIST-model with appropriate generator parameter values and a suitable fault resistance artificial fault. No multi-mass was used, and instead the turbine was represented by a single mass. The voltage source used in the model was the original one, which was in ideal mode, i.e. an infinite bus. The input torque to the simulation was the same as earlier used for the validation of another model active and reactive power shorn in Figure 91 and Figure 92. In Figure 104 is shown the voltage dip created by a fault, and in Figure 105 and Figure 106 the active power and reactive power comparisons respectively with the measured quantities.

The simulated active and reactive power output during and after the fault differ significantly from the measured ones. To begin with, the reactive power in pre-fault state is different from the measured. Reactive power (or active power to that matter) does not have a control (compare Q_{set} in the model discussed in section 4.8.1) parameter for user to determine. The variation of the measured active or reactive power is barely visible in Figure 104 and Figure 105, and thus the difference between the simulation and measurement is absolutely unacceptable. One should refer to Figure 91 and Figure 92 for the actual response seen in the active and reactive power measurements during and after the fault.

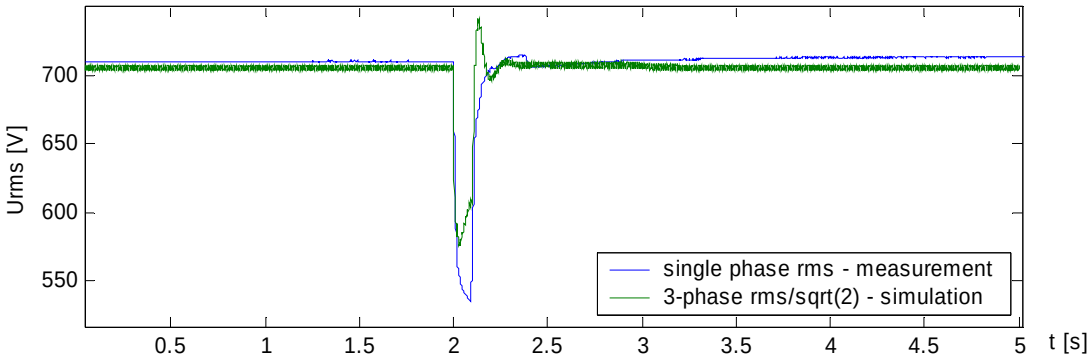

Figure 104. Measurement rms-voltage and the rms-voltage in voltage source during an artificial fault.

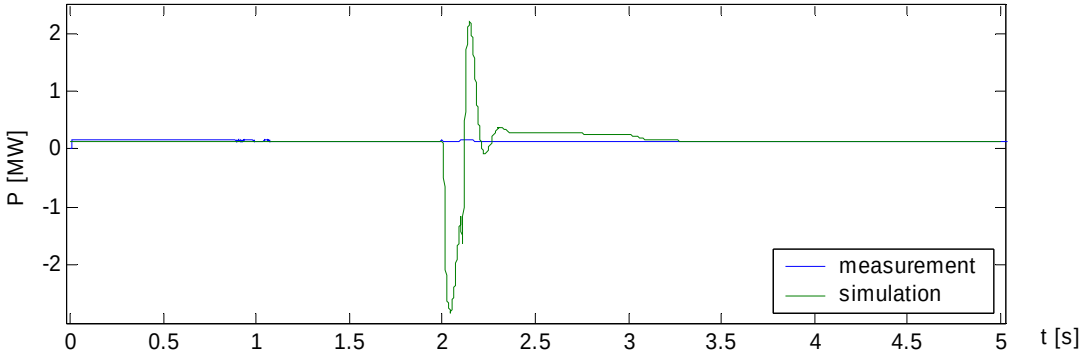

Figure 105. Measured and simulated active power in voltage source simulation during an artificial fault.

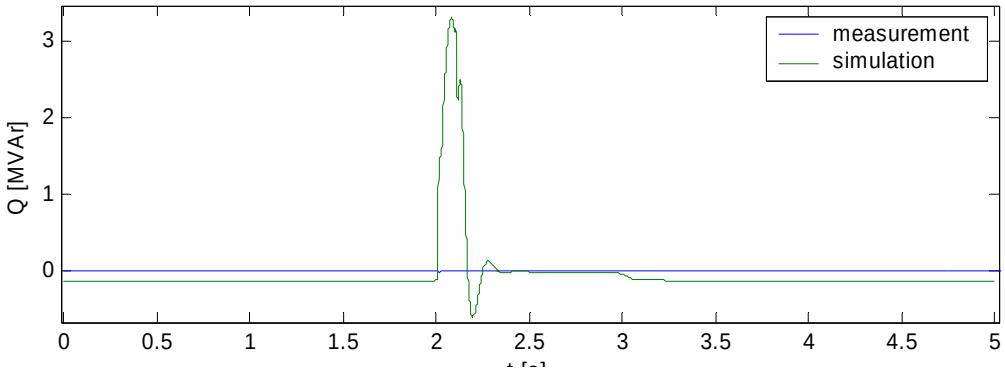

Figure 106. Measured and simulated reactive power in voltage source simulation during an artificial fault.

4.9 Aggregation

There has been no synchronous dynamic voltage dip response measurement data available from both a DFIG equipped wind farm and a single turbine within the farm. Thus no aggregation study nor analysis was possible to be done. A deduction based on the aggregation simulations and study on fixed speed wind farm is done here, however. The fixed speed wind

farm aggregation was concluded in sections 3.4 and 3.7 to be possible by forming an aggregate model identical to single turbine model by replacing the model turbine rating by the sum of ratings of all turbines in the farm. An analysis of possible small error in reactive power was also done regarding fixed speed wind turbine aggregation. Fixed speed wind turbine is not controlled much if at all – consider the passive or active stall control at nominal power – in normal operation, or during a grid fault. Thus the fixed speed wind turbine aggregation accuracy is probably the most dependent on the model unlinearities of the three major wind turbine concepts mentioned in this report. It was shown, however, that the unlinearity of P-Q relationship of fixed speed wind turbine does not cause a large error in aggregate model P-Q relationship. However, in case of variable speed concept as the turbines are very much controllable, operation of each turbine is not necessarily identical, ignoring the power variations due to wind speed – the reactive power of the turbines may be controlled to be of different magnitude. In addition, the behavior of reactive power due to a grid fault is not really dependent of the magnitude of the reactive power production or consumption. Thus, the aggregate turbine reactive power could most likely be controlled for the farm as it would be controlled for a single turbine.

In HElib DFIG-model aggregation the rotor/converter circuit component parameters (capacitances, inductances and resistances) which are given in SI-units, need to be taken into account in addition to the multi-mass and generator rated power. Also the P_{set}- and Q_{set}-values are given in MW and MVAr, as well as the control algorithm uses power measurements in SI-units. However, it does not seem to be enough to grade up these parameters to obtain a reasonable simulation results. There must be some other things in the model that need to be taken into account as well.

5 Conclusions

There has been lot of modeling of wind turbines in the field and these models are presented in some extent in publications. The models themselves are not distributed, though. Quite a little validation against measurements is done or reported to have been done on the models.

Fixed speed wind turbine model, which are quite simple and easy to construct, are today quite good. The parameter acquisition and selection for the specific turbines is probably the most difficult task, as well as it is difficult for the other wind turbine types.

It is quite difficult to get into the models created by others. The models may be not documented thoroughly, and even if the documentation was rather good, it still is quite a task to figure out how the model really works and the designing basics of it, as well as the parameter selections etc. The most challenging part of DFIG-machine construction and modification to another machine of e.g. of different size and with different parameters, is the control circuit. The control schemes and the parameters of wind turbines are business secrets of turbine manufacturers. The control circuits are somewhat complex and include several control parameters which need to be given a value. This makes it a hard task to succeed.

There is quite limited selection of measurement data of voltage dip response available and suitable for model validation purposes. The model validation cases and procedure should not be limited only to a single measurement case against which the simulations are compared. Instead the model should be validated under different circumstances.

References

[1] http://www.windpower.org/en/tour/wres/index.htm Available December 2006.
[2] Wind power in power systems. Edited by T. Ackermann. John Wiley & Sons, Ltd, 2005. ISBN 0-470-85508-8.
[3] S. Seman, Transient performance analysis of wind-power induction generators, Doctoral Dissertation. Espoo, 2006. ISBN 951-22-8422-7.
[4] J. Niiranen, "Voltage dip ride through of a doubly-fed generator equipped with an active crowbar", Nordic Wind Power Conference, 1-2 March, 2004, Gothenburg, Sweden.
[5] T. Petru, Modeling of wind turbines for power system studies, Doctoral dissertation. Chalmers University of Technology, Gothenburg, Sweden, 2003. ISBN 91-7291-306-1.
[6] T. Petru, Modeling of wind turbines for power system studies, Licentiate Thesis. Chalmers University of Technology, Gothenburg, Sweden, 2001.
[7] http://www.energy.sintef.no/wind/IEA.asp Available December 2006.
[8] J.O.G. Tande, E. Muljadi, O. Carlson, J. Pierik, A. Estanqueiro, P. Sørensen, M. O'Malley, A. Mullane, O. Anaya-Lara, B. Lemström, "Dynamic models of wind farms for power system studies – status by IEA Wind R&D Annex 21". EWEC'04, 22-25 November, London, UK.
[9] V. Akhmatov, Analysis of dynamic behaviour of electric power systems with large amount of wind power. Electric Power Engineering, Ørsted-DTU, Technical University of Denmark. Kgs. Lyngby, Denmark, April 2003.
[10] S. Uski, S. Hänninen, Muutosilmiöiden mittaaminen ja analysointi hajautettua tuotantoa sisältävässä verkossa, in Finnish. VTT-R-08322-06, Espoo, September 2006.
[11] J. Niiranen, "About the active and reactive power measurement in unsymmetrical voltage dip ride through testing". Nordic Wind Power Conference, 22-23 May, 2006, Espoo, Finland.
[12] A. Perdana, S. Uski, O. Carlson, B. Lemström, "Validation of aggregate model of wind farm with fixed-speed wind turbines against measurement". Nordic Wind Power Conference 2006, Espoo, Finland, 22-23 May, 2006.
[13] J.O.G. Tande, I. Norheim, O. Carlson, A. Perdana, J. Pierik, J. Morren, A. Estanqueiro, J. Lameira, P. Sørensen, M. O'Malley, A. Mullane, O. Anaya-Lara, B. Lemström, S. Uski, E. Muljadi, "Benchmark test of dynamic wind generation models for power system stability studies". In review.
[14] S. Uski, S. Hänninen, B. Lemström, "Electrical network faults seen by a wind farm – analysis of measurement data". European Wind Energy Conference 2006, Athens, Greece, February 27 – March 3, 2006.
[15] S. M. Bolik, "Grid connection of wind turbines, a never ending story?", 6th International Workshop on Large-Scale Integration of Wind Power and Transmission Networks for Offshore Wind Farms. Delft, Netherlands, 26-28 October 2006.
[16] S. Uski, B. Lemström, J. Kiviluoma, S. Rissanen, P. Antikainen, "Adjoint wind turbine modeling with ADAMS, Simulink and PSCAD/EMTDC". Nordic Wind Power Conference 1-2 March, 2004, Göthenburg, Sweden.
[17] http://wind.nrel.gov/designcodes/preprocessors/ Available in December 2006.
[18] http://wind.nrel.gov/designcodes/simulators/aerodyn/ Available in December 2006.
[19] J. Kiviluoma, S. Uski, S. Rissanen, B. Lemström, P. Antikainen, E. Peltola, Transient Load and Control Simulation of Wind Turbines Using Simulink, ADAMS and PSCAD/EMTDC, T3SULAWIND project report PRO2/P5107/04. Confidential. VTT Technical Research Centre of Finland, 2004.

[20] S. Rissanen & S. Uski, “Modelling and Measurements of Dynamic Loads of an Arctic Wind Turbine”. Boreas VII Conference, Saariselkä, March 2005.
[21] User’s guide on the use of PSCAD – PSCAD Power Systems Computer Aided Design. Manitoba HVDC research Centre. 2003.
[22] T. Thiringer, J. Luomi, “Comparison of reduced-order dynamic models of induction machines,” *IEEE Trans. on Power Systems*. vol. 16, no. 2, pp. 119-126, Feb 2001.
[23] P. Rosas, “Dynamic influence of wind power on the power system”, PhD Thesis. Technical University of Denmark, March 2003.
[24] H. Ganander, G. Ronsten, “Design load aspects due to ice loading on wind turbine blades”. Proceedings of the 2003 BOREAS VI Conference, Pyhätunturi, Finland, April 2003.
[25] DIgSILENT, Dynamic modelling of doubly-fed induction machine wind-generators, Technical documentation. DIgSILENT GmbH, Germany, 2003.
[26] D.J. Trudnowski, A. Gentile, J.M. Khan, E.M. Petritz, ”Fixed-speed wind-generator and wind-park modeling for transient stability studies”, IEEE Transactions on Power Systems, vol. 19, No. 4, Nov. 2004.
[27] H. Saadat, Power system analysis. McGraw-Hill Primis Custom Publishing, 2002. ISBN-10 0072848693, ISBN-13 978-0072848694.
[28] IEA Annex XXI database. Restricted access to Annex participants.
[29] Bonus 600/120 kW generator data-sheet, ABB.
[30] J.O.G. Tande, Power quality measurements from Smøla 40 MW wind farm. 2006-18-12. Confidential.
[31] M. A. Pöller, “Doubly-fed induction machine models for stability assessment of wind farms”. Proceedings of IEEE Power Tech Conference 2003, Bologna, Italy, Vol. 3, June 23-26, 2003. pp.6-13.
[32] P. Ledesma, J. Usaola, “Effect of neglecting stator transients in doubly fed induction generator models”. IEEE Transactions on Energy Conversion, Vol. 19, No. 2, June 2004, pp. 459-461.
[33] W.E. Leithead, S. de la Salle, D. Reardon, “Role and objectives of control for wind turbines”. Generation, Transmission and Distribution, IEE Proceedings-C, vol. 138, No. 2, March 1991, pp. 135-148
[34] A.D. Hansen, F. Iov, P. Sørensen, F. Blaablerg, “Overall control strategy of variable speed doubly-fed induction generator wind turbine”. Nordic Wind Power Conference, 1-2 March, 2004, Gothenburg, Sweden.
[35] Müller, S., Deicke, M., De Doncker, R.W., ”Doubly fed induction generator systems for wind turbines”. IEEE Industrial Applications Magazine, Vol. 8, Issue 3, May-June 2002. pp.26-33.
[36] M. Høgdahl, J.G. Nielsen, “Modelling of the Vestas V80 VCS wind turbine with low voltage ride-through”. 5th International Workshop on Large-Scale Integration of Wind Power and Transmission Networks for Offshore Wind Farms. Glasgow, Scotland, 7 -8 April 2005.
[37] P. Novak, I. Jovik, B. Schmidtbauer, “Modelling and identification of drive-system dynamics in a variable-speed wind turbine”, Proceedings of the Third IEEE Conference on Control Applications, 24-26 Aug. 1994, Vol. 1, pp. 233-238
[38] V. Akhmatov, “Variable-speed wind turbines with doubly-fed induction generators, Part I: Modelling in dynamic simulation tools”, Wind Engineering, Vol. 26, No. 2, 2002, pp. 85-108
[39] Y. Lei, A. Mullane, G. Lightbody, R. Yacamini, “Modeling of the wind turbine with a doubly fed induction generator for grid integration studies”. IEEE Transactions on Energy conversion, Vol. 21., No. 1, March 2006, pp. 257-264

[40] P. Ledesma, J. Usaola, “Doubly fed induction generator for transient stability analysis”. IEEE Transactions on Energy Conversion, Vol. 20, No. 2, June 2005, pp. 388-397.
[41] A. Petersson, Analysis, modeling and control of doubly-fed induction generators for wind turbines. Doctoral Dissertation. Gothenburg, 2005. ISBN 91-7291-600-1.
[42] http://www.lmglasfiber.com/Products/Wing%20Overview/800-1200.aspx, available July 2006.
[43] Analysis of the Unsteady Aerodynamics Experiment for National Full-Scale Aerodynamics Complec Testing.
Available : http://wind.nrel.gov/amestest/LoadsAnalysisDocument.pdf, July 2006.
[44] Kong, C., Bang, J. Sugiyama, Y., “Full Scale Structural Experimental Investigation of an E-glass/Epoxy Composite”,
Available: http://www.sme.org/gmn/data/events/000140/papers/1809.doc, July 2006.
[45] R. Pena, J.C. Clare, G.M. Asher, “Doubly fed induction generator using back-to-back PWM converters and its application to variable-speed wind-energy generation”. IEE Proceedings Electric Power Applications, Vol. 143, No. 3, May 1996.
[46] S. Seman, “Analysis of a 1.7 MVA doubly fed wind-power induction generator during power systems disturbances”, Proceedings of NORPIE 2004, 14-16 June 2004, Trondheim, Norway.
[47] G. Tsourakis, C.D. Vournas, “Simulation of low voltage ride through capability of wind turbines with doubly fed induction generator”. European Wind Energy Conference 2006, Athens, Greece, February 27 – March 3, 2006.
[48] T. Sun, Z. Chen, F. Blaabjerg, “Voltage recovery of grid-connected wind turbines with DFIG after a short-circuit”. 35th Annual IEEE Power Electronics Specialists Conference. Aachen, Germany, 2004.
[49] E. Muljadi, C.P. Butterfield, “Pitch-Controlled Variable-Speed Wind Turbine Generation”, IEEE Transactions on Industry Applications, Vol. 37, No., 1, January/February 2001. pp. 240-246.
[50] F. Lescher, J.Y. Zhao, A. Martinez, “Multiobjective H2/H∞ Control of a Pitch Regulated Wind Turbine for Mechanical Load Reduction”. International conference on renewable energies and power quality (ICREPQ’07), Sevilla, Spain, 28-30, March, 2007.
[51] C. Jauch, ”Wind Turbine Pitch Angle Controllers for Grid Frequency Stabilisation”, European Wind Energy Conference 2006, Athens, Greece, February 27 – March 3, 2006.
[52] J.G. Slootweg, W.H. de Haan, H. Polinder, W.L. Kling, ”General model for representing variable speed wind turbines in power system dynamics simulations”. IEEE transactions on Power Systems, Vol. 18, No.1, February 2003.
[53] Turbine Description REpower MM 82, by J-W. Derksen. SD-2.2-WT-TD-1-B-EN. 22.3.2005.
[54] C. Jauch, ”Stability and Control of Wind Farms in Power Systems”, Risø-PhD-24(EN). ISBN 87-550-3547-7.
[55] M. Rasila, ”Torque- and Speed control of a Pitch Regulated Wind Turbine”, Master Thesis, Chalmers University of Technology, Gothenburg, Sweden, 2003.
[56] US Patènt # 6856039, Variable speed wind turbine generator. June 26, 2003. Available http://www.uspatentserver.com/685/6856039_c.html in December 2006.
[57] Technical description FL 1500-70/65. Fuhrländer. Available http://rewhc.org/wind/downloads/FL_1570_65_Technical_Paper.pdf in December 2006.
[58] Characteristics of Vestas Wind Turbines, by Henrik Kanstrup Jørgensen, Vestas.

[59] Miksi Vestas-tuulivoimala, 23.10.99 Amm-esite2.doc. Edustaja Suomessa Insinööritoimisto Erkki Haapanen Oy. in Finnish
[60] Windenergie 1999. Bundesverband WindEnergie e.V. ISBN 3-9806657-0-4.
[61] Windenergie 2002, Bundesverband WindEnergie. ISBN 3-9808-236-0-1.
[62] Workshop material. DIgSILENT Workshop – Wind Power Integration October 6.-7., 2003.
[63] P.M . Anderson, A. Bose, ”Stability Simulation Of Wind Turbine Systems”. IEEE Transactions on Power Systems , Vol.PAS-102, No.12, December 1983.
[64] L. Tang, R. Zavadil, “Shunt capacitor failures due to wind farm induction generator self-excitation phenomenon”. IEEE Transactions on Energy conversion, Vol.8, No.3, September 1993.
[65] A. Perdana, O. Carlson, J. Persson, “Dynamic response of grid-connected wind turbine with doubly fed induction generator during disturbances”. Nordic Workshop on Power and Industrial Electronics, 14-16 June, 2004, Trondheim, Norway.
[66] S. Heier, “Grid integration of wind energy conversion systems”. John Wiley & Sons, 1998. ISBN-10 047197143X, ISBN-13 978-0471971436.
[67] N60/1300 kW N62/1300 kW-brochure. Nordex.
[68] http://www.windpower.org, available December 2006.
[69] http://www.dgsee.umist.ac.uk/dfig/index.html Available in 2004.
[70] K. Kauhaniemi et al., Simulointiympäristö Loppuraportti. VTT Prosessit, Vasan Yliopisto 31.3.2005.
[71] HElib model library created by VTT and University of Vaasa.
[72] P. Giroux, G. Sybille, H. Le-Huy, “Modeling and simulation of a distribution STATCOM using Simulink’s Power System Blockset”, Industrial Electronics Society, 2001. IECON’01. The 27th Annual Conference of the IEEE. Vol. 2, 29 Nov-2 Dec, 2001.
[73] O. Anaya-Lara, X. Wu, P. Cartwright, J.B. Ekanayake, N. Jenkins, “Performance of doubly fed induction generator (DFIG) during network faults”. Wind engineering, Vol. 29, No. 1, 2005. pp. 49-66.
[74] http://www.iet.aau.dk/Research/wts.htm Available 2004.
[75] M. Hokkanen, Kaksoissyötetyn generaattorin ohjaus ja säätö. VY-VTT: PSCAD tutkimusraportti. Vaasa 15-08-2004. In Finnish

Appendix A1

Matlab-code laske_fundUI.m

```
% Makro laskee myötäverkon arvoja käyttäen vaiheiden RMS-jännitteet,
% pätö- ja loistehon arvot jne.
% Koodi sovellettuna Niirasen NWPC'06 paperista */

% Huom! datan vaiheiden on oltava oikeassa järjestyksessä! (b vaihe 120
% degr. a:ta jäljessä ja c 120degr a:ta edellä = 240degr jäljessä)

% Etukäteen pitää olla määritetty muuttujat: */
% nsample = näytteiden lkm jaksolla - ei tarvitse olla kokonaisluku */
% ua_array = ua-hetkellinen data matriisina */
% ub_array = ub-hetkellinen data matriisina */
% uc_array = uc-hetkellinen data matriisina */
% ia_array = ia-hetkellinen data matriisina */
% ib_array = ib-hetkellinen data matriisina */
% ic_array = ic-hetkellinen data matriisina */

clear x_incr f_scale Ldataset half k Ua1_rms Ub1_rms Uc1_rms u_pos1_cos
u_pos1_sin;
clear i_pos1_cos i_pos1_sin P_pos1 Q_pos1 U_pos1_rms I_pos1_act_rms
I_pos1_sinact_rms;
clear cosphi_pos1 ua_sin ub_sin uc_sin ua_cos ub_cos uc_cos ia_sin ib_sin
ic_sin;
clear ia_cos ib_cos ic_cos x sinx_dt cosx_dt n koo;
clear ua_sin ub_sin uc_sin ua_cos ub_cos uc_cos ia_sin ib_sin ic_sin;
clear ia_cos ib_cos ic_cos Ua1_rms Ub1_rms Uc1_rms;
clear u_pos1_cos u_pos1_sin i_pos1_cos i_pos1_sin P_pos1 Q_pos1 U_pos1_rms;
clear I_pos1_act_rms I_pos1_sinact_rms cosphi_pos1;

% Laskenta alkaa

x_incr = 2*pi/nsample;      % radiaanejen lisäys ayhdellä aika-askeleella

f_scale=2./nsample;         % integraaliyhtälön skaalauskerroin

Ldataset=length(ua_array);  % datasetin pituus

half=round(nsample/2);

% Alustetaan taulukoiden alut (puolen jakson pituudelta) nolliksi
for k=1:1:half
    Ua1_rms(k)=0.;
    Ub1_rms(k)=0.;
    Uc1_rms(k)=0.;

    u_pos1_cos(k)=0.;
    u_pos1_sin(k)=0.;

    i_pos1_cos(k)=0.;
    i_pos1_sin(k)=0.;

    P_pos1(k+half)=0.;
    Q_pos1(k+half)=0.;

    U_pos1_rms(k)=0.;

    I_pos1_act_rms(k)=0.;
    I_pos1_sinact_rms(k)=0.;

    cosphi_pos1(k)=0.;
end

k=1;

% Käydään läpi
while k<=Ldataset-nsample+2
    ua_sin=0.;
    ub_sin=0.;
    uc_sin=0.;

    ua_cos=0.;
    ub_cos=0.;
```

```
    uc_cos=0.;

    ia_sin=0.;
    ib_sin=0.;
    ic_sin=0.;

    ia_cos=0.;
    ib_cos=0.;
    ic_cos=0.;

%koo=k  %printataan missä laskennassa mennään

% Käydään läpi yhden jakson ajan integrointi alkaen mittausdatapisteestä
    for (n=0:1:nsample-1)
        x=n*x_incr;
        sinx_dt=f_scale*sin(x);
        cosx_dt=f_scale*cos(x);

        ua_sin = ua_sin+ua_array(k+n) * sinx_dt;
        ub_sin = ub_sin+ub_array(k+n) * sinx_dt;
        uc_sin = uc_sin+uc_array(k+n) * sinx_dt;

        ua_cos = ua_cos+ua_array(k+n) * cosx_dt;
        ub_cos = ub_cos+ub_array(k+n) * cosx_dt;
        uc_cos = uc_cos+uc_array(k+n) * cosx_dt;

        ia_sin = ia_sin+ia_array(k+n) * sinx_dt;
        ib_sin = ib_sin+ib_array(k+n) * sinx_dt;
        ic_sin = ic_sin+ic_array(k+n) * sinx_dt;

        ia_cos = ia_cos+ia_array(k+n) * cosx_dt;
        ib_cos = ib_cos+ib_array(k+n) * cosx_dt;
        ic_cos = ic_cos+ic_array(k+n) * cosx_dt;
    end

% Lasketaan suureille arvot ja tallenetaan arvot integrointidatasetin
% (=jakso) puoleen väliin
    Ua1_rms(k+half)=sqrt((ua_cos*ua_cos + ua_sin*ua_sin)/2.);
    Ub1_rms(k+half)=sqrt((ub_cos*ub_cos + ub_sin*ub_sin)/2.);
    Uc1_rms(k+half)=sqrt((uc_cos*uc_cos + uc_sin*uc_sin)/2.);

    u_pos1_cos(k+half)=(2.*ua_cos-ub_cos-uc_cos-sqrt(3)*(uc_sin-ub_sin))/6.;
    u_pos1_sin(k+half)=(2.*ua_sin-ub_sin-uc_sin-sqrt(3)*(ub_cos-uc_cos))/6.;

    i_pos1_cos(k+half)=(2.*ia_cos-ib_cos-ic_cos-sqrt(3)*(ic_sin-ib_sin))/6.;
    i_pos1_sin(k+half)=(2.*ia_sin-ib_sin-ic_sin-sqrt(3)*(ib_cos-ic_cos))/6.;


P_pos1(k+half)=3.*(u_pos1_cos(k+half)*i_pos1_cos(k+half)+u_pos1_sin(k+half)*i_po
s1_sin(k+half))/2.;

Q_pos1(k+half)=3.*(u_pos1_cos(k+half)*i_pos1_sin(k+half)-u_pos1_sin(k+half)*i_po
s1_cos(k+half))/2.;


U_pos1_rms(k+half)=sqrt(3.*(u_pos1_sin(k+half)*u_pos1_sin(k+half)+u_pos1_cos(k+h
alf)*u_pos1_cos(k+half))/2.);

    I_pos1_act_rms(k+half)=P_pos1(k+half)/(sqrt(3)*U_pos1_rms(k+half));
    I_pos1_sinact_rms(k+half)=Q_pos1(k+half)/(sqrt(3)*U_pos1_rms(k+half));


cosphi_pos1(k+half)=P_pos1(k+half)/sqrt(P_pos1(k+half)*P_pos1(k+half)+Q_pos1(k+h
alf)*Q_pos1(k+half));

    k = k+1;
end
end
```